POLITECNICO DI TORINO

Master degree course in Mechanical Engineering

Master Degree Thesis

Design, testing and hydrodynamic analysis of a submerged Point Absorber

Supervisor
Prof. Giuliana Mattiazzo

Cosupervisor:
Ing. Giovanni Bracco

Candidate
Simone Sardo
Student ID: s242919

Academic year 2018 – 2019

To my family

Abstract

In recent years the scientific community has expressed a considerable interest in marine energy in order to deal with the serious environmental problems of our planet. The main purpose of the research in the specific field is to obtain clean energy production systems at low cost and with good efficiency. In this thesis was designed a point absorber intended to be placed in the Mediterranean sea, which is less energetic than the oceans. In these conditions you could still realize an efficient WEC with the due measures and obtaining a good power cost ratio. Initially after the choice of the location of the point absorber a preliminary assessment of the energy production near the coast of the island of Pantelleria was made. Falnes studies were followed to design an optimal WEC. In addition, a Matlab Simulink model has been developed that simulates the behavior of the point absorber in reality using the Cummin's equation. A small scale (1:32) prototype has been built in the laboratory for experimental analysis. Different types of buoys have been designed using the same method and their behavior has been assessed. Finally, the experimental and theoretical results were compared.

Keywords: Submerged point absorber, Wave energy device, island of Pantelleria.

Acknowledgements

This thesis marks for me the end of a course of study but also of an important chapter of my life. A beautiful path, full of people, places, moments, memories (and exams, of course) that I will always carry with me, that made me grow and become the person I am. If I have come this far, it certainly is not just because of me. The first people I have to thank cannot but be my parents, who have always supported me both emotionally and economically, and have always maintained total trust in me, even in the moments when I was the first to doubt myself. I would like to thank Professor Giuliana Mattiazzo again, for the opportunity given to me. A special thank goes to dr. Panagiotis Dafnakis and Ing. Giovanni Bracco who closely followed the drafting of the thesis. Thanks also to all the family members, near and far, and to old friends. Finally, a very special thank you goes to all my fellow adventurers of these years in Turin. In particular I want to spend a few words for the most faithful companions of adventure Bruno, Cristina and Andrea each of them gave me so much with whom I shared good and bad moments.

Simone

Contents

List of Tables

List of Figures

Chapter 1

Introduction

The increase of pollution that has been recorded in recent years together with the great growth of the oil price have led many states to shift their attention to new sources of energy. in this way the experimentation of energy production from renewable sources has increased recently. This fact was taken very seriously because even the European Union has moved to deal with these problems, which are local and global interest. In fact, the latter set the goal of increasing the share of clean energy in the global energy mix of the continents before 2020. A form of clean energy that is currently largely underutilised is Ocean energy, Oceans cover 70 percent of the earth's surface and contains energy in several forms:

- Salinity ;
- Temperature differential (OTEC,SWAC);
- Tide;
- Marine currents;
- Wave power;

As said in [1] the OES well known as Ocean Energy System the association has determined the amount of the several type of energy in the ocean. The global tidal energy resource is estimated at 1200 TWh/year (OES, 2012)The potential of wave energy correspond to 29500 TWh/year (OES, 2012), the energy from the thermal gradient (OTEC) is estimated to 83340 TWh/year. Moreover there is the energy from the salinity gradient has been estimated 5 177 TWh (IRENA, 2014b). With the energy from the ocean can be possible to cover the 2/3 of the global energy need (160000 TWh/year)[2].

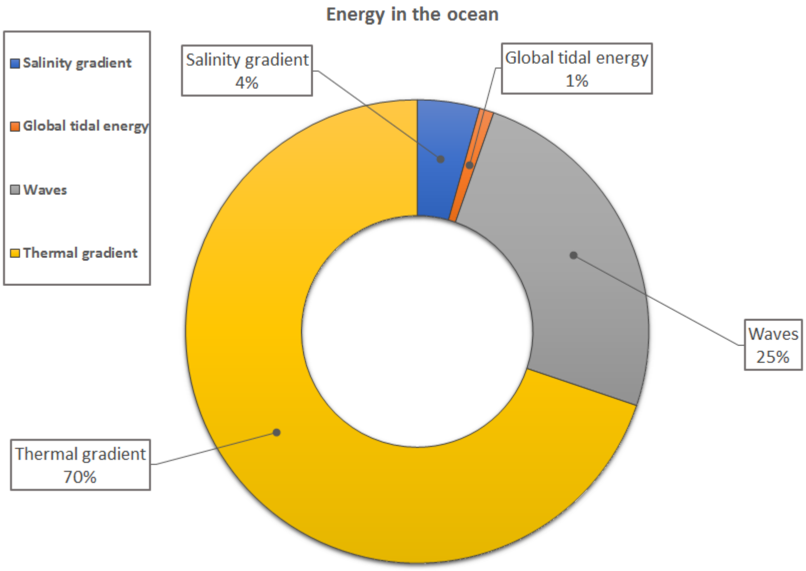

Figure 1.1. Energy in the ocean.[1]

Wave power is one of the largest and most broadly accessible of the marine resources. " It is estimated that harvesting the 0.2% of the ocean's untapped energy will provide power for the entire world. "[3] Waves are therefore a very dense energy source. Unfortunately WECs are not able to harvest 100% of the incoming power...

Chapter 2

Wave Energy

2.1 Energy in the ocean

Currently the researchers are working hard on new medics to capture the energy present in the ocean. However, only in recent years technologies are improving greatly due to the increase in the price of fossil fuels and the problems of global warming affecting our planet. It is also important to remember that in the past marine technologies were considered very expensive with low efficiency to be used as an alternative to other renewable sources. The main types of energy contained in the ocean are mechanical and thermal. Mechanical forces are created by rotation of the earth an the moon's gravitation. The process of wave formation originates due to the rotation of the earth. Furthermore tides are caused by the gravitation pull attraction of the moon and sun. In addition to the previous phenomena two there are ocean current formed by forces including breaking waves, wind, the Coriolis effect, cabbeling, and differences in temperature and salinity. Instead the sun create a temperature difference between the surface and the seabed. From this phenomenon can be dropped thermal energy.

2.2 Wave generation

Waves are created by the wind blowing over water, and will occur only in water near the sea surface. Wind energy is a derived of solar energy. Afterwards wind energizes the sea water therefore even wave energy is eventually concentrated solar energy. The wave formation is complex and not completely understood.

- The wind exerts a tangential stress on the water surface inducing the formation of waves.
- Then by the Bernoulli effect the faster air in point A is at lower pressure than point B, further increasing the wave height.

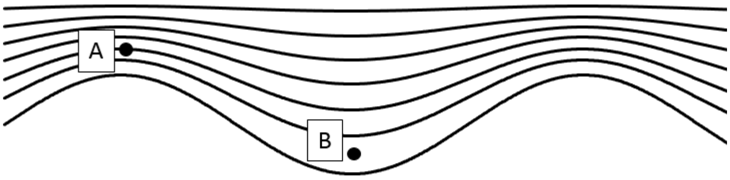

Figure 2.1. Bernoulli effect in the wave formation.

The ocean waves propagate faster than the wind, this causes a transfer of energy. The waves grow thanks to the friction of wind on the water's surface and pressure differences between the upwind and the lee side of a wave crest.[4] Growth and wave formation depends on 5 factors: [5]

- Wind speed, necessary for the energy exchange;
- The fetch is the area of water surface over which the wind blows;
- Width of area affected by fetch ;
- Wind duration;
- Water depth;

As it is possible see in the next figure there are different phases of an ocean surface. At first the Wave Crest, where the water masses of the surface layer are moving horizontally in the same direction as the wind. of ocean or lake surface over which the wind blows in an essentially constant direction; subsequently there is the falling wave. After there is the trough, where the water masses of the surface layer are moving horizontally in the opposite direction of the wind and finally the rising wave.

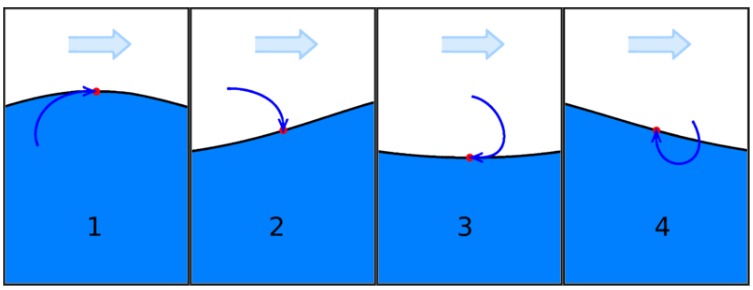

Figure 2.2. Phases of a ocean waves[6].

In the first movement the water's particles motion expected is only vertical but the real trajectory is circular. As it is possible see in the next figure the oscillatory motion is highest at the surface and decreases with depth. With this type of motion the ocean carries kinetic energy witch can be captured by Wave energy converter (WEC).

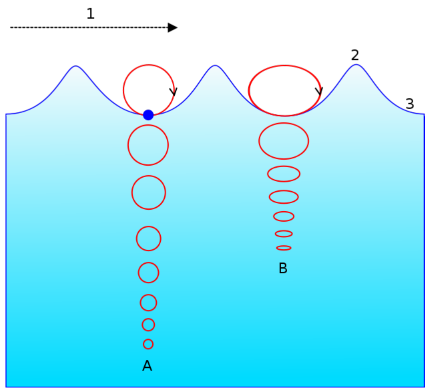

Figure 2.3. Water's particels movement (seabed with different deph)[7].

The Water's particles velocity is composed by vertical and horizontal component. This second component transport the waves on the ocean and it is called group velocity. However the vertical component is know as wave energy flux and it express the energy through a vertical plane of unit width, parallel to a wave crest. The wave are able to transport for hundred kilometres a big amount of energy with little losses. It is important known that the motion of the water's particles depend by the height of the seabed. There are different condition: deep water, shallow water and intermediate water.
The main physical parameters describing waves are:

- Height expressed in meters is vertical distance from trough to crest;
- Length expressed in meters is distance from crest to crest;
- Period expressed in seconds is time interval between two consecutive crest;
- Wave propagation direction;

The first two are the most important. With this parameters it is possible describe the size of the ocean waves and the structure of the flow within them. In the figure it is possible s understand how the period and wave height change in the world.

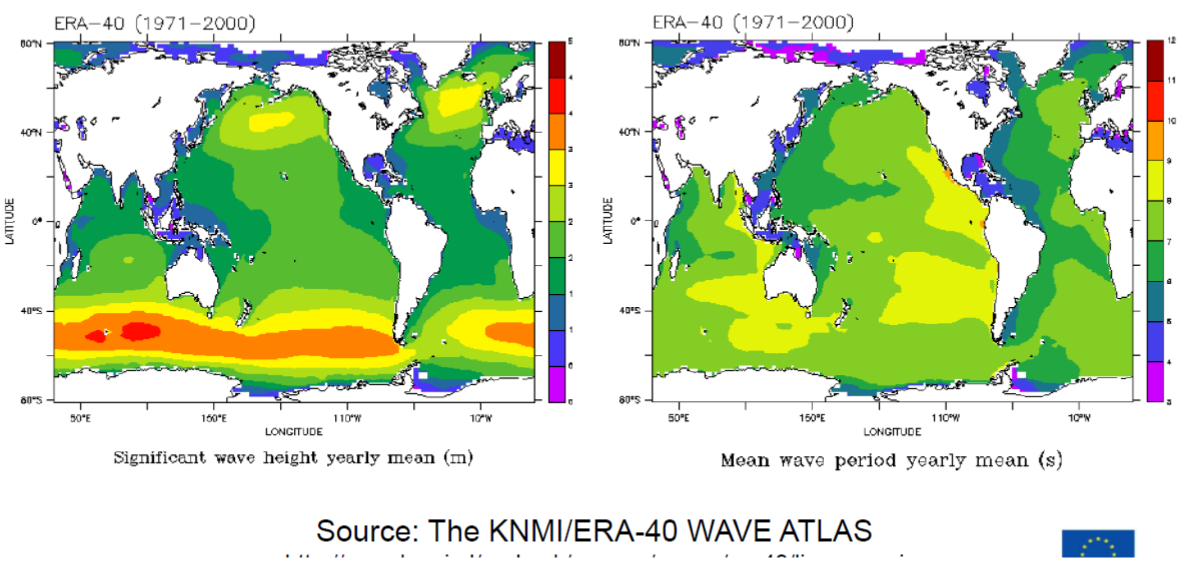

Figure 2.4. Global Average Wave Parameters [8].

The wave power is normally expressed with that average annual power per meter of wave crest width parallel to the shoreline. As it is possible see in the figure the wave energy is distributed unevenly around the world like other types of clean energy.

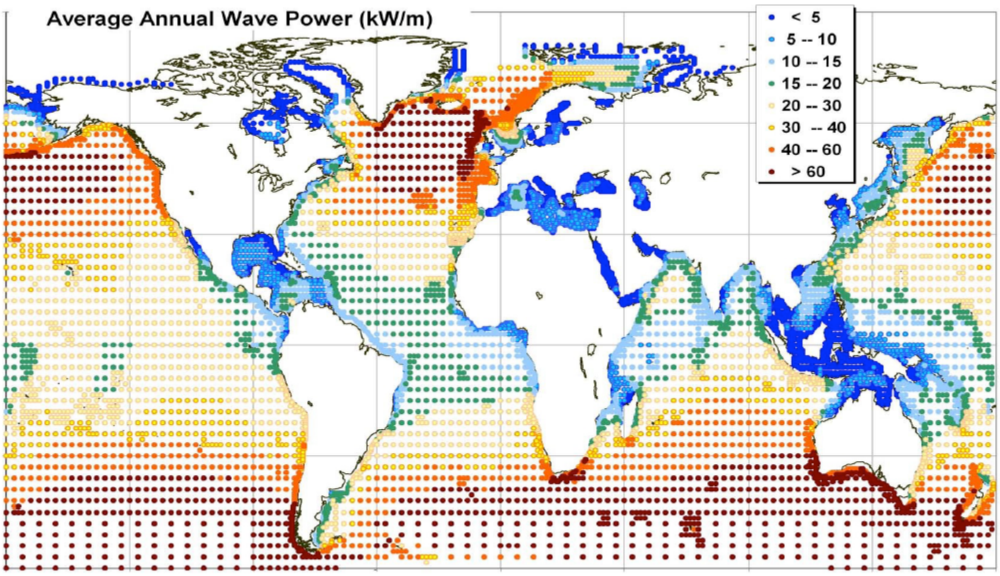

Figure 2.5. Distribution of Wave Energy levels in KW/m of crest length [8].

As it is possible see in the maps there are zone with wave energy level very hight. In these spot strong wind have travelled over long distance and the exchange of energy continue without interruption. In fact increased wave activity is found between the latitudes of approximately 30° and 60° in both the hemispheres.[9]. For these reasons the countries best suited for wave energy conversion are Great Britain, Ireland, Norway, New Zealand, Southern Australia, Chile, followed by Northern Spain, France, Portugal, North and South American coasts and South Africa.This map with the annual power level is very important but must be known that the wave distribution depend by the season.

2.3 Regular wave

The oceans waves are a very complicated phenomena and in the first approximation can be considered as linear wave. Regular waves can be easily described by mathematical model applying the correct laws of physics. This is a simply way to describe this phenomenon[10]. In the linear theory of regular wave work under the assumption of:

- the crests of the wave are infinitely long with constant elevation in the transversal direction, and the wave fronts are infinite parallel plans;
- Semplified treatment consider waves as bi-dimensional waves ;
- The water is incompressible, the continuity equation applies as a result of conservation of mass. ;
- The motion of the fluid (the flow) is irrotational;
- sea bottom is assumed to be impermeable and therefore the velocity component along z must be null at all times;

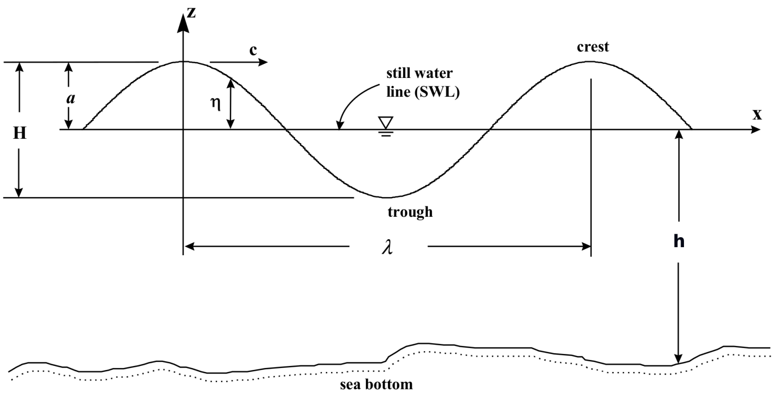

Figure 2.6. Linear wave representation.

$$\eta(x,t) = asin(\omega t - \kappa x)$$

Where:

- η = the magnitude of the maximum displacement from the mean sea-level;
- $a = \frac{H}{2}$ = middle of the wave height (vertical distance from trough to crest);
- $\omega = \frac{2\pi}{T}[rad/s]$ = wave periodicity in time;
- $\kappa = \frac{2\pi}{\lambda}$ wave number, periodicity in space;
- $T[s]$ = wave period;
- $\lambda[m]$ = wavelength (horizontal distance between two crests along the wave direction);

There are different type of waves and depend to the depth of the seabed. In order to distinguish between shallow and deep water, we can use the following rule:

- $h > \lambda/2$ refer to deep water;
- $h < \lambda/20$ refer to shallow water;

For deep water we have:

$$\lambda = \frac{g}{a\pi}T^2(\approx 1.56T^2)$$

The phase velocity, c_p, of a regular wave is defined as:

$$c_p = \frac{\omega}{\kappa} = \frac{L}{T}$$

Which is, for instance, the speed of the top (crest) of the wave as it moves along. From the dispersion relation we obtain different equation.

2.3.1 Linear Wave Theory

All the equations for describing linear waves are present in the following figure. All relevant terms are present and success in the various cases a second one of the depth of the sea. The complete linear wave theory is exposed.

Linear Theory of Regular Waves Review			
Wave property	**SHALLOW WATER** $(h/\lambda < 1/20)$	**INTERMEDIATE WATER** $(1/20 < h/\lambda < 1/2)$	**DEEP WATER** $(h/\lambda > 1/2)$
Velocity potential $(\boldsymbol{u} = \nabla\phi)$	$\phi = \frac{ag}{\omega}\frac{\cosh k(z+h)}{\cosh kh}\cos(\omega t - kx)$	$\phi = \frac{ag}{\omega}\frac{\cosh k(z+h)}{\cosh kh}\cos(\omega t - kx)$	$\phi = \frac{ag}{\omega} e^{kz}\cos(\omega t - kx)$
Dispersion relation	$\omega^2 = gk^2h$	$\omega^2 = gk\tanh kh$	$\omega^2 = gk$
Wave length - wave period relation	$\lambda = T\sqrt{gh}$	$\lambda = \frac{g}{2\pi}T^2\tanh\frac{2\pi h}{\lambda}$	$\lambda = \frac{g}{2\pi}T^2 \quad (\approx 1.56\ T^2)$
Wave profile	$\eta = a\sin(\omega t - kx)$	$\eta = a\sin(\omega t - kx)$	$\eta = a\sin(\omega t - kx)$
Dynamic pressure	$p_d = \rho ga\sin(\omega t - kx)$	$p_h = \rho ga\frac{\cosh k(z+h)}{\cosh kh}\sin(\omega t - kx)$	$p_h = \rho ga\, e^{kz}\sin(\omega t - kx)$
Horizontal particle velocity	$u = \frac{\omega a}{kd}\sin(\omega t - kx)$	$u = \omega a\frac{\cosh k(z+h)}{\sinh kh}\sin(\omega t - kx)$	$u = \omega a e^{kz}\sin(\omega t - kx)$
Vertical particle velocity	$w = \omega a\frac{z+h}{h}\cos(\omega t - kx)$	$w = \omega a\frac{\sinh k(z+h)}{\sinh kh}\cos(\omega t - kx)$	$w = \omega a e^{kz}\cos(\omega t - kx)$
Horizontal particle acceleration	$\dot{u} = \frac{\omega^2 a}{kh}\cos(\omega t - kx)$	$\dot{u} = \omega^2 a\frac{\cosh k(z+h)}{\sinh kh}\cos(\omega t - kx)$	$\dot{u} = \omega^2 a\, e^{kz}\cos(\omega t - kx)$
Vertical particle acceleration	$\dot{w} = -\omega^2 a\frac{z+h}{h}\sin(\omega t - kx)$	$\dot{w} = -\omega^2 a\frac{\sinh k(z+h)}{\sinh kh}\sin(\omega t - kx)$	$\dot{w} = -\omega^2 a\, e^{kz}\sin(\omega t - kx)$
Group velocity	$c_g = c$	$c_g = \frac{1}{2}c\left(1 + \frac{2kh}{\sinh 2kh}\right)$	$c_g = \frac{1}{2}c$

$\omega = 2\pi/T,\ k = 2\pi/\lambda$ T = wave period λ = wave length a = wave amplitude g = acceleration of gravity $c = \lambda/T$ = phase speed	t = time x = direction of propagation z = vertical co-ordinate positive upward, origin at still water level h = water depth	p_h = dynamic pressure $p_h - \rho gz + p_o$ = total pressure in the water ($-\rho gz$ = hydrostatic pressure, p_o = atmospheric pressure). $E = \frac{1}{2}\rho ga^2$ = wave energy (per unit surface area) $P = Ec_g$ = wave energy flux (per unit width along the wave crest)

Figure 2.7. Linear theory of regular wave [11].

2.3.2 Energy transported by the wave

The total energy is the sum of potential energy and kinetic energy. For a progressive, plane, harmonic wave the time-average stored energy per unit (horizontal) area is:

$$E = E_p + E_k$$

$$\begin{cases} E_p = mg(\triangle z) \\ E_k = \frac{1}{2}mv^2 \end{cases}$$

Let us consider the potential energy associated with the elevation of water from the wave troughs to the wave crests. Per unit (horizontal) area the potential energy relative to the sea bed equals the product of $\rho g(h+\eta)$, the water weight per unit area, and $(h+\eta)/2$, the height of the water mass centre above the sea bed:

$$\rho g/2(h+\eta)^2 = \rho g/2h^2 + \rho gh\eta + \rho g/2\eta^2$$

The increase in relation to calm water is:

$$\rho gh\eta + \rho g/2\eta^2,$$

Where the first term has a vanishing average value.

$$E_p|_{m^2} = \frac{mg(\triangle z)}{cl\lambda} = \frac{\rho Vg(2z_G)}{cl\lambda} = \frac{\rho\frac{a\lambda}{\pi}clg(\frac{2a\pi}{8})}{cl\lambda} = \frac{\rho ga^2}{4}[J/m^2]$$

Where cl is the crest length.

2.3.3 Total stored energy

By the equation of energy, the average potential energy is equal to the kinetic energy and therefore the total energy of wave is:

$$E|_{m^2} = E_p|_{m^2} + E_k|_{m^2} = 2E_p|_{m^2} = \frac{(\rho ga^2)}{2}[J/m^2]$$

The energy travels at the group velocity, that for deep water waves is half of the phase velocity. This quantity can be called Wave energy transport.[12]

$$P_w = Ec_g = \frac{1}{2}\rho ga^2\frac{c}{2} = \frac{1}{4}\rho ga^2\frac{\lambda}{T} = \frac{1}{8\pi}\rho g^2a^2T = \frac{\rho g^2}{32\pi}H^2T[W/m_cl](\approx H^2T[kW/m_cl])$$

Waves are therefore a very dense energy source. Unfortunately WECs are not able to harvest 100% of the incoming power.

2.4 Irregular wave

Irregular waves can be seen as overlapping amounts to other regular waves as the next figure. In an irregular wave there are different wavelengths and different heights. Maximums are reached when the waves are those that are in bands and amplitudes and add up.[10]

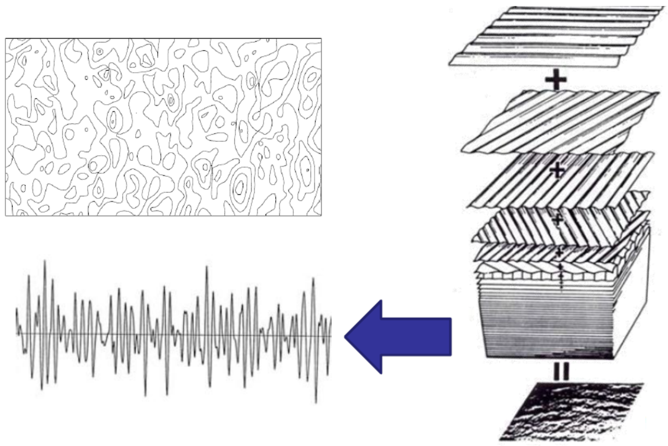

Figure 2.8. The sea surface obtained from the sum of many sinusoidal waves.[10]

For describe the irregular wave is used the Fourier series. The overlapping of regular wave with different amplitude and wave length produce irregular wave:

$$\eta(t) = \sum_{(n=1)}^{N} \eta_n \cos(k_n x - \omega_n t + \varepsilon_n)$$

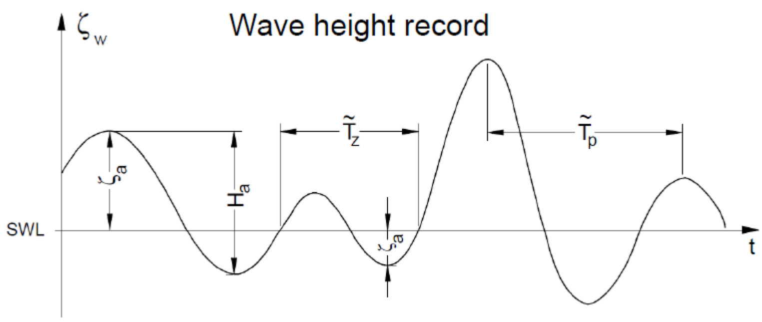

Figure 2.9. Sample of a wave record.

From a wave record it is possible create a wave spectrum energy that is way for represent the sea state as it is possible see in the next figure.[10]

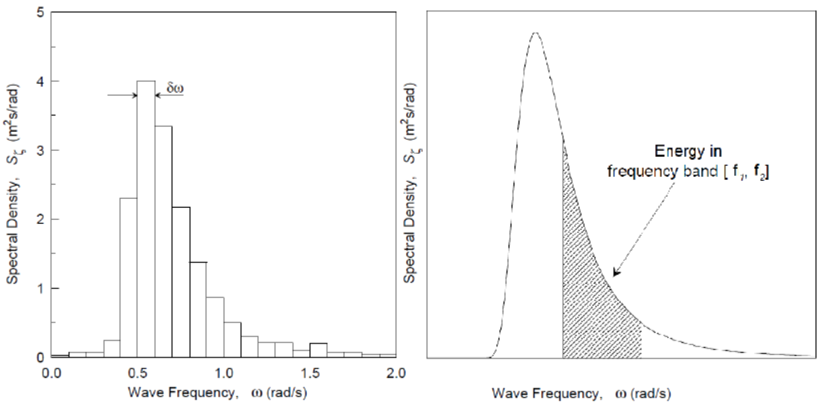

Figure 2.10. Wave spectrum.[10]

The form of a wave spectrum is usually expressed in terms of the moments of the distribution (spectrum). The n-th spectral moment is defined as as follows[10]:

$$m_n = \int_0^\infty f^n S(f) df$$

All the previous parameters can be derived from the spectral moments:

- Peak period: $T_p = \sqrt{\frac{m_2}{m_4}}$
- Zero-crossing period $T_z = \sqrt{\frac{m_0}{m_2}}$
- Mean period $T = \frac{m_0}{m_1}$
- Significant wave period height $H_s = 4\sqrt{m_0}$
- Energy period $T_e = \frac{m_{-1}}{m_0}$

Then the power is:

$$P = \frac{\rho g^2}{64\pi} {H_s}^2 T_e \left[\frac{W}{m_{cl}}\right] \left(\approx 0.5 {H_s}^2 T_e \left[\frac{W}{m_{cl}}\right]\right)$$

Different kinds of spectra have been elaborated to describe sea state. To describe irregular waves in open sea where the wind is blowing regularly over a wide "fetch" the Bretscheider spectrum is usually used (as advise by the international Towing Tank Conference, ITTC-1966)[10]

$$S_\xi^B(\omega) = \frac{A}{\omega^5} e^{\frac{-B}{\omega^4}}$$

The Bretscheider spectrum describes a growing, fully developed, or a decay sea. If the sea is fully developed (the wind blow into the sea fetch for sufficient time to stabilize its condition), the Bretscheider spectrum assumes the expression of the Pierson-Moskovitz wave in witch A and B as evaluated as follows.

$$A = 0.0081g^2$$

$$B = 0.74(\frac{g}{V_W})^4$$

$$S_\xi^B(\omega) = \frac{(0.0081g^2)}{\omega^5} e^{-0.74(\frac{g}{V_W\omega})^4}$$

Where V_W is the wind velocity $[m/s]$ measured at 19.5 m over the sea level. In the fetch is limited, the Bretscheider and the Pierson-Moskovitz wave spectra are not able to describe properly the energy distribution over the frequencies. To describe the JONSWAp (join North Sea Wave Project, Hasselman 1973) was developed. The JONSWAP spectrum is used to describe close seas and the Bretschneider spectrum for oceanic sites. [10]

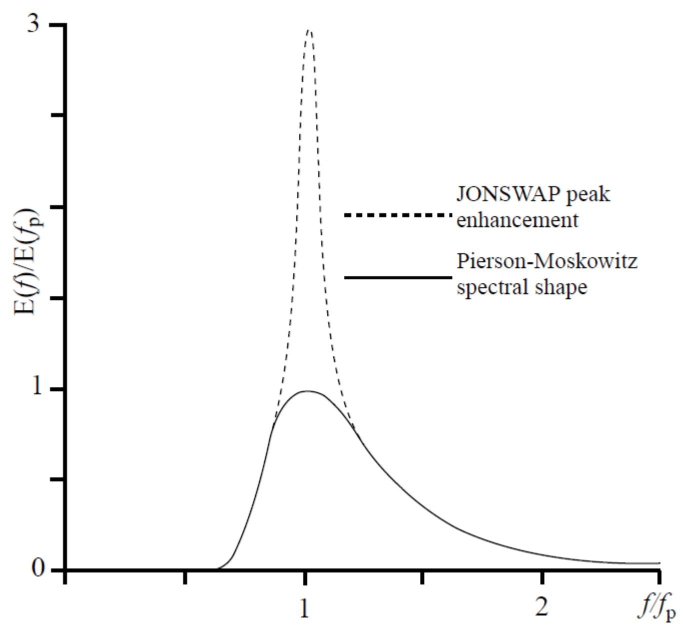

Figure 2.11. Difference between JONWAP and Bretschneider spectrum [10].

Chapter 3

Wave Energy converter

3.1 Wave energy converter

For extract the power of wave and transform it in electricity is used a wave energy converter usually called WEC. This devices can be divided into different categories depending on the position at sea:[13]

- Offshore devices
- Near-shore devices
- Shoreline devices

There are many types of WEC and they can be classified according to the principle of, the position at sea or from the type of PTO. The Capture Width (measured in meters) is related to the wave power capabilities of a WEC. It is defined as the ratio between the output power and the incoming wave power density [14].

$$CW = \frac{P_e}{P_w}$$

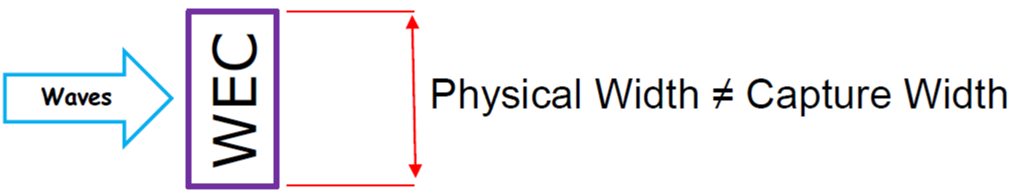

Figure 3.1. Presentation of physical width.[14]

In order to establish a sort of " efficiency " for a WEC, it was defined the relative capture width as the ratio between the capture width and the actual device width[14].

$$RCW = \frac{CW}{Device\ Width} = \frac{P_e}{WP_w}$$

A WEC can have a RCW great than 100%, because of the interactions between the radiated wave and the incoming wave (as the heaving point-absorber).

3.2 Classification by type

WECs can be classified in the first moment with respect to their dimension and orientation respect to the wave. A Point Absorber is a device with horizontal dimensions negligible with respect to the wave length. Terminators and Attenuators have definite dimensions with respect to the wave and usually a domain the horizontal dimension. Terminators physically intercept the incoming wave where as Attenuator extract energy as the wave passes through their length.

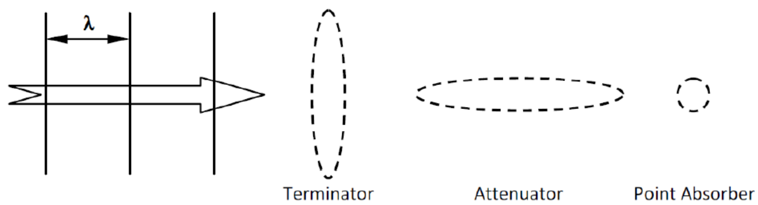

Figure 3.2. Types of WEC.

In addition to the previous types there are other different technologies in the following part are explained all the main devices.

3.2.1 Attenuator

The attenuator is composed of several floating segments which are positioned parallel to the predominant wave direction. This device follows the movement of the wave and captures the energy counteracting the movement along its length. The movement of these segments drives hydraulic rams, which pump high-pressure fluid through hydraulic motors. In the next figure it is possible to see the most successful attenuator that is the Pelamis Wave Energy Converter. As it is possible see it is parallel to the predominant wave direction (perpendicular to the wave front). [13]

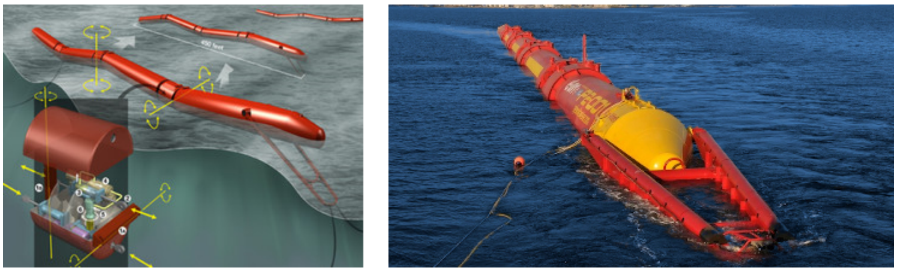

Figure 3.3. Pelamis (Scotland).[15]

3.2.2 Point Absorber

This device has small dimensions relative to the incident wavelength. The point absorber can have different position on the sea. It can be a floating structure or submerged. In the first case it heave up and down on the surface, in the second below the surface relying on pressure differential. An advantage of this device in that the direction is not important because have a small size. The point absorber is composed by aa buoy witch oscillate in the sea and pull a tensioned tether. This mooring line is connected to a PTO for the production of energy.[13]

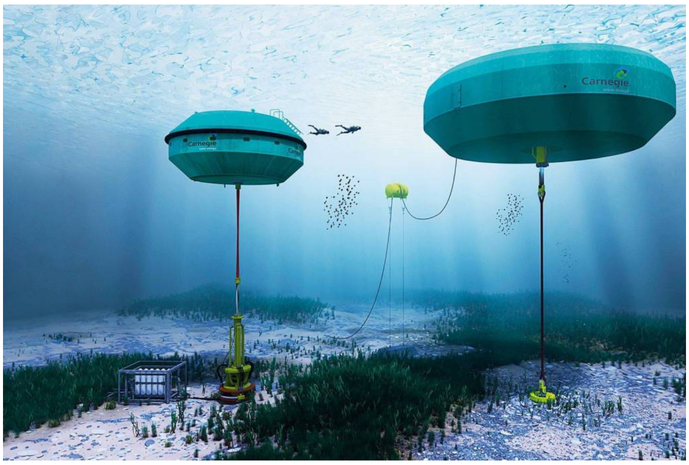

Figure 3.4. Example of Point Absorber.[16]

3.2.3 Oscillating Wave Surge Converter (OWSC)

This device defeated the dead in a sea wave surge. The OWSC have one end fixed to a structure or the seabed while the other end is free to move near the surface. This last part have a surge motion as an inverted pendulum due to the movement of the ocean's wave.[13] In Figure, the Oyster is a buoyant, hinged flap which is attached to the seabed at around ten metres depth, around half a kilometer from shore. The hinged flaps ways backwards and forwards driving two hydraulic pistons which push high pressure water on shore to drive a conventional hydro-electric turbine.

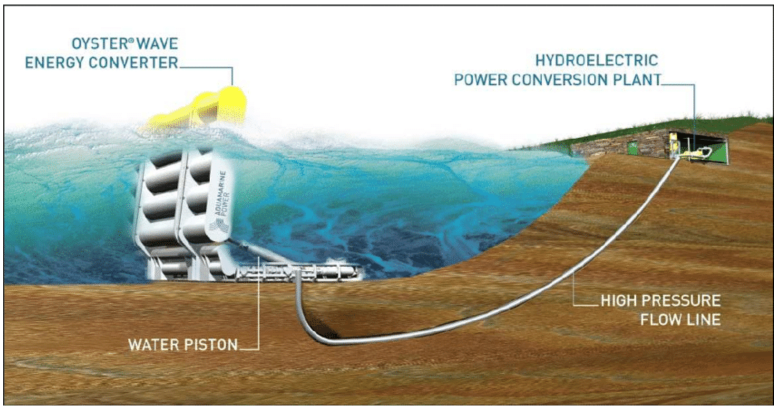

Figure 3.5. Aquamarine Oyster-Scotland [17].

3.2.4 Oscillating Water Column (OWC)

These devices can be located on shore or in deeper water offshore. The Oscillating Water Column(OWC) is a device composed mainly of an air chamber and a turbine.The air chamber is partially submerged and open below the water line thus the heave motion of the sea surface forces the air contained in the chamber through the turbine. The air is pushed or pulled through the turbine, resulting in an alternate flow. In order to use this alternate flow, the PTO(PowerTakeOff) is usually composed of a Wells turbine because of its capacity to rotate continuously in one direction in spite of the direction of the air flow.

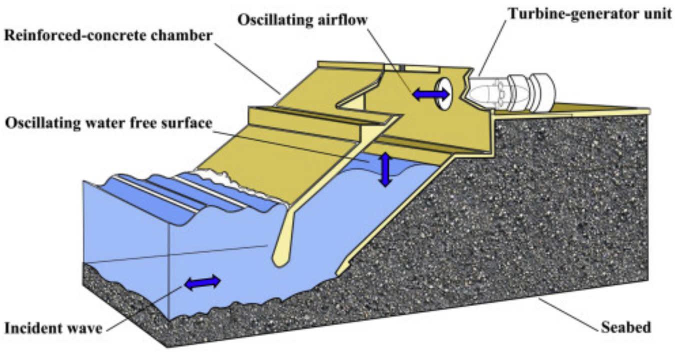

Figure 3.6. Example and operating principle of an Oscillating Water Column device [18].

3.2.5 Overtopping device

This device is usually usually a large structure that captures incident waves in a reservoir above sea level and releases water with a turbine. the latter is connected to a generator that produces electric energy. An overtopping device needs to have a minimum storage capacity. They can be located either on shore or floating offshore. This device is composed by a main body with doubly curved (elliptical circular) ramp, Two wave reflectors, Mooring system and PTO (Low head Kaplan turbines Permanent Magnet Generators).

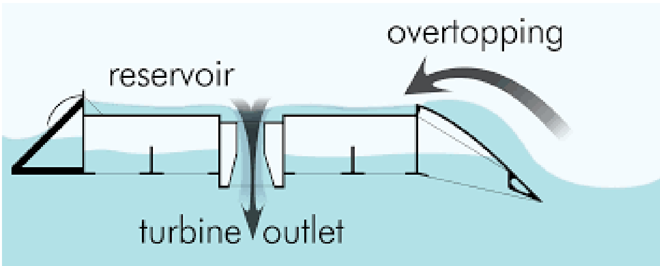

Figure 3.7. Example of Overtopping Device [19].

3.2.6 Submerged Pressure Differential

This device is composed of a part connected to the seabed and the other free to move vertically. The difference in pressure that is created due to the movement of the waves. this device is usually placed near the shore. When properly designed for the sea state, this category also has significant point absorbing characteristics.[13]

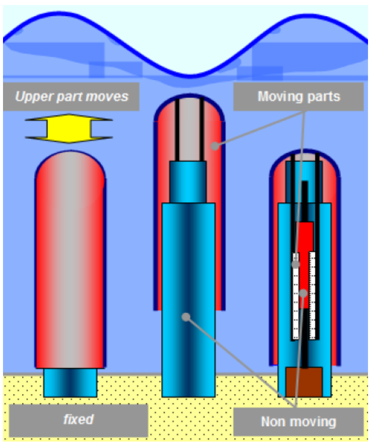

Figure 3.8. Example of Submerged Pressure Differential device[20].

Chapter 4

Point Absorber Project

This thesis treat about only the point absorber and the design of one of this device. This chapter explain how this types working. A point absorber is a wave energy converter which absorbs energy through its movement created by the excitation forces caused by the passing waves. The Point Absorber which is being developed by Politecnico di Torino operates under the sea surface [21] for two important reasons:

- The survivability of the wave energy converter is increases during storms with extreme wave conditions;

- Public requirement for minimised visual impact;

4.1 Point Absorber

This device is composed of a buoy that moves under the effect of the waves and can be superficial or submerged. The buoy is kept in position by cables connected to the bottom. The motion of the point absorber usually starts a hydraulic pump and generates electricity. The part of the device called PTO can be of different types depending on the manufacturer, such as directly through linear generators or generators driven by mechanical linear-rotary converters or hydraulic pumps. The presence of this device in the sea can cause some marine ecosystem problems [22] such as:

- Electric fields generated by the various cables for electric transmission;

- The energy left to the waves could cause problems, in fact it is recommended that they be applied away from the coast;

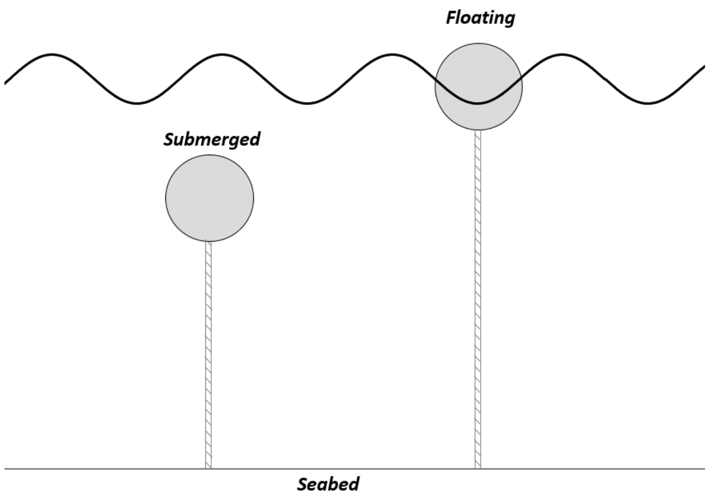

Figure 4.1. Schematic representation of floating and submerged Point Absorber.

Furthermore, another characteristic of the function of the WEC is the fact that both surge and heave motion are utilised in order to absorb energy. According to [23], point absorbers which use several modes of motions have a significant advantage because the power generation is higher. A Fundamental dimension to be selected during the design and the development of the wave energy converter is the volume of the hull. In order to identify the total volume of the buoy, a method was proposed [23] [12] called 'Budal Diagram' which takes into account the sea state of the deployment of the WEC. The objective is the optimization of the power generation always always regarding the how big the hull is and so the final cost of the function of the machine. A good point absorber has the same characteristics as a good wave-maker. The wave energy is absorbed by radiating a wave with destructive interference to the incoming waves. Buoys use the rise and fall of swells to generate electricity in various ways including directly via linear generators, or via generators driven by mechanical linear-to-rotary converters or hydraulic pumps. EMF generated by electrical transmission cables. Falnes claims [12] that for design of the WEC must take into account the realistic limits of the wave absorption. First of all it is important to remember that any wave has a certain energy and all this amount of energy can't be converted completely into electric energy. There are two limits for the absorbed power that will be subsequently exposed , they are High Frequency Limit(P_a) and Low Frequency limit (P_b). These limit are explained carefully in the next chapter. The hull's ability to destroy waves is expressed by the limit P_a. The excitation force of the wave causes oscillatory movement. A oscillating body in the water produces waves known as radiated waves. If the produced waves are equally large with the passing ones, means that they ' destroy

' each other and power generation becomes maximum. The previous statement can become more clear by understanding the Figure.

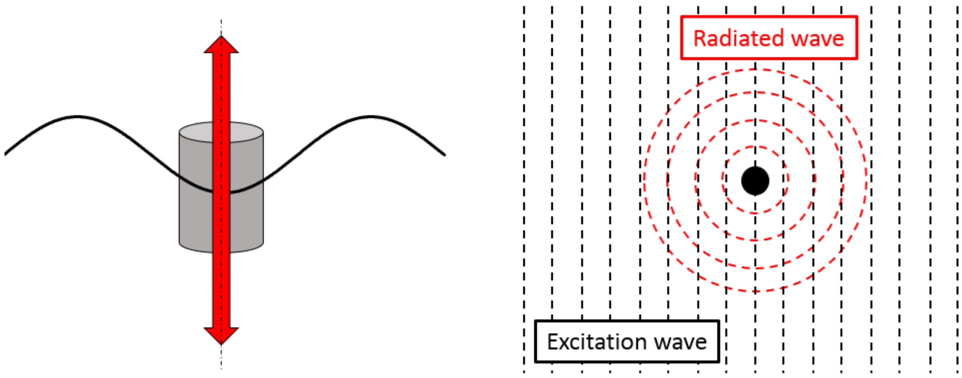

Figure 4.2. Oscillating body, excitation wave and radiated wave.

In schema a, a regular wave of height H and period T is presented. It is supposed that the body is oscillating with optimal conditions as it is presented in schemata b and c, producing radiated waves with direction to the right. As a result, the produced radiated waves destroy 100% the passing wave, as it is shown in schema d. In other words, all this theory of the wave destructions means that the hull vibrates with optimal conditions, absorbs all the energy of the interfacing wave and consequently the sea behind the device is calm.

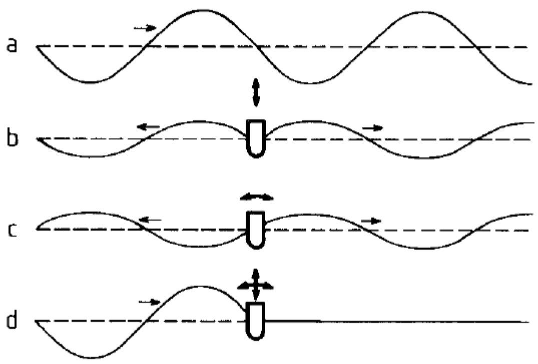

Figure 4.3. Wave interface – Power absorption.[12]

In this point, it must be mentioned that this kind of 100% wave energy absorption is utopian because the assumptions that have been made are not realistic

(Friction loses etc.) However, this instruction should be followed to achieve as maximum power absorption as possible. The quality of the body's vibration and wave generation depends on the mode of the oscillation and the degrees of freedom of the motion. When the displacement of the body is only heave, it is considered to be a source radiator which Is presented in Figure b. Moreover, a body which moves in pitch or in surge, is considered to be a dipole radiator. The difference between a source radiator and a dipole radiator is the fact that the first one generates a circular wave which expands towards all the direction while a dipole radiator generates two waves with the same period and height but they are in antiphase.

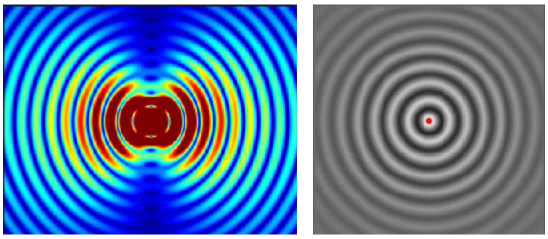

Figure 4.4. Source and dipole radiator.

After these considerations it is possible to say that the maximum power can be obtained with a Point Absorber that behaves as both and sources mentioned above. The optimal situation is when the buoy is able to move in heave, surge and pitch or with three degrees of freedom. The Point Absorber developed by the Politecnico di Torino will in fact be free to move with these three degrees of freedom to achieve maximum power.

4.2 Model of Point Absorber system

In Figure 4.1 an initial schematic representation of the point absorber is presented. The first hull geometry which has been studied is the sphere(subsequently the cylinder), while it is totally submerged just under the surface of the sea. The buoy is moored through a tether to a heavy weight (anchor) located in the bottom of the sea. The mooring line is considered to be linear and always in tension, responsible for the recovery forces acting in the hull and the stiffness of the system. Power generation can be achieved through the energy absorption from the passing waves and conversion into electrical energy using Power Take Off system and an electric generator. Also in order to maximize the energy production, a control system aims to configure the characteristics of the system in order to keep the whole system in resonance. For the design and the development of the WEC a mathematical model has been constructed simulating the dynamic response of the hull. The software used to build the numerical model is Matlab Simulink, and all the hydrodynamic parameters (added mass, radiation damping etc.) have been obtained by Hydrodynamic Diffraction of ANSYS Aqwa. For the evaluation of the model, a comparison has been carried out between the mathematical tool and the Hydrodynamic Response of ANSYS Aqwa and a small experimental campaign as well. In the future, CFD analysis and an extensive experimental campaign will take place for the optimization of the project and the validation of the current mathematical model.

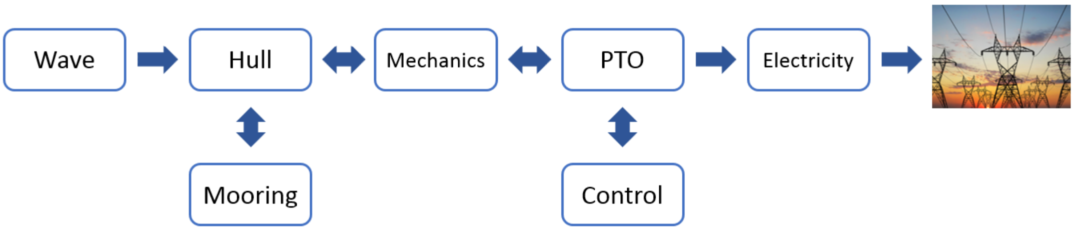

Figure 4.5. Technology concept.

4.3 State of the art

Intensive research and development on the field of the wave energy technology started in the 1970s, a fact that was stimulated from the emerging oil crisis of the specific era [24]. Since then, a lot of Wave Energy Converters have been proposed, and many of them belong to the category of the point absorbers.

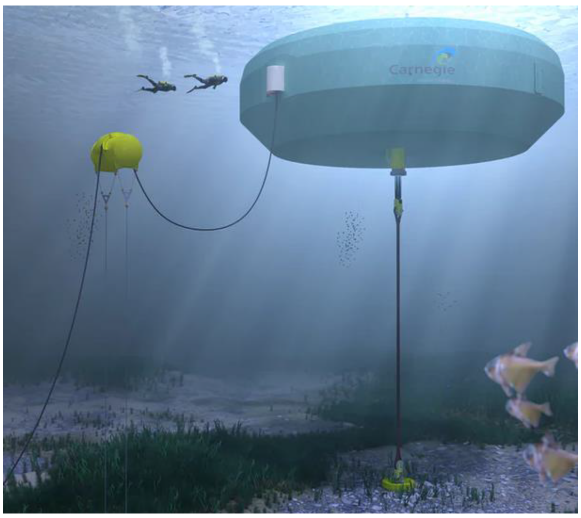

Figure 4.6. Schematic representation of Ceto 6 Wave Energy Converter [25][26].

CETO 6 is a fully submerged ocean technology developed by the Australian Carnegie Wave Energy Limited, a WEC which converts ocean swell into zero-emission renewable power and desalinated fresh water.[25]. Ceto 6 is one of the most developed and efficient point absorber technology with a capacity of 1MW per single unit. Some other technologies are: The point absorber developed by University of Uppsala [27], Powerbuoy developed by Ocean Power Technologies [28], Wavebob developed by Wavebob Ltd. [29] and many others.

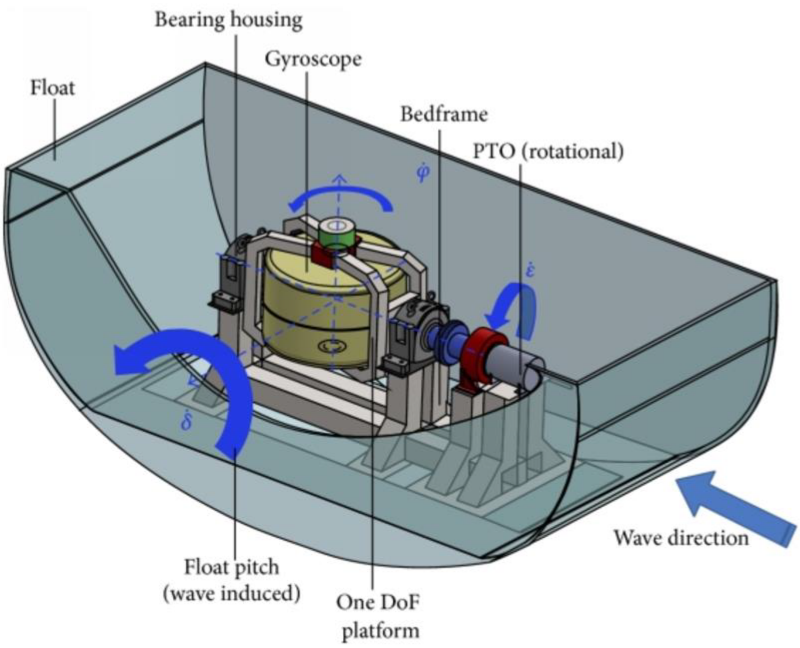

Figure 4.7. 3D model of ISWEC[30].

The main difference between the technologies mentioned above and the point absorber being developed at Politecnico Di Torino, is the fact that the targeting deployment site of the WEC is not the Ocean but the Mediterranean Sea, and specifically the island of Pantelleria. In the past another wave energy converter was deployed in Pantelleria Called ISWEC (Inertia Sea Wave Energy Converter) [30]. The energy potential of the Mediterranean Sea is lower in comparison to the Ocean, however, this doesn't mean that a sustainable wave energy technology cannot be used efficiently in closed seas. The most important factor is the design of the device is to take into account the targeting deployment site and select all the characteristic of the converter in order to sustainable in the specific sea environment.

4.4 Politecnico di Torino project

The previous part of the chapter treat generally about the point absorber technology and how it works.the goal of this thesis is design a real point absorber. After this first part, design a small scale device. Furthermore realize this one and test in laboratory for validate the model realized. And the last part is the data analysis. This project was done with two different geometries: spherical and cylindrical. The device in small scale realized at Politecnico di Torino is different from the other realized in the world.it is represented in the next figure.

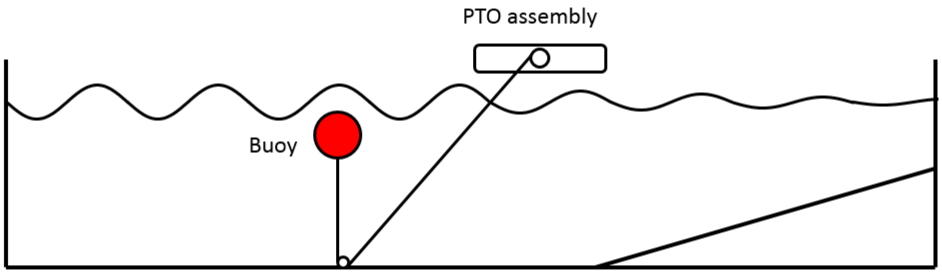

Figure 4.8. Point absorber system.

As it is possible observe in figure the system in composed by small-scale buoy, anchor and the PTO assembly. The following points have been followed to design this system:

- Find the site of application;
- select the project wave;
- Build the Budal diagram;
- Find the Volume of the device;
- Simulate the behavior of the device with a mathematical model;
- Experimental campaign with a small scale prototype;

After this design part the dimension of the real buoy was scaled for the small scale model.Subsequently in laboratory the model was realized and tested.

Chapter 5

Island of Pantelleria - Application

5.1 Selection of sea site

To deal with the problems related to pollution afflicting our planet it was decided to focus on renewable energy sources. A clean energy source capable of satisfying the entire planet 1-10 TW [31] is the marine one, ninth still very widespread because it is under development and needs to be optimized. The Politecnico di Torino has also decided to contribute to the development of a point absorber to be placed in the Mediterranean sea. This sea is not at the level of an energetically speaking ocean because it is closed and is considered of intermediate level.

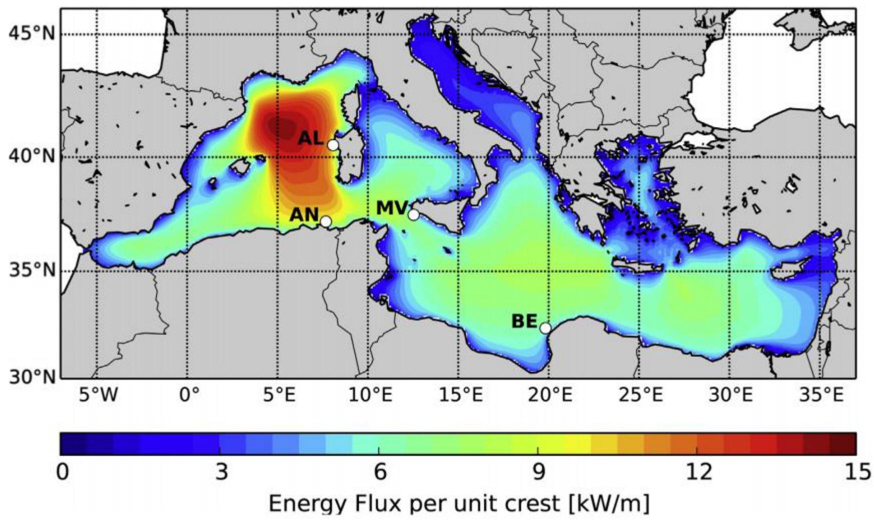

Figure 5.1. Mean energy flux per unit crest [Kw/m] for the 1979-2013 period [32].

The best area is located between the northern coast of Algeria, the Balearic Islands, Sardinia (10 kW / m along the coast). The average potential is around 6-7 Kw / m. The point absorber wave energy converter which is under development in the Politecnico di Torino was designed by following a specific path in order to produce a device, able to operate with the highest possible efficiency in Mediterranean Sea. The most important step for the development of a point absorber is to identify the site where it will be installed. The methodology of Falnes [23] was used to design the point absorber, which requires to find a regular wave of design. The features of this wave will be used in the next step to determine all the characteristic parameters of the device. To maximize the power produced it is necessary to make a WEC that work in resonance to obtain the best amplitude of oscillation. To reach this condition, optimal control is used to modify the rigidity and damping of the system.

5.2 Determining project wave

The project wave is identified according to the method of Falnes [23] which is composed by the following points:

- Find the site at sea and a value of power $JT(kW/m)$ that exceeded only a third of the year;
- Identify the most frequent waves characterized by a peak period or a peak of energy (T_p, T_e);
- Combine the two previous results J_T and $T_p(T_e)$ to find the height of the wave corresponding to a regular wave using the following formula:

$$J_T = \frac{\rho g^2 H^2 T}{32\pi}$$

The resulting regular wave of the specific procedure can be used as starting point for the development of the point absorber. After numerous evaluations it was decided to collocate the research site in the Mediterranean sea near the island of Pantelleria. Pantelleria is located in the Mediterranean Sea, among the Island of Sicily and Tunisia and Malta. In comparison to the places in Mediterranean Sea, a satisfying energy potential can be found available in the coast of Pantelleria. The average value of the sea depth is about 30 meters. In order to begin designing the point absorber some statistical data for what concerns the waves in the specific are are need.

Figure 5.2. Pantelleria Island [33].

As it is possible to see in the next figure there is a scatter of the wave occurrences. A big quantity of wave have H_s between 0.3 and 1.5 meters. the most frequent period instead is between 4.5 and 5.8 seconds.

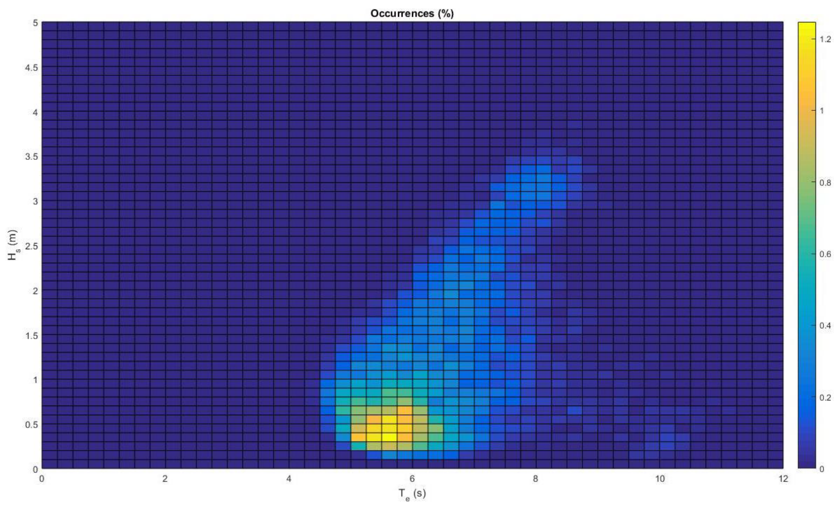

Figure 5.3. Occurrences of the various waves in Pantelleria.

However, the energy potential of the waves depends on both the height and period. In the next figure the power density of the waves is exposed.

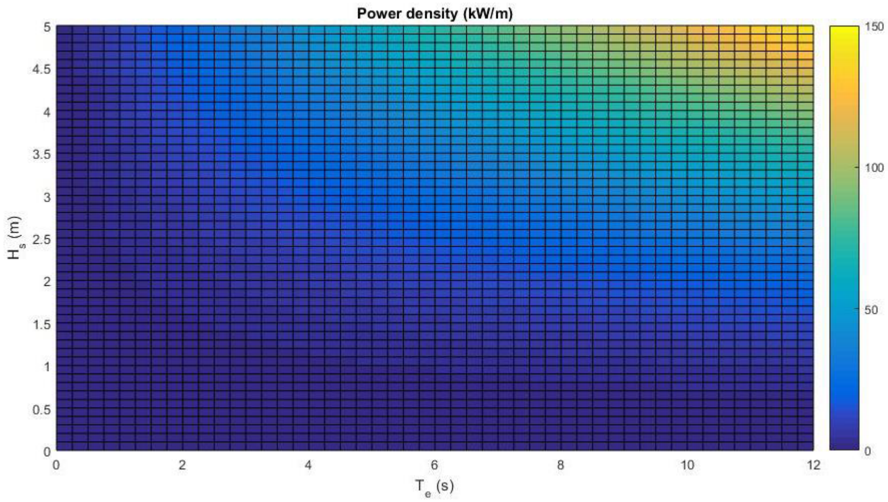

Figure 5.4. Power density of the waves.

Combining the previous two scatter the energy density of the waves in Pantelleria is obtained.

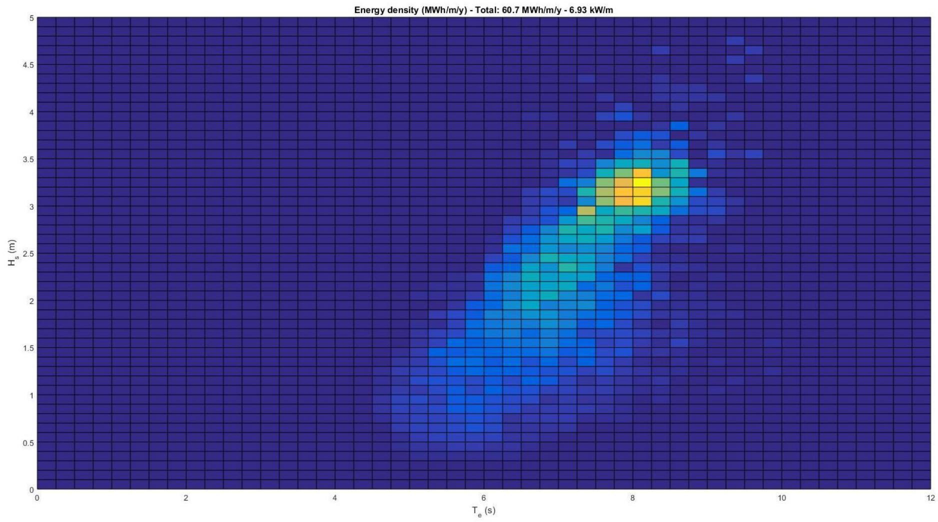

Figure 5.5. Energy Density in Pantelleria.

The selection of the principal wave of the design, is a tricky decision. Consequently, in order to calculate the main wave, the proposed method by Falnes is followed. The threshold $J_T(kW/m)$ is the power that is exceeded by only a third of the year. In the next figure it is possible to see the power threshold $J_T(kW/m)$ of the waves in Pantelleria :

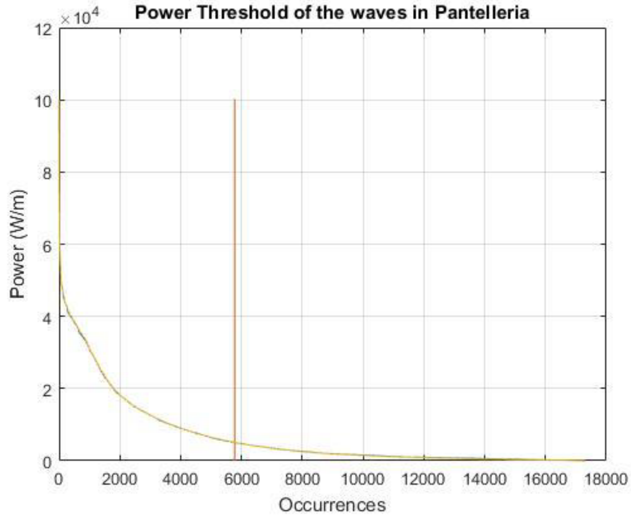

Figure 5.6. Power threshold of the waves in Pantelleria.

The figure above represents a cumulative diagram of power occurrences. At 5774 there is a third of the year. the power threshold is 5,048 W / m and is exceeded a third of the year. The Falnes [23] method aims to efficiently design a point absorber that works for at least a third of the year.

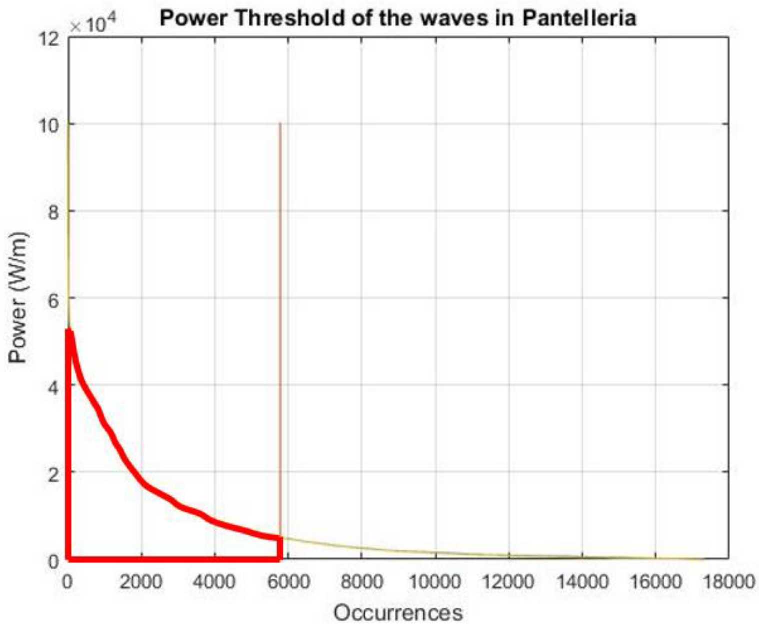

Figure 5.7. Selected waves.

In this way the proportion cost of the wave energy converter and power production will be optimized. Consequently, the point absorber of Politecnico di Torino will be designed in order to function at full capacity at the critical power threshold of $5.048 W/m$. The main disadvantage of the specific strategy is the fact the converter will not be able to receive the additional energy of the waves that have a higher potential of the calculated power threshold. However, lower nominal capacity means lower cost and in this way the wave energy converter will be enough cost effective. It is more favourable to design correctly one technological unit and deploy many of them in an array that develop a bigger one with higher capacity and cost. The crucial characteristic is to be economical with respect to itself, and result in the end the best possible LCOE (Levelized Cost Of Energy in $/Kw).
The next step is to define the peak period or, or the peak energy period of the most frequent waves (T_P *or* T_e). In order to implement the second step, only the waves that exceed the critical power threshold of $5.048 W/m$, in other words only the 5774 occurrences that result the higher power potential for one third of the year. With these waves, another diagram is created, a graph that the vertical axis represents the occurrences and the horizontal axis express the available power from the waves inW/m. The red circle represent the selected most repeated wave with power 1151.2 W/m.

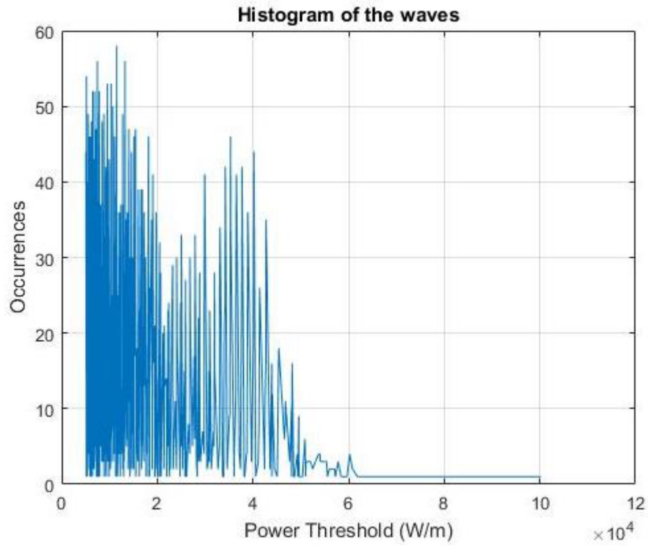

Figure 5.8. Histogram of the most repeated waves.

From the scatter the period of the most frequent wave is $T_P = 6.5 seconds$ and with the theory of Pierson-Moskowitz spectrum the resultant regular wave have $T = 0.858T_P = 5.577sec$. In the previous figure the red circle represent the most frequent waves with 1151.2 W/m The final step is to relate J_T and $T_P(T_e)$to the regular wave of period. In order to determine the wave height of the corresponding regular wave using the equation (14). The resulting regular wave of the project has $T = 5.57s$ and $H = 1m$.

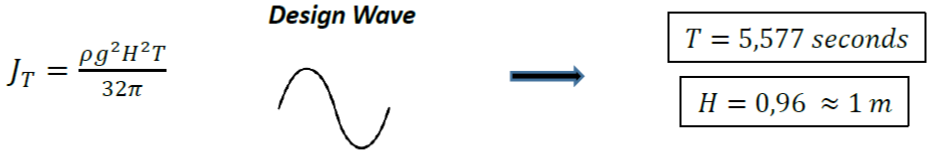

Figure 5.9. Result wave.

Chapter 6

Design of Point Absorber

This chapter explain how to design correctly a point absorber. First of all it is important to remember that any wave has a certain energy and all this amount of energy can't be converted completely into electric energy. As Falnes [12] claims, the conversion of wave energy remains a dream. In fact there are realistic limits to the energy failure for the optimal design of a WEC[23] [24] [34].
These limits are:

- P_a: High Frequency Limit
- P_b: Low Frequency limit

The following figure show the entire procedure for the design of a wave energy absorber. This action plan allows you to design a project starting from the place where you want to place the device. Subsequently from the specific characteristics of the site there will be a project wave that will be used to define the previously mentioned limits. The limits can be represented on a graph by which the size of the device will be determined. Subsequently it will be possible to proceed with the simulations with the mathematical model having all the data available. Finally optimization and experimental tests will be carried out.

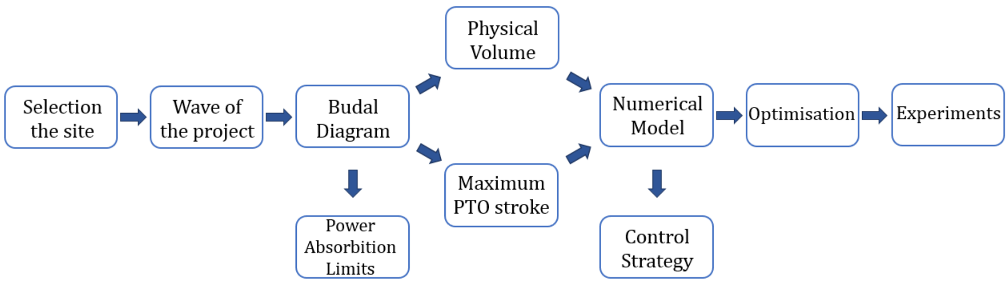

Figure 6.1. Different phase of design.

6.1 High Frequency Limit – Bubal limit

The hight frequencies limit assuming deep water conditions ($\omega^2 = \kappa g$) is:

$$P_a = \alpha \frac{J}{\kappa} = \alpha \frac{\rho g^3 A^2}{4\omega k} = \alpha \frac{\rho g^3 \left(\frac{H}{2}\right)^2}{4\omega \kappa} = \alpha c_\infty T^3 H^2$$

where:

$$J = \frac{\rho g^2 D(\kappa h) A^2}{4\omega}$$

this term is the wave energy transport per unit frontage of the interfacing wave. The coefficient α depend to the motion type and is showed in the next figure:

- $\alpha = 1$ for heave;
- $\alpha = 2$ for surge or pitch;
- $\alpha = 3$ when the hull moves in heave, surge and pitch;

Moreover ρ is the water density ω is the wave frequency, κ is the wave number, A is the wave amplitude, , and $D(kh)$ is the depth function which is equal to 1 for deep water assumption, also the coefficient c_∞ is equal to:

$$c_\infty = \frac{\rho \left(\frac{g}{\pi}\right)^3}{128}$$

As it is shown in the equation the high frequency limit is increased for big periods, and it depends a lot in the coefficient α. It is obvious that a device which vibrates in three degrees of freedom can absorbs three time more energy than a heaving buoy.

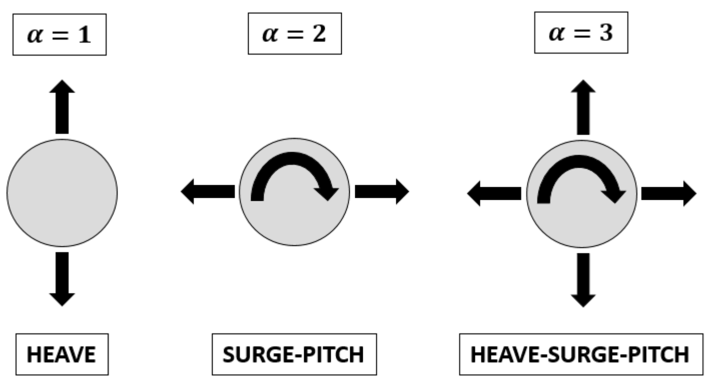

Figure 6.2. Coefficient α or different type of oscillation.

In conclusion, high frequency power absorption limit is the first of the existing two to consider during the designing of a point absorber. Coefficient α, period and height are the three important parameters which influence the efficiency and should be chosen correctly in order to reach the maximum productivity. In the following pages the second limit is presented. It is very important remember that this is the same for buoy with different geometric shape.

6.2 Low Frequency Limit – Bubal limit

The bound previously exposed includes optimum conditions and unreasonable movements without logic. Instead the low frequency limit P_B indicates the power of a point absorber in a realistic way which can be absorbed[23]. In order to define the philosophy and the content of the second power absorption bound, the quantity Swept Volume must be explained. Considering a heaving floating point absorber, Swept Volume V_s is called the volume between the maximum and the minimum displacement.

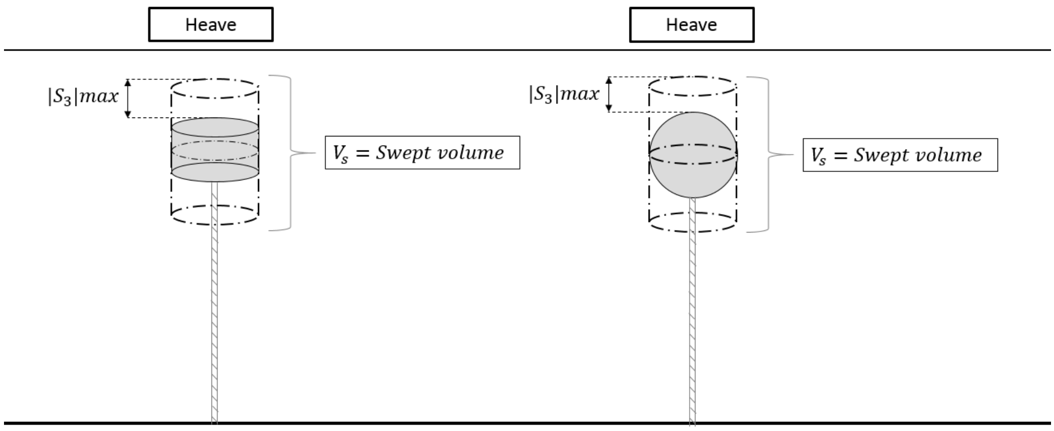

Figure 6.3. Swept Volume of Spherical and cylindrical Point Absorber.

In the occasion of the heaving spherical buoy with water plane area S_w and maximum oscillation amplitude of $|S_3|_{max}$, Swept Volume equals to the volume of cylinder:

$$V_s = S_w 2|S_3|_{max}$$

During the initial design of the submerged wave energy converter, it is essential to decide both the S_w, in other words the physical Volume V of the buoy and the $|S_3|max$, in other words the maximum allowed stroke of the PTO system. In order

to choose wisely these quantities, the targeting deployment site should be taken into account. In order to maximize the power absorption, the velocity u_3 of the converter is also a very crucial quantity and plays an important role.
The total absorbed power is [12]:

$$P_{absorbed} = P_{excitation} - P_{radiation}$$

With Excitation Power:

$$P_{excitation} = \frac{1}{2}|F_ej||u_j|cos(\gamma)$$

And Radiated Power:

$$P_{radiation} = \frac{1}{2}R_jj|u_j|^2$$

The optimal can be achieved only when the hull oscillates with optimal velocity $u_{3,opt}$ and zero phase difference between the incoming wave and the system's vibration($\gamma = 0$). In this case:

$$P_{absorbed} = P_{radiation} \rightarrow P_{radiation} = \frac{P_{excitation}}{2} \Rightarrow u_{opt} = \frac{|F_{ej}|}{2R_{jj}}$$

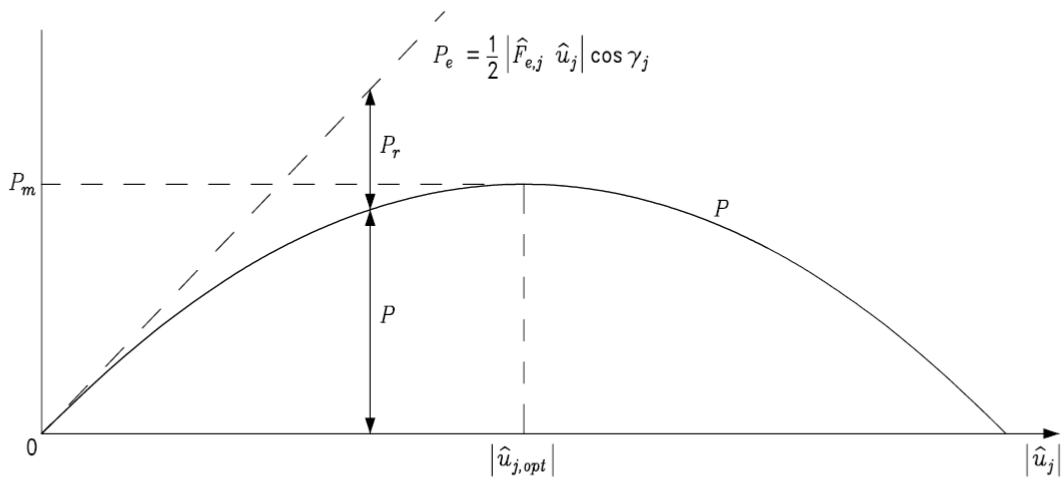

Figure 6.4. Power absorbed (solid curve) versus velocity amplitude. Radiated power P_r is the difference between excitation power P_e (dashed line) and absorbed power P [12].

In figure the property of a point absorber which claims that a solid body is able to absorb energy if it is capable to radiate waves and destroy the incoming ones, is obvious. The optimal point in the graph is located in the middle of the curve where $P_r = P$ and $u_3 = u_{3,opt}$. The excitation force on the body coming from the incident wave with amplitude A is :

$$|F_e j| < \rho g S_w A$$

and the heave velocity is

$$|u_3| < \frac{\omega V}{2S_w}$$

Combing the previous inequalities we obtain the inequality

$$\frac{P}{V} < \frac{\rho g \omega A}{4} = \frac{\pi \rho g A}{2T} = \frac{\pi \rho g H}{4T}$$

Finally, the low frequency limit for a floating heaving point absorber is:

$$P_b = \frac{c_0 V_s H}{T}$$

Where V_s is the maximum swept volume of the wave energy converter, H is the height of the incident wave, T is the period of the incident wave and $c_0 = 4\pi g \rho$. As it is shown, P_B are inversely proportional to the period. The previous equation is valid only for a floating one degree of freedom (heave) point absorber. Falnes [23] claimed that the bound P_b was not taken into account in the beginning of the wave energy era, at the mid-1970s, and as a result, no technology has ever reached in commercial stage. In the next pages the low frequency limit is presented for submerged hulls and for multi-DOF motions.

6.3 Submerged case

6.3.1 Submerged Sphere

One of the main differences between floating and submerged point absorbers for what concerns the limits of the power absorption is the fact that the submergence of the body influences the hydrodynamic parameters of the system such as excitation forces, radiation coefficients etc. Furthermore, when a WEC can absorb energy not only from heave, it means that the bounds will be higher. Consequently, the power gain limit for a submerged sphere is [35]:

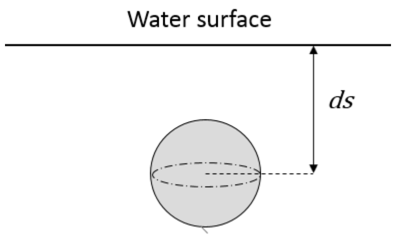

Figure 6.5. Dimensions for spherical PA.

$$P_b = 4\pi^3 \rho e^{kd_s} S_{3,max} \frac{VH}{T^3}$$

where:

- ρ: Density $[Kg/m^3]$;
- k: Wave number;
- d_s: Depth location $[m]$;
- V: Swept volume $[m^3]$;
- T: Wave Period $[s]$;
- H: Wave Height $[m]$;
- c_0: coefficient $c_0 = \frac{\pi}{4}\rho g$;

As it is obvious, in the equation, the term $e^{-\kappa s}$ express the influence of the submergence of the body in the sea. When the body oscillate with multiple degrees of freedom the low frequency limit P_b become the double because the swept volume increase as it is possible to see in the next figure.

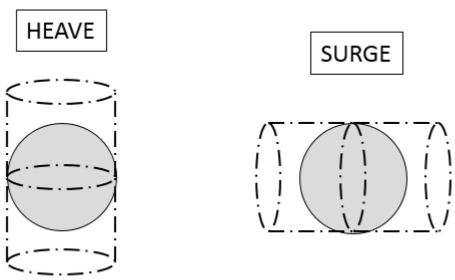

Figure 6.6. Swept volumes for heaving and surging point absorbers.

6.3.2 Submerged Cylinder

Moreover, the geometry plays also an important role in the construction of the equation. As a result, the for a submerged cylinder the equation changes to [35]

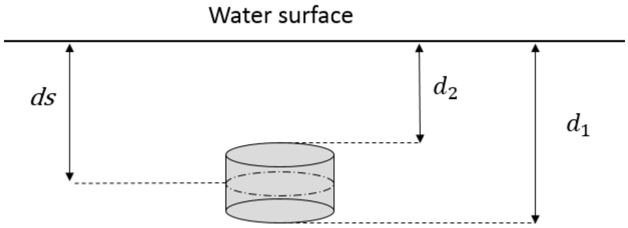

Figure 6.7. Dimensions for cylindrical PA.

$$P_b = \frac{\pi^2 a\rho a H}{T} S_{3,max} \left(\frac{2J_1(ka)}{kJ_0(ka)\cosh(kd_1)} - ae^{kd_2} \right)$$

Where:

- ρ: Density $[Kg/m^3]$;
- k: Wave number;
- d_s: Depth location of centre of mass $[m]$;
- d_1: Depth location of upper edge $[m]$;
- d_2: Depth location of lower edge $[m]$;
- $S_{3,max}$: Max amplitude vibration $[m]$;
- V: Swept volume $[m^3]$
- T: Wave Period $[s]$;
- J_0, J_1:Bessel functions;
- H: Wave Height $[m]$;
- c_0: coefficient $c_0 = \frac{\pi}{4}\rho g$;

When the body oscillate with multiple degrees of freedom the low frequency limit P_b become the double because the swept volume increase as the spherical case.

6.4 Budal diagram general

The existing two upper bounds P_a and P_b for the power P that can be received for a sinusoidal wave of height $H = 2|A|$ and period $T = a\pi\omega$, is a useful indicator for the potential of the point absorber. Using the two bound, it is possible to construct a very useful tool called Budal Diagram. The specific diagram shows exactly the limits of the power absorption in the frequency domain:

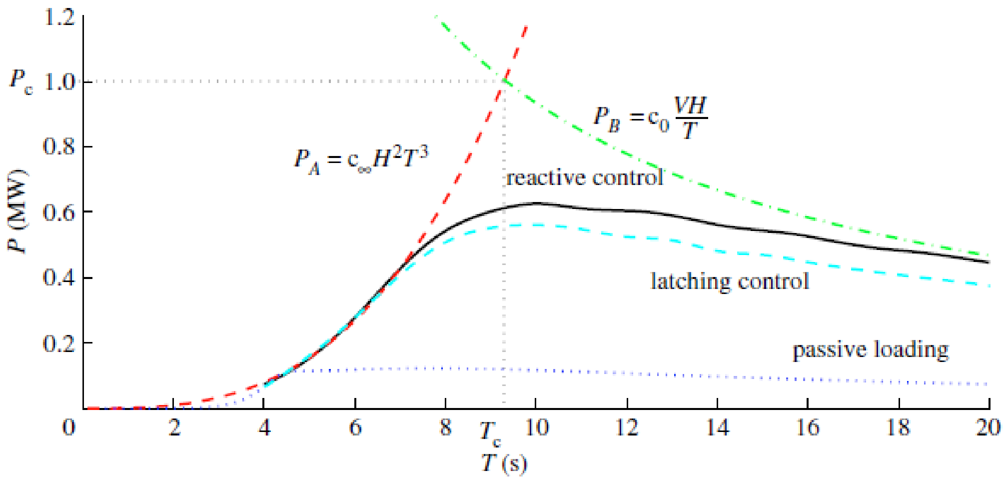

Figure 6.8. Budal Diagram for a floating point absorber [23].

In the figure, red dashed line represents the high frequency limit, and the green dashed line expresses the low frequency limit. In the area below these two lines the possible achievable values of power generation can be found. The continues black line represents the power absorbed from a WEC applying optimal control, the dashed blue line express latching control and the dotted line expresses passive control [23]. The specific diagram describes a the a situation with $H = 2.26m$ and physical volume of $V = 524m^3$. However, the important advantage of the Budal diagram is the fact that it can be used as a design tool in order to choose the optimal volume for a specific Sea state. For instance, in Figure 16, the intersection between the two upper bounds is found at 9.3 seconds which is also the frequency that results the highest absorption, 1 MW. In order to find the most suitable physical volume for a specific regular wave (Specific Height H and Period T), it is suggested to make Budal diagram having the intersection of the two lines in the desirable frequency and calculate the swept volume

$$P_a = P_b \Rightarrow V_S = \frac{C_\infty}{C_0} H T^4$$

According to Falnes, the swept volume cannot be bigger than the physical volume. We consider that $V_s = V$. It can be claimed that the resulting volume is the best choice for what concerns the power productivity of the point absorber in the selected regular wave. It must be cleared that the previous equation is only for a floating point absorber. The high frequency limit is the same for every kind of system (Attention only to choose the correct coefficient a), while the second one changes as it was demonstrated in the previous pages. In any case, the physical volume of the hull can be calculated, for every working principle, by choosing the correct P_B bound.

6.5 Budal Diagram of the Point Absorber

6.5.1 Submerged Sphere design process

The first step of the project is to identify the volume of the point absorber. To obtain the exact value to produce the maximum power it is necessary to set $P_a = P_b$. From this equation the optimal value of swept volume is obtained. To calculate the actual volume of the buoy, a coefficient is used to relate the two volumes. Falnes claims that the swept volume cannot be greater than the physical volume. For ecomonic reasons it would be better to have a smaller physical volume possible, at the same time in this situation it will not be easy to reach the project swept volume. This happen because a different phase could be obtained between the incident wave and the oscillating body, to solve this problem advanced control methods are used. In this way, chorus volumes can reach the same swept volume.

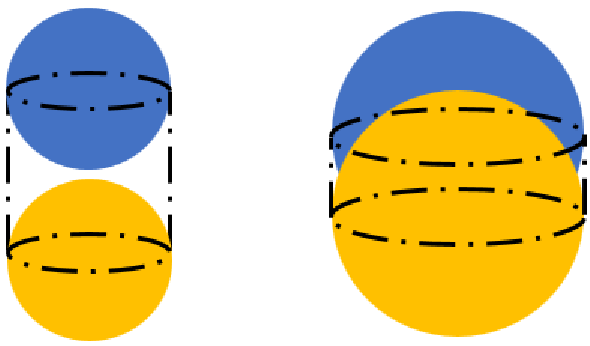

Figure 6.9. Different buoys reach the same swept volume with different amplitude of the oscillation. The blue spheres express the body in the maximum displacement, while the yellow one show the opposite.

The best scenario would be to select the smaller physical possible volume and achieve the targeted swept volume ($V = V_S$) with the optimal velocity. In this way the proportion between cost and power production would be ideal. Using the project wave and considering $V = V_S$, the Budal diagrams were designed for floating and submerged case.

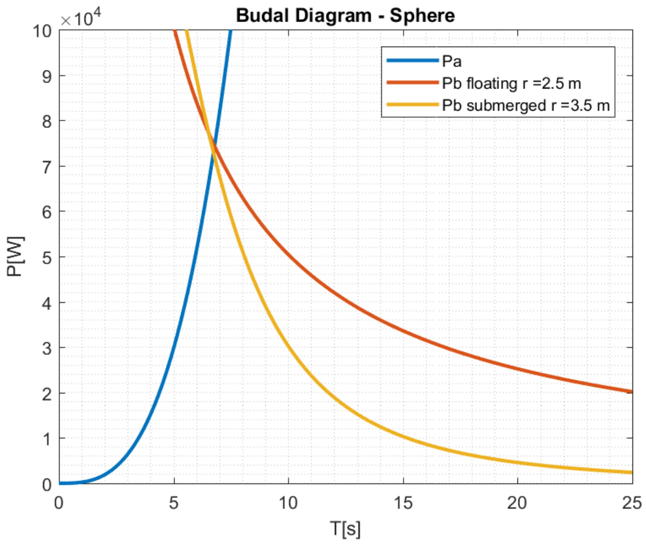

Figure 6.10. Budal diagram for floating and submerged spherical case.

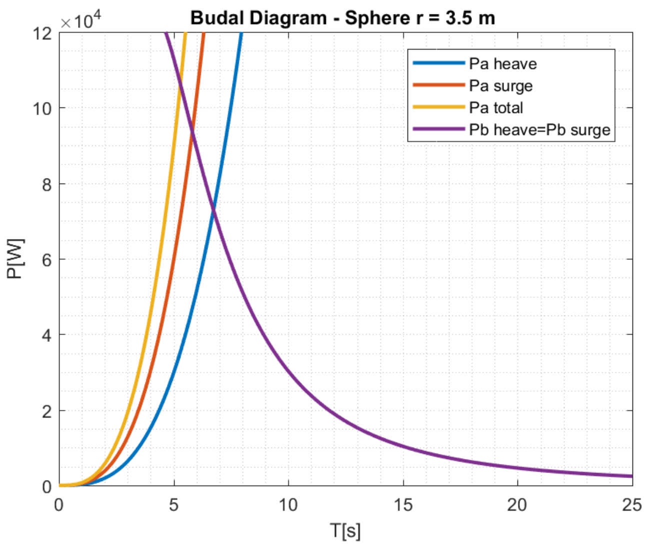

Figure 6.11. Power absorption bounds for heaving, surging spherical point absorbers.

As it is shown in figure 6.10 both floating and submerged hulls can give the same pick of the diagram. However, the floating one has radius of 2.5 m and the submerged one 3.5 m. The submerged sphere has $|S_3|_{max} = 1.75m$ and d_s (submergence) equal to 6.3 m. This is an advantage of the floating converter because can reach the same level of absorption with less cost. The previous analysis in figure 6.10 was only for a heaving point absorber. For a heaving/surging point absorber the limits of the submerged case are presented in the figure 6.11.

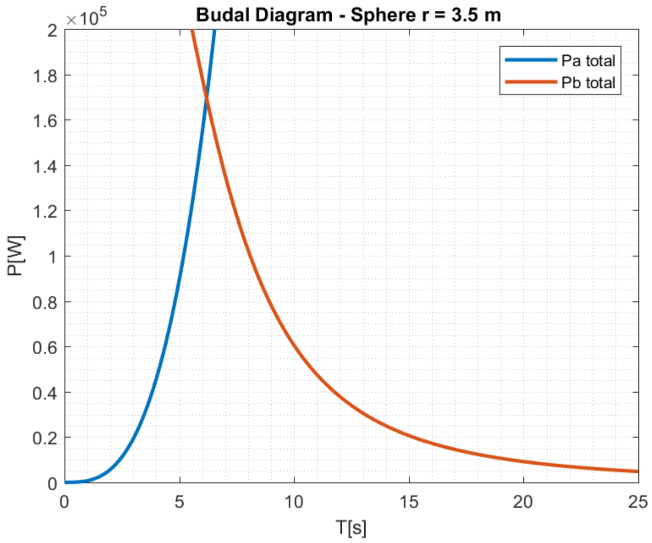

Figure 6.12. Total Budal diagram for a heaving and surging spherical point absorber.

Figure there is the total Budal Diagram for a multiple degree of freedom point absorber such as the one which is being developed at Politecnico di Torino. In this point it must be explained that in the submerged case there are some quantities which must be identified and given as an input before the calculation of the optimal swept volume. These quantities are: submergence of the COG of the hull ds, maximum displacement, or maximum stroke of the PTO (Power Take Off) $|S_3|_{max}$ and the relation between physical and swept volume. In order to test and evaluate different systems which have exactly the same power absorption bounds presented in Figure, but different technical characteristics all the variables must be expressed as a function of the Radius r of the sphere. Always the analysis starts from the 1DOF heaving absorber. The coefficient b is introduced which expresses the connection between the Swept Volume and the physical one:

$$V_s = b \cdot V \rightarrow 1 \leq b \leq 0.1$$

The maximum value of b is 1, when the swept volume is the same with the physical one. As it is shown in figure , the swept volume of a heaving point absorber is a cylinder:

$$V_s = 2\pi r^2 S_{3,max}$$

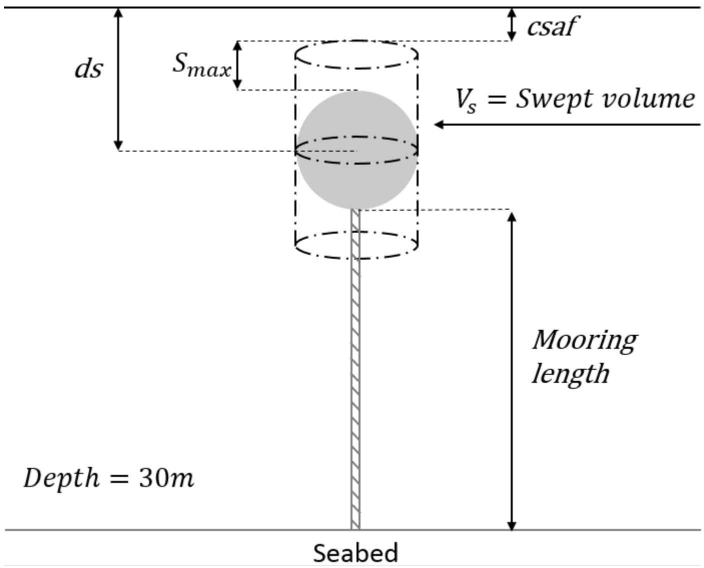

Figure 6.13. Technical Characteristics of PA.

Combining the previous equations:

$$V_s = 2\pi r^2 S_{3,max} = bV = b\frac{4}{3}\pi r^3$$

And finally :

$$S_{3,max} = b\frac{2}{3}r$$

A safety coefficient has been added to ensure that the buoy does not reach the surface defined as follows:

$$safety\ factor\ c \geq 1 \longrightarrow csaf = d_s - (r + S_{3,max})$$

where d_s the submergence of the centre of gravity of the submerged hull:

$$d_s = c\left(r + b\frac{2}{3}r\right)$$

It was demonstrated above that all the input variables necessary for the construction of the Budal Diagram depend on the radius of the spherical buoy. So as to determine different versions of the point absorber, different values of the coefficient b are inserted in the equation:

$$P_a = P_b$$

$$c_\infty T^3 H^2 = 4\pi^3 \rho e^{-kd_s} s_{3,max} \frac{VH}{T^3}$$

$$r^4 e^{-kr(c+cb\frac{2}{3})} = \left(\frac{18}{64}\right) \frac{c_\infty T^6 H}{b^2 \pi^4 \rho}$$

The inserted values of b are: 1, 0.9, 0.6, 0.5, 0.4, 0.,3. In this way six different systems are going to be determined which have the same peak of absorption (when $P_b = P_a$) and the swept volume is 100%, 90%, 60%, 50%, 40%, and 30% of the physical volume respectively to the values of the coefficient b. In order to calculate the characteristics, the equation is solved numerically in Matlab with the following code:

Matlab

```
syms a
eqn = a^4*exp((-k)*a*(c+c*b*4/6)) == (18/64)*(coo*T^6*H)/(b^2*pi^4*density);
sola = double(vpasolve(eqn,a,[0 10]))
```

Figure 6.14. Matlab code for the numerical solving of the equation for spherical point absorber.

6.5.2 Submerged Cylinder design process

As the spherical geometry different size boys reach the same swept volume with different amplitude of the oscillation. In the next figure the blue cylinder express the body in the maximum displacement, while the yellow one show the opposite.

Figure 6.15. Different cylindrical buoys with their swept volume.

The best scenario would be to select the smaller physical possible volume and achieve the targeted swept volume ($V = V_S$) with the optimal velocity. with this assumption is built the following Budal diagram.

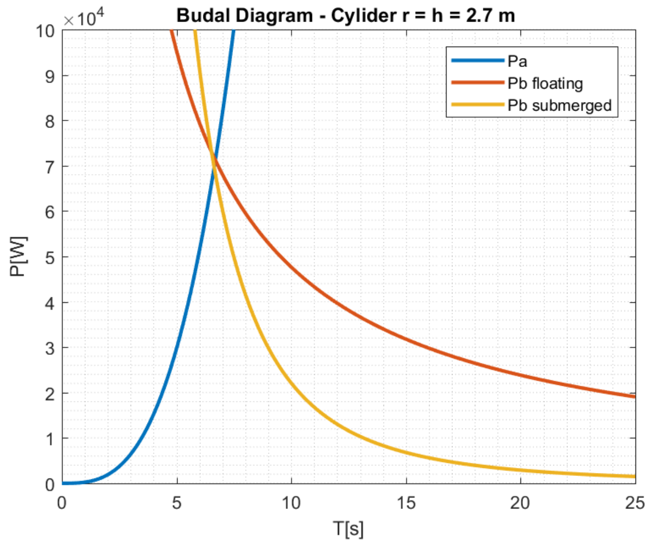

Figure 6.16. Budal diagram for floating and submerged cylindrical case.

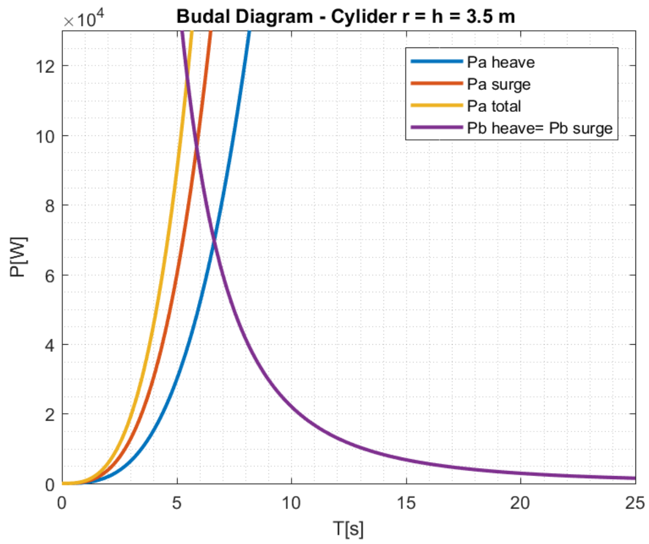

Figure 6.17. Budal diagram for a heaving and surging cylindrical point absorber.

As it is shown in figure 6.16 both floating and submerged hulls can give the same pick of the diagram. However, the floating one has radius of 2.7 m and the submerged one 3.5 m. The submerged cylinder has $|S_3|_{3,max} = 1.75m$ and d_s (submergence) equal to 3.6 m. This is an advantage of the floating converter because can reach the same level of absorption with less cost. The previous analysis in figure 6.16 was only for a heaving point absorber. For a heaving/surging point absorber the limits of the submerged case are presented in the figure 6.17.

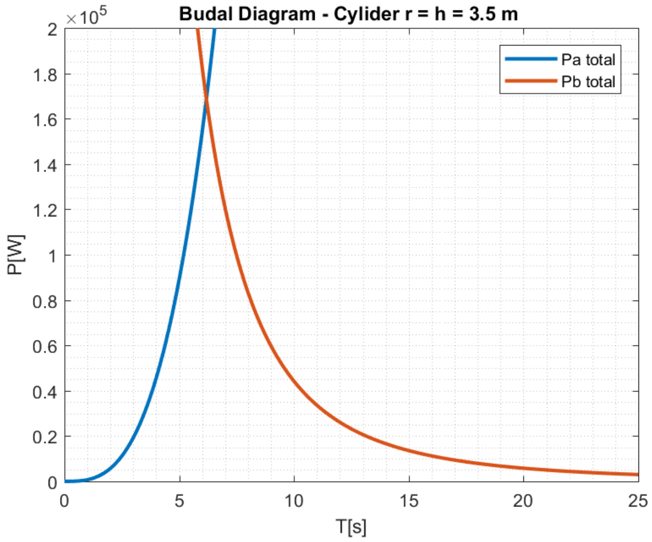

Figure 6.18. Total Budal diagram for a heaving and surging cylindrical point absorber.

In the figure there is the total Budal Diagram for a multiple degree of freedom point absorber. In this point it must be explained that in the submerged case there are some quantities which must be identified and given as an input before the calculation of the optimal swept volume. These quantities are: submergence of the COG of the hull ds, maximum displacement, or maximum stroke of the PTO (Power Take Off) $|S_3|_{max}$ and the relation between physical and swept volume. In order to test and evaluate different systems which have exactly the same power absorption bounds presented in figure, but different technical characteristics all the variables must be expressed as a function of the Radius r of the cylinder. Always the analysis starts from the 1DOF heaving absorber. The coefficient b is introduced which expresses the connection between the Swept Volume and the physical one:

$$V_s = b \cdot V \longrightarrow 1 \leq b \leq 0.1$$

The maximum value of b is 1, when the swept volume is the same with the physical one. As it is shown in the previous figure , the swept volume of a heaving point absorber is a cylinder:

$$V_s = 2\pi r^2 S_{3,max}$$

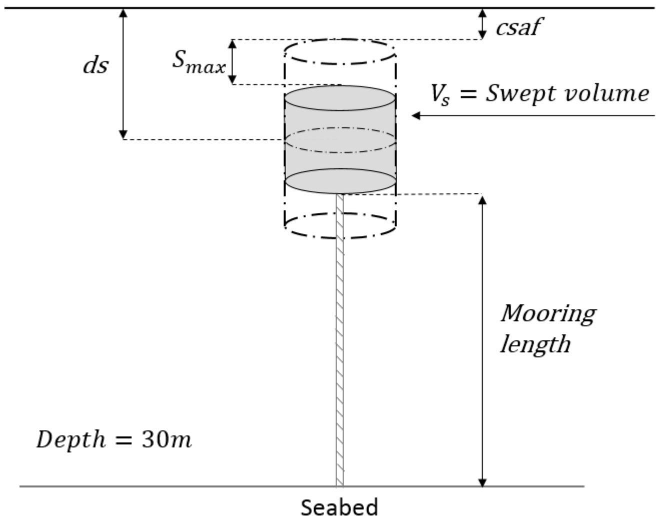

Figure 6.19. Technical Characteristics of cylindrical PA.

Combining the previous equations:

$$V_s = 2\pi r^2 S_{3,max} = b \cdot V = bh\pi r^2$$

And finally :

$$S_{3,max} = \frac{bh}{2}$$

A safety coefficient has been added to ensure that the buoy does not reach the surface defined as follows:

$$safety\ factor\ c \geq 1 \longrightarrow csaf = d_s - (h/2 + S_{3,max})$$

Where d_s the submergence of the centre of gravity of the submerged hull:

$$d_s = c\left(\frac{h}{2} + \frac{bh}{2}\right)$$

It was demonstrated above that all the input variables necessary for the construction of the Budal Diagram depend on the radius of the spherical buoy. So as to determine different versions of the point absorber, different values of the coefficient b are inserted in the equation:

$$P_a = P_b$$

$$c_\infty T^3 H^2 = \frac{\pi^2 a\rho g H}{T} s_{3,max} \left(\frac{2J_1(ka)}{kJ_0(ka)cosh(kd_1)} - ae^{-kd_2} \right)$$

where J_0 and J_1 are Bessel functions of the first kind of order 0 and 1 respectively, k is the real solution of the dispersion equation.

$$c_\infty T^3 H^2 = \frac{\pi^2 a\rho g H}{T} s_{3,max} \left(\frac{a}{cosh(kd_1) - ae^{-kd_2}} \right)$$

Where:

$$a = r$$

$$a = radius$$

$$h = ma$$

then:

$$d_s = c\left(\frac{h}{a} + \frac{bh}{2}\right) = c\left(\frac{ma}{2} + \frac{mab}{2}\right)$$

$$d_1 = d_s - \frac{h}{a} = c\left(\frac{mb}{2} + \frac{mab}{2}\right) - \frac{ma}{2}$$

$$d_2 = d_s + \frac{h}{a} = c\left(\frac{ma}{2} + \frac{mab}{2} + \frac{ma}{2}\right)$$

The inserted values of b are: 1, 0.9, 0.6, 0.5, 0.4, 0.,3. In this way six different systems are going to be determined which have the same peak of absorption (when $P_b = P_a$) and the swept volume is 100%, 90%, 60%, 50%, 40%, and 30% of the physical volume respectively to the values of the coefficient b. In order to calculate the characteristics, the equation is solved numerically in Matlab with the following code:

$$eqn = \ alpha * cinf * T^3 * H^2 =$$
$$= \ (pi\text{^}2 * rho * g * H * b * m(t) * a\text{^}3)/(2 * T) * ((1/(cosh(k * (c * (a * m(t)/2 + b * m(t) * a/2) - a * m(t)/2)))) - exp(-k * (c * (a * m(t)/2 + b * a * m(t)/2) + a * m(t)/2)))$$

Figure 6.20. Matlab code for the numerical solving of the previous equation (cylindrical case).

6.6 Result of design

6.6.1 Submerged Sphere result

The design previous exposed was done different time with several value of b. It was found six different hull different swept volumes, different physical volumes, different submergence of the centre of gravity and maximum PTO strokes but with the same power absorption limits. the aim is to find the best point absorber with the lower cost.

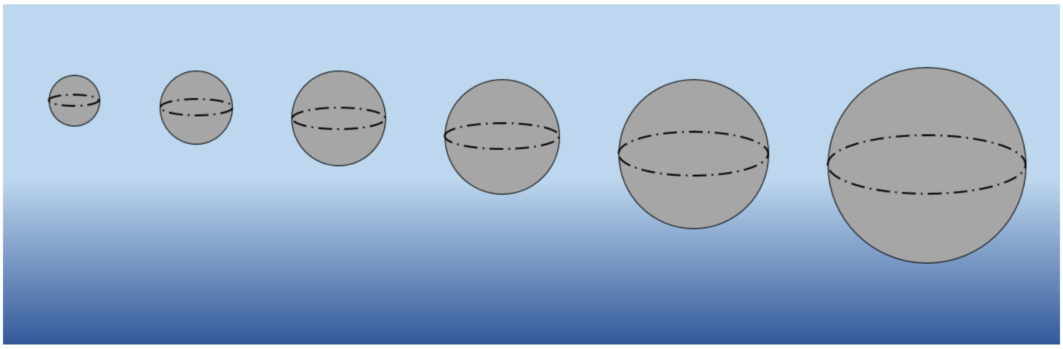

Figure 6.21. Schematic representation of the six different buoys.

Bigger volume, means bigger surface, and as a results bigger excitation forces from the wave. However, this does not mean that the small hull is not able to be competitive, it depends of the swept volume and the velocity oscillation. In the next figure are exposed the 6 hull found with the technical details [34]:

Symbol	Hull 1	Hull 2	Hull 3	Hull 4	Hull 5	Hull 6
$m(kg)$	56085	66088	126045	169851	246565	404449
$R(m)$	2.44	2.58	3.2	3.53	4	4.71
$V(m^3)$	60.8	71.64	136.63	184.12	267.13	438.44
$Vs(m^3)$	60.8	64.48	81.98	92.06	107	131.53
c	1.1	1.1	1.1	1.1	1.1	1.1
$csaf$	0.41	0.41	0.45	0.47	0.51	0.57
b	1	0.9	0.6	0.5	0.4	0.3
$ds(m)$	4.47	4.53	4.92	5.18	5.57	6.22
$s3max(m)$	1.63	1.55	1.28	1.18	1.07	0.94

Table 6.1. Technical details of the six different hulls [34].

In this point, it must be mentioned that every hull has a density of 90% of the water density. Consequently, as the volume of the buoy is increased from number 1 to number 6, also the mas is increased. As it is shown for body number 1 the coefficient b equals to 1 and as a result, physical volume and swept volume have the same value. For every system, the safety factor equals to 1.1 and the $Smax$ is inversely proportional with the physical volume. It is reminded that the whole analysis focuses in a submerged heaving point absorber. However, as it was demonstrated at [35], surge power bound is the same with heave bound and consequently the low frequency power limit becomes double for a submerged heaving surging point absorber. For the validation of the performance, a mathematical model built in Matlab Simulink is going to be used. It is a 3 DOF considering motions in heave, surge and pitch and uses optimal control [34]:

$$K = \omega^2(m + A(\omega))$$

and

$$B_{PTO} = B(\omega)$$

where B_{PTO} is the PTO damping and K the damping. The added mass is expressed by $A(\omega)$ and the radiation damping coefficient is $B(\omega)$. Both the hydrodynamic properties have been obtained by the software. In the next an analytical presentation of the numerical model is presented. In figure the Budal Diagram plus the performance calculated with the mathematical model of the six different devices are presented [34]:

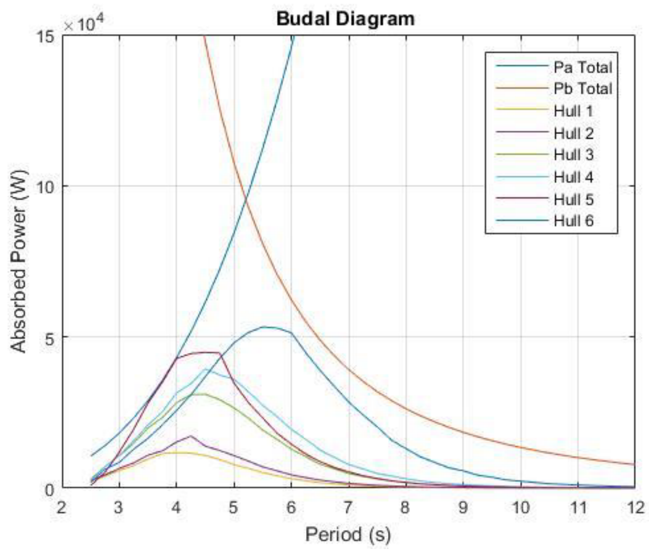

Figure 6.22. Hydrodynamic performances of the six different devices.

In this analysis, the technical characteristics, that have been derived by the process above, are going to be used for the design of a multiple degree of freedom device (heave, surge, pitch) considering that the optimization in of the system in heave is also optimization is surge power absorption. How it is possible to see the power production rise with the volume. Moreover, it must be mentioned that the objective is to design a submerged point absorber which will resonant at 5,5 second which is the period of the project wave which has been determined for the deployment site of Pantelleria. Hull 6 has the higher performance, however, it should not be forgotten that the target is to design a technological unit which will be feasible maximising the power output, not with respect to the available wave potential but to itself and resulting a competitive LCOE. As it was referred, an important factor for the cost of investment and maintenance of the wave energy converter is physical volume. Falnes [35] supported that ‘ small is beautiful ’ meaning that small technological units installed in an array could be the solution in the immaturity of the wave energy conversion. In figure 34 the power per volume performance of the six different devices is presented. Not surprisingly, hull 6 which has 438,44 m^3 volume and 404449.66 kg mass, has the poorest power per volume performance. Hull 2 reached the higher results, a hull which has 66087.79 kg mass, 71.64 m^3 physical volume, 64.48 m^3 swept volume, CoG submergence of 4.53 m, 1.55 m maximum displacement S_3max, volume relation factor equal to 0.9, radius equal to 2.58 m. Taking into account the targeted period is 5.5, it would be fruitful to move the pick of the productivity lightly to the right in the domain of frequency in order to catch the efficiently specific waves. Furthermore, hulls 1,3,4 have also pretty good performances.[34]

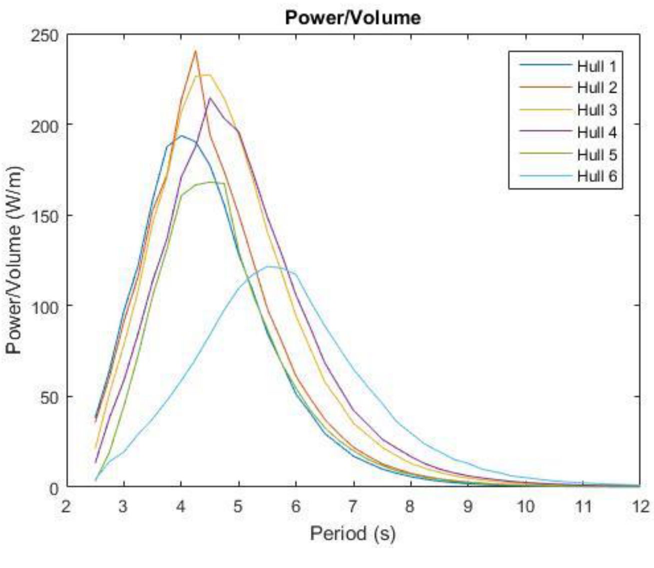

Figure 6.23. Power per volume performance.

In conclusion, as it was demonstrated, the power production is not the only indicator for the successful design of the wave energy converter. Volume is also another very important characteristic to take into account. For this reason, hull 2 is selected for the development of the point absorber of Politecnico di Torino. The next figure presents all the necessary technical details for the modelling of the device.

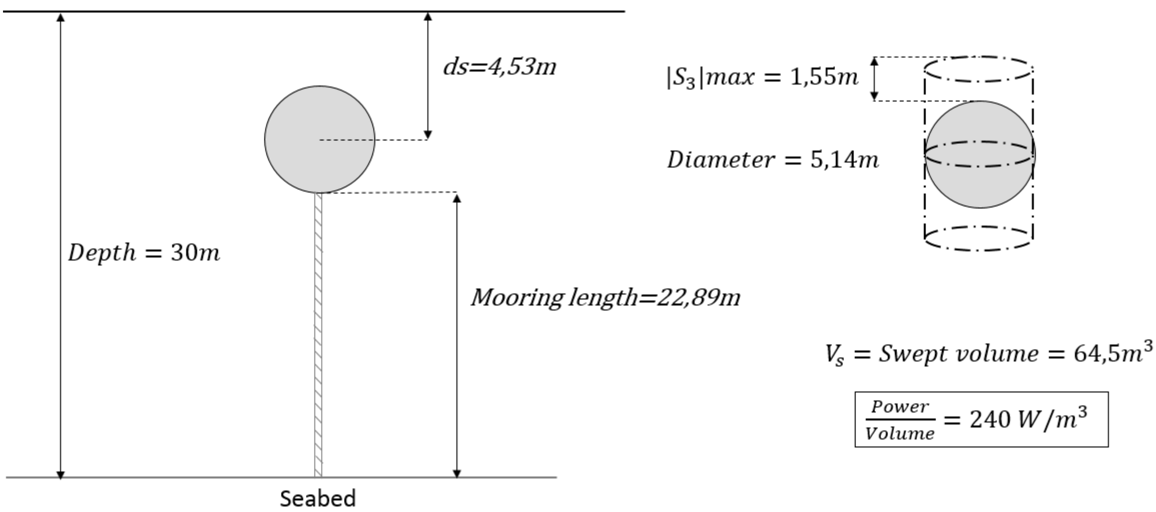

Figure 6.24. Selected characteristics for the development of the point absorber.

Chapter 7

Mathematical model

In this section the mathematical model of the point absorber is presented. The whole system dynamics depend on many different phenomena such as the interaction between the waves and the submerged hull, the submerged hull and the mooring system, the existing damping phenomena etc. The mathematical model is 3 degrees of freedom taking into account surge, heave and pitch motions of the device [34].

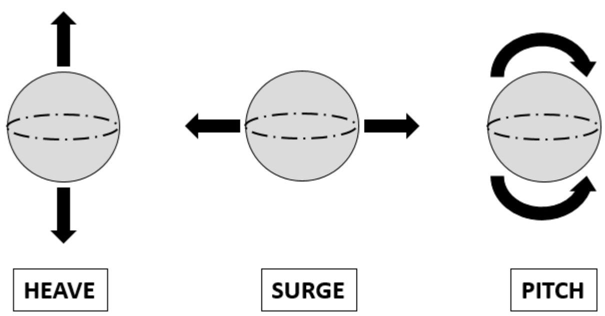

Figure 7.1. Degrees of freedom in the model.

The model created with Matlab Simulink calculates the dynamic response of the system subjected to the action of an incident wave. I can be created with the regular and irregular waves model but only the regular ones were used. Using an axisymmetric body will not matter the direction of incidence of the wave. In the model the Froude – Krylov forces, radiation damping and viscosity phenomena are evaluated. Not only was the motion of the buoy considered but also the remains of the system used by inserting a block relative to the PTO. Furthermore the Ansys Aqwa program was used for the determination of the hydrodynamic coefficients that depend on geometry, materials and orientation [34].

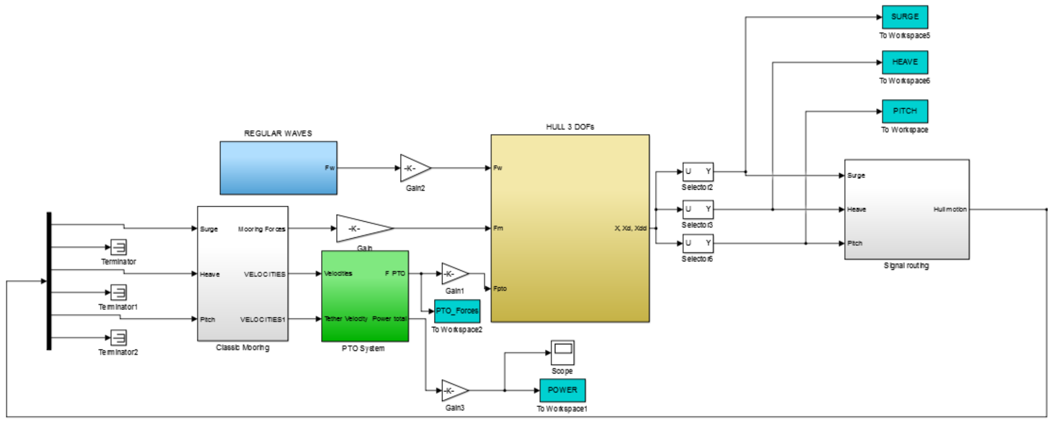

Figure 7.2. Mathematical Model at Matlab Simulink.

The time step used for the simulation of the model is 0.01 second and solver used ode45. The mathematical model that has been realized refers to the layout in the next figure, or to the system realized in the laboratory.

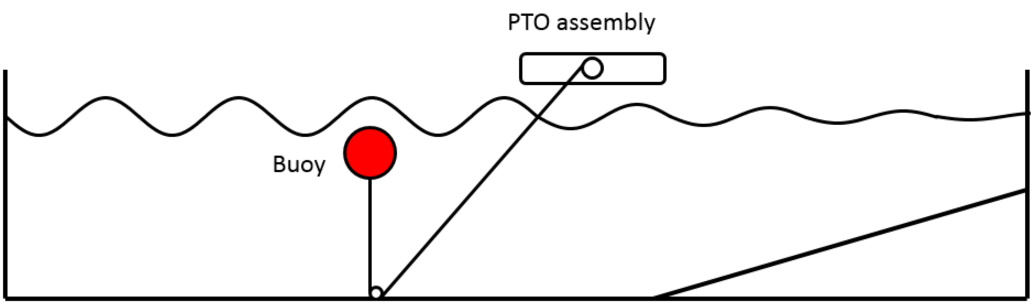

Figure 7.3. Simplified WEC model system.

As can be seen in the figure there is a submerged buoy which can be of different geometries, spherical or cylindrical. Furthermore, there is a pre-tensioned tether that connects the buoy with a pulley mounted on the electric PTO shaft. The motion of the buoy drives the pulley. In the following part there is the modelling of every part of the system.

7.1 Movement of a floating structure

For describe the motion of the buoy was used the the 'Cummins Equation'. This equation analyze the behavior of a general oscillating body under effect of an incident wave in the ocean. [36]

In frequency domain the equation written is [37]

$$[M + A(\omega)]\ddot{X} + B(\omega)\dot{X} + KX = F_W(j\omega)$$

Where:

- M = is the mass matrix of the oscillating body;
- $A(\omega)$ = the added mass matrix;
- $B(\omega)$ = the potential damping matrix;
- K = Hydrostatic stiffness (bouyancy forces). This term there isn't in the submerged case;
- $FW(j\omega)$ = Wave forces vector calculated with the following equation

  $$F_W(j\omega) = \frac{H}{2} f_w(j\omega)$$

  The term H/2 is the wave height and $fW(j\omega)$ is the wave amplitude Named Froude-Krylov coefficients.
- X is the position vector(6 DOF);

It is very important remember that this equation is based linear theory and is valid for small amplitude motions. The Cummin's equation in time domain becomes

$$[M + A(\infty)]\ddot{X} + \int h_r(t-\tau)\dot{X}d\tau + KX = F_w(t)$$

The last equation represents the added mass matrix evaluated for infinite oscillation frequency, while $hr(t-\tau)$ is the impulse response function of the radiation forces. The convolution term of equation models the radiation hydrodynamic problem in an ideal fluid, with a linear force pressure distribution. In particular, the impulse response functions of the radiation forces take into account the fluid memory effect and incorporates the energy of the radiated waves generated by the body motion. It is important to highlight that the time-domain equation can be involved with the introduction of non linear effects and it is very useful for the calculation of the hull response in irregular waves. On the other hand, the frequency domain equation involves linear quantities, steady state conditions conditions and it is valid only for monochromatic wave excitation forces. [34]

7.2 Newton equation

In this section are explained all the forces acting on a submerged point absorber. Subsequently is created the equation which describe the motion in the mathematical model.

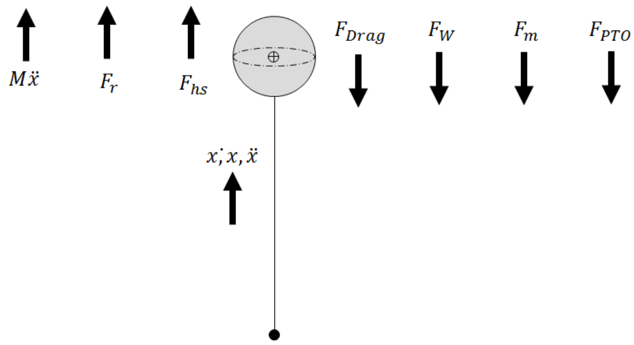

Figure 7.4. Free-body diagram of the point absorber.

In the model are used only regular wave under the liner wave theory. In this case is essential the assumption of incompressible fluid with zero viscous losses. The linear wave theory in not very useful in this case with higher order dynamics of buoy-fluid interaction. The dynamic equation for the buoy motion is (Falnes, 2007) [39]

$$M\ddot{x} + F_r + F_{hs} = F_w + F_{drag} + F_m + F_{PTO}$$

In this equation x is a displacement vector that represents all the type of motion. The motion in surge direction is expressed with the letter x and the heave direction with z, and pitch with θ. All this parameters refers to the centre of gravity (COG) of the buoy:

$$x = [\ x\ z\ \theta\ ]^T$$

M is the mass matrix that is composed by the buoy mass m and the inertia moment I along the diagonal axis, the other terms are zero.

$$M = \begin{bmatrix} m & 0 & 0 \\ 0 & m & 0 \\ 0 & 0 & I \end{bmatrix}$$

F_w, is called excitation force and is the force produced by the incident waves on an fixed body.
F_r, is the radiation force produced by an oscillating body creating waves on calm

sea.
F_{hs} is the hydrostatic fore that represents the restoring force due to buoyancy and can be calculated with the following equation:

$$F_{hs} = (\rho V_b - m)g$$

The term ρ is the density of the sea water, V_b is the total volume of the buoy, g is the gravitational acceleration. This force is always in the same direct and maintains a tension force on the tether.
F_{drag} is the drag force is a non linear viscous damping. This force act opposite to the relative motion of the buoy to the surrounding sea water. The value of this term depend to the geometrical shape of the body. Normally is very difficult calculate this term but in the case of submerged sphere and cylinder is simple. The drag force can be calculated by the formula:

$$F_{drag}(sphere) = \begin{bmatrix} -\frac{1}{2}\rho C_{Dx} A_x |\dot{x}|\dot{x} \\ -\frac{1}{2}\rho C_{Dz} A_z |\dot{z}|\dot{z} \\ -\frac{1}{2}\rho C_{D\theta} A_\theta |\dot{\theta}|\dot{\theta} \end{bmatrix}$$

$$F_{drag}(cylinder) = \begin{bmatrix} -\frac{1}{2}\rho C_{Dx} A_x |\dot{x}|\dot{x} \\ -\frac{1}{2}\rho C_{Dz} A_z |\dot{z}|\dot{z} \\ -\frac{1}{2}\rho C_{D\theta} D^5 |\dot{\theta}|\dot{\theta} \end{bmatrix}$$

	Sphere	Cylinder
C_{Dx}	0.42	0.7
C_{Dz}	0.42	1.22
$C_{D\theta}$	0.42	0.22

Table 7.1. Table of drag coefficient (cylinder ceto)[40].

How it is possible see the drag force is a vector and contain the terms for the surge and heave direction. The term ρ is the density of the water, C_D represents the dimensionless drag coefficient in a specific direction, A_x and A_z are the cross-section areas of the buoy along surge and heave axes, $\dot{x}$ and $\dot{z}$ are the velocity of the full in surge and heave respectively. [38]
F_m is the mooring force, it is a vector that contain all the component in different direction.

$$F_m = \begin{bmatrix} Force\ x \\ Force\ z \\ Moment \end{bmatrix}$$

F_{PTO} is the PTO force absorbed from the PTO

$$F_{PTO} = \begin{bmatrix} PTOForce\ x \\ PTOForce\ z \\ PTOMoment \end{bmatrix}$$

The analysis of the system is conduced in the time domain with the Cummins equation that is used for studies WECs response to sea waves. The equation of motion become:

$$(M + A_{\infty})\ddot{x}(t) + \int B(t-\tau)\dot{x}(t)d\tau + F_{hs} = F_w + F_{drag} + F_m + F_{PTO}$$

The variable B is the radiation impulse response function matrix, and A_{∞} is the added mass matrix. These variables can be computed using the commercial program ANSYS Aqwa, where the geometry is created with the dimension found with the Budal process.

7.3 Mooring

The mooring system of the submerged point absorber is modelled as a linear mooring with a constant linear stiffness. The block in Matlab Simulink receives as an input the motion of the hull and produces as an output the generated mooring forces on the hull.

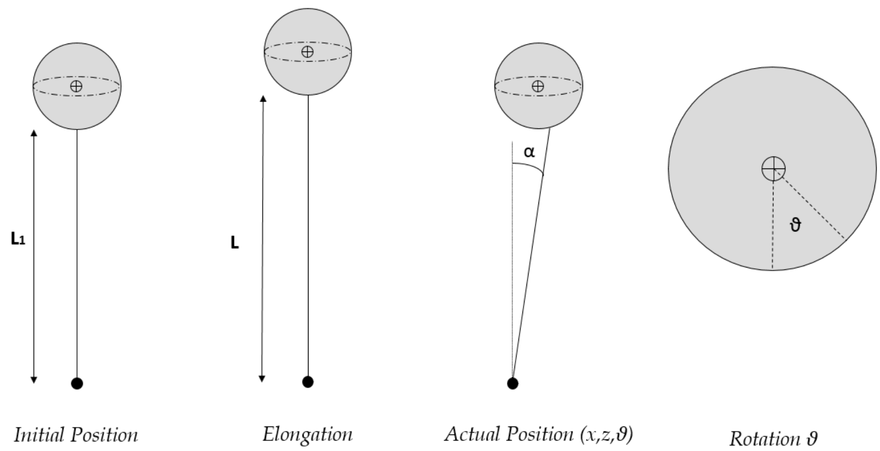

Figure 7.5. Modelling of motion of the point absorber [34].

In figure is exposed a 2D mooring model of the submerged point absorber. As it is possible to see in the figure there are big difference between the initial position $O(x, z, \theta)$ end the actual position when the buoy are moving around his COG. It is very important remember that the vector of the buoy motion is the input of he model expressed in the system reference O. In the following part are exposed the equation used for calculate the parameter of the mooring:[34]

$$X = x + (Rsin\theta)$$

$$Z = L_1 + z + R(1 - cos\theta)$$

The actual length of the mooring line is calculated

$$Actual\ length : L = \sqrt{X^2 + Z^2}$$

Consequently, the elongation is

$$\triangle L = L - L_1$$

And the tension

$$T = K \cdot \triangle L$$

Where K is the linear stiffness of the mooring. The tether is always in tension thanks to the buoyant force.

One other important parameter for the analysis is the angle α presented in the previous figure. The angle α represent the interaction between the mooring and the buoy.

$$sin\alpha = \frac{X}{L}$$

and

$$cos\alpha = \frac{Z}{L}$$

These trigonometric variable are used in order to calculate the final mooring forces:

$$Forcex = Tension \cdot sin\alpha$$

$$Forcez = Tension \cdot cos\alpha$$

$$Moment : Forcex \cdot R \cdot cos\alpha + Forcez \cdot R \cdot sin\alpha$$

These forces are the output of the mooring block and the input in the main body of the model.

$$F_m = T \cdot \begin{bmatrix} sin\alpha \\ cos\alpha \\ 0 \end{bmatrix} = \begin{bmatrix} Forcex \\ Forcez \\ Moment \end{bmatrix}$$

7.4 PTO

In this section there is the modelling of the power take off system. The input of this block are the elongation velocity of the tether and the linear damping of the system. [34]

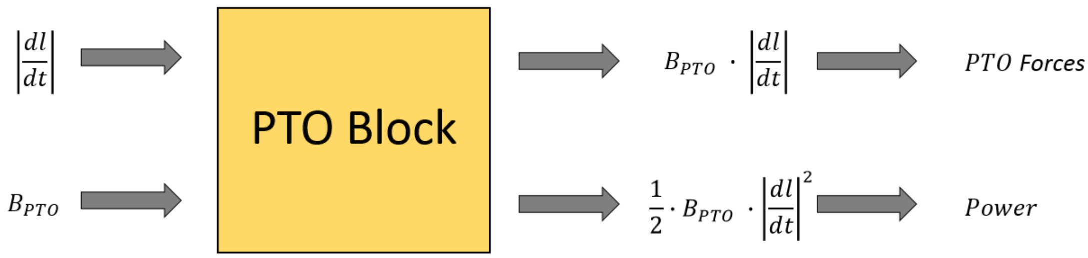

Figure 7.6. Strategy of the Power Take Off modelling [34].

More precisely the equation used are:

$$PTOForce\ x = Damping \cdot velocity \cdot sin\alpha$$

$$PTOForce\ z = Damping \cdot velocity \cdot cos\alpha$$

$$PTOMoment = PTOForce\ x \cdot R \cdot cos\alpha + PTOForce\ z \cdot R \cdot sin\alpha$$

In order to calculate the power, the formula is used:

$$Power = \frac{1}{2} \cdot B_{PTO} \cdot |\dot{x}|^2$$

$$F_{PTO} = \begin{bmatrix} PTO\ Force\ x \\ PTO\ Force\ z \\ PTO\ Moment \end{bmatrix}$$

Chapter 8

Experimental setup

In January 2019, the second experimental campaign of the submerged point absorber took place at Politecnico di Torino. The objective of the experiments was to make an initially validation of the mathematical model and gain some experience and sensibility of the dynamics of the whole system. From the previous design of the point absorption we obtain the real scale buoy with the diameter of 5.14 m. After the scaling process the small scale model have the diameter of 16 cm. To have a direct comparison with a different geometry it was decided to create two cylinders with the same volume but with different geometric characteristics. The difference between the two is the ratio $m = r/H$.

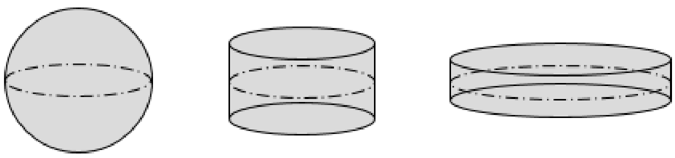

Figure 8.1. Prototypes used.

	Sphere	Cylinder	Cylinder
$m = r/H$		0.6	1
$Diameter\ [m]$	0.16	0.202	0.162
$Height\ [m]$		0.067	0.104
$Volume\ [m^3]$	0.0021	0.0021	0.021

Table 8.1. Theorical dimension of the small scale prototype.

Due to the small size of the wave test flume, a small scale device of a realistic point absorber was constructed. The full scale device has diameter of 5.14 meters, 66088 Kg mass and the objective was to simulate a sea of 45 meters' depth.

Type	Real Scale Pantelleria	Small scale (1:32)
Diameter $[m]$	5.16	0.1612
Radius $[m]$	2.58	0.0806
Volume $[m^3]$	71.64	0.021
Mass $[Kg]$	66088	2.01
Density $Kg/m^3]$	922	922
Sea Depth $[m]$	22.4	0.7
Wave type	regular	regular
Smallest Period $[s]$	3.5	0.6187
Highest Period $[s]$	9	1.5910

Table 8.2. Theorical dimension of the real and small scale Spherical prototype.

Due to the small budget of the experimental campaign the need of some quick results and experience with the technological concept, the prototype was constructed in a simple way. For what concerns the scaling process, the Froude method was used. The objective was to construct a sphere which has a geometry one third of the width of the flume. The reason of the specific geometrical choice is the reflection phenomenon which takes place in the walls of the tank. Consequently, if the body is not enough small respect to the flume, there is a big danger that the body will not encounter the waves that were sent. In the following table, all the information necessary for the Froude scaling is presented. The Froude number is $\lambda = 32$. [38]

Characteristic	Dimension-Froude	Real Number
Length	λ	32
Area	λ^2	1024
Time	$\sqrt{\lambda}$	5.6568
Velocity	$\sqrt{\lambda}$	5.6568
Acceleration	-	-
Volume flow	$\lambda^{\frac{5}{2}}$	5792.61
Mass	λ^3	32768
Force	λ^3	32768
Pressure	λ	32
Power	$\lambda^{\frac{7}{2}}$	185363.8

Table 8.3. Froude scaling parameter.

8.1 Preparation of the prototypes

8.1.1 Sphere prototype

This chapter discusses the implementation of models used for laboratory tests. For the ball has been purchased a plastic ball used in furniture of 16 cm of diameter as that present in the figure. Subsequently the two parts were sealed with two-component glue, and a 3 mm hole was made with the drill to fill it. Moreover the surface has been prepared for the painting using the paper glass as in figure 6.3 on the right.

Figure 8.2. Right: The starting plastic sphere; Left: The sphere ready for to be painted.

After this step the sphere was painted red to be more easily recognized by the tracking motion software. Finally it has been filled with the oil which has a density of 0.9 Kg/l, perfect characteristic to obtain the desired weight.The hole was plugged using simply two-component glue being very small.

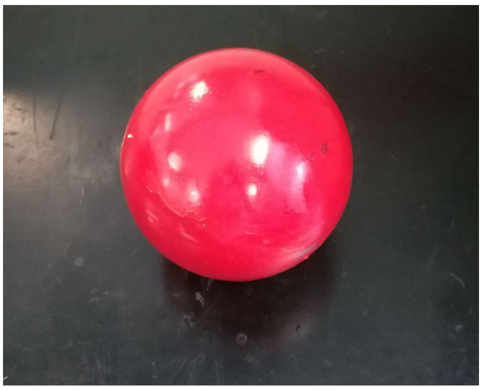

Figure 8.3. The final sphere prototype.

The sphere purchased proved to be perfect because it already had a small hole that was used to secure the anchor rope. The final sphere prototype have the following features:

- Weight 1,9776 Kg
- Diameter 0.16 m

8.1.2 Cylinder prototype

As for the cylinders, for the realization of the prototype we started from the PVC tubes of external diameter 20.2 cm and 16.2 cm, which have been cut to the correct size to obtain the desired volume of 6.3 cm and 8.8 cm respectively.

Figure 8.4. Right:the plastic plug Left: the pvc pipe.

As for the smaller one the caps have been applied. (one of the two is perforated) suitable and sealed with two-component glue. One of the two holes will be used to obtain a support to secure the rope of the mooring. To obtain the desired weight, a cast iron weight placed in the centre of mass was used. Instead for the bigger one the caps were not available so they were made from a wooden panel and fixed with two-component glue and screws.

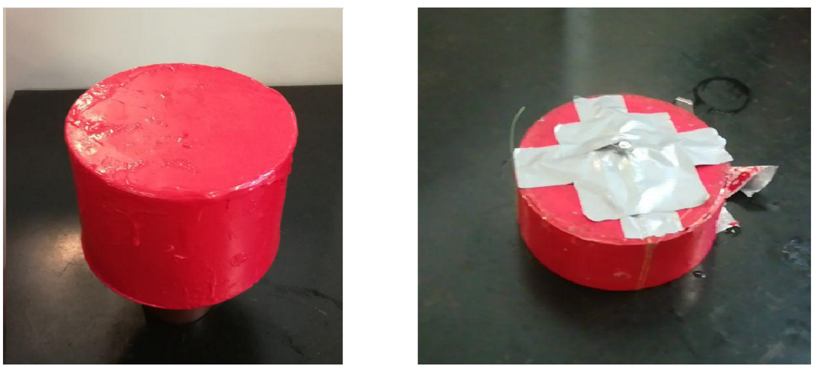

Figure 8.5. Left the 16 cm prototype; Right: the 20 cm prototype.

First of all, the wooden parts have been sealed and sealed using silicone and two-component glue. This time the caps are both perforated, One of the two holes will be used to obtain a support to secure the rope of the mooring and the other to fill the prototype with oil. The prototype with diameter of 16cm is called cylinder1 the other prototype with diameter of 20cm is called cylinder2. The final cylinder1 prototype have the following features:

- Weight 2,014 Kg
- Diameter: 0,162 m
- Height: 0,103 m

The final cylinder2 prototype have the following features:

- Weight 1,854 Kg
- Diameter: 0,202 m
- Height: 0,0668 m

We will call the prototype 20 cm tied in low cylinder2-1 and the one with an intermediate fixing cylinder2-2. These two prototypes are the same only changes the mood in which they were ditched.

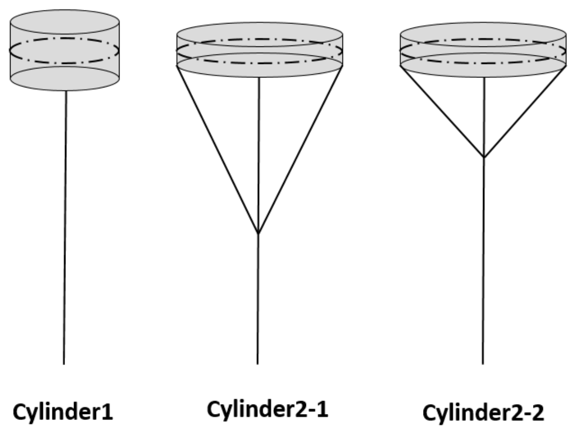

Figure 8.6. All the cylinder used with the name used.

8.2 Preparation of PTO and acquisition system

8.2.1 PTO assembly

In this chapter we talk about how the pto system including data acquisition system has been reactivated. The starting structure is that of a small scale model of the ISWEC to which the gyroscope has been removed because our prototype will work in a different way.

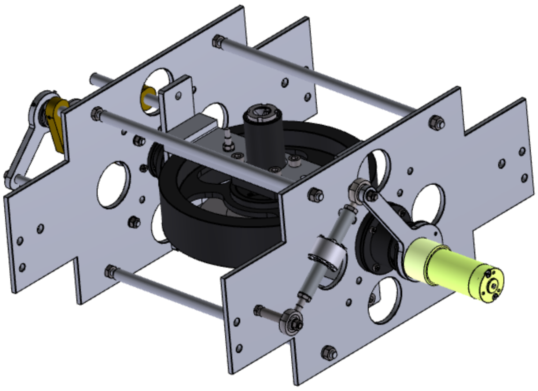

Figure 8.7. Small scale 3D CAD prototype of ISWEC.

The aim was to create a system to absorb power from the movement of the point absorber tied to a rope. Therefore the best solution has been studied and realized on Solidworks that consists in the substitution of the gyroscope with a tree on which a pulley will be mounted.

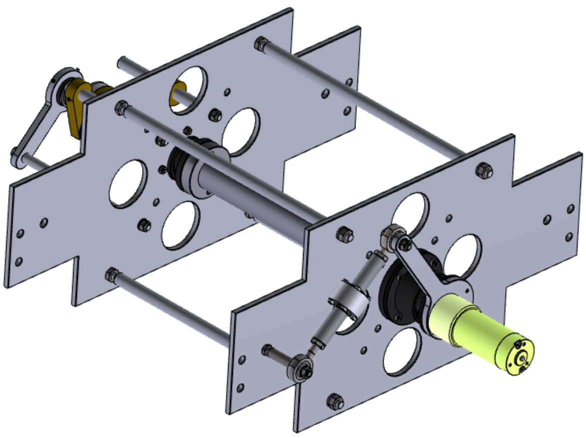

Figure 8.8. CAD 3D of the PTO assembly.

In order to realize the prototype presented in the previous figure the tree with the following measures has been realized, so as to enter the previous structure and have the least possible inertia. In addition, there are two central 4 mm holes used to clamp the pulley on it.

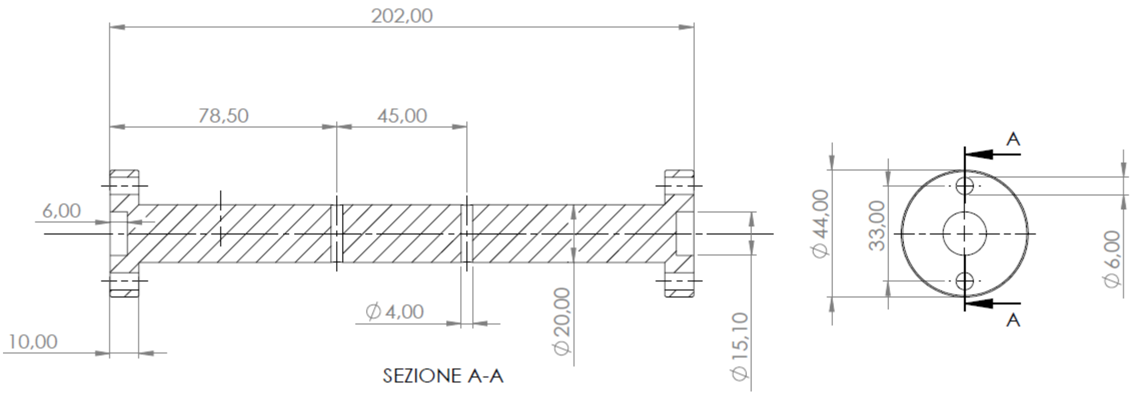

Figure 8.9. Draws of the shaft with dimension.

The spindle was made of aluminum so as to have a minor put possible. This component was made from a 50 mm diameter turning bar and finally the column drill was used. In the figure below you can see the realization of the tree and a 3D drawing in the design environment.

Figure 8.10. 3D CAD of the shaft.

The next component to be realized was the pulley to be set on the tree. In the figure below are shown the dimensions and as you can see the pulley has been divided into two parts for ease of assembly and realization.

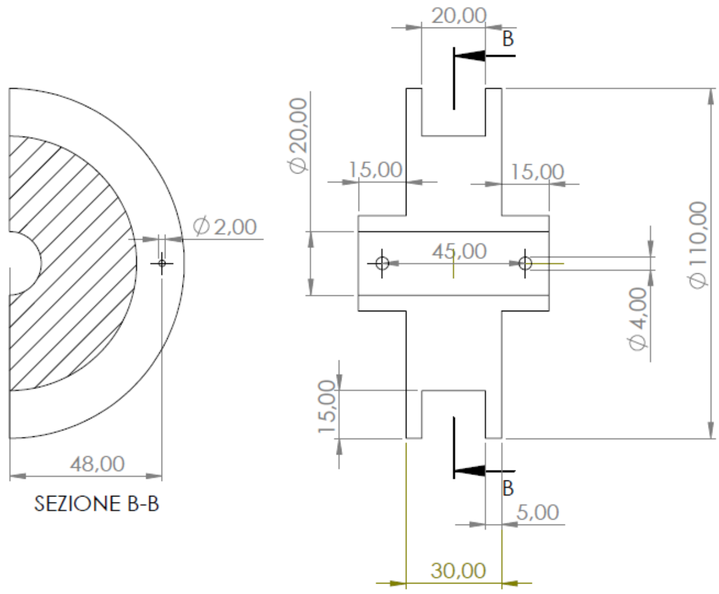

Figure 8.11. Draws of the pulley with dimension.

In order to reduce the inertia of the system, the pulley was made with a 3D printer, Because using such a small model you will have considerable friction and any detail is important to ensure data acquisition during laboratory tests. As you can see in the figure there is a lateral hole of 2 mm diameter that will be used to fix the rope of the mooring.

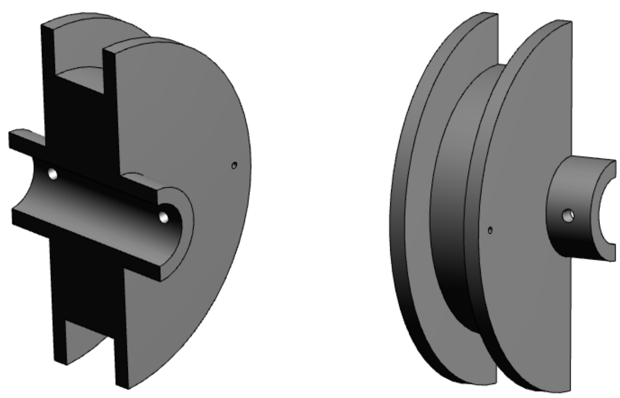

Figure 8.12. 3D CAD of the pulley.

There are also two holes 4 mm complementary to those on the shaft. Subsequently the pulley was taped onto the tree as you can see in the next figure.

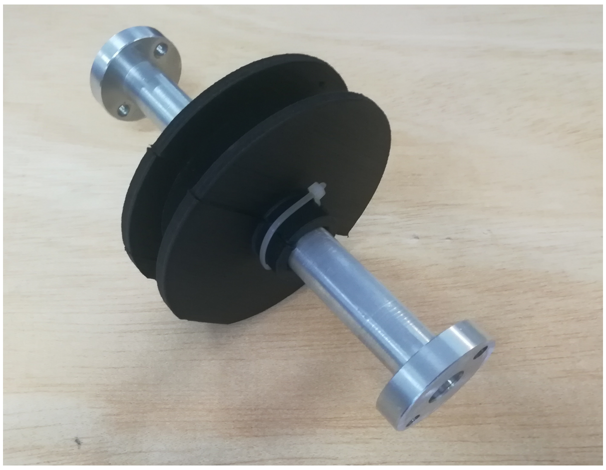

Figure 8.13. Pulley mounted on the shaft.

Finally this last part will be mounted on the supporting structure through four screws M8. In this way the central part is complete, and all threaded bars with spacers are pulled to respect the various games present and the distances given by the project.

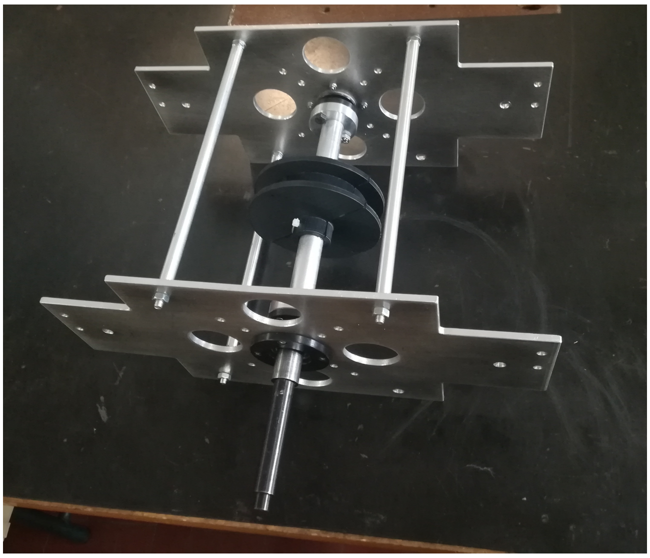

Figure 8.14. Pulley and shaft mounted on the structure.

On the bearing structure there are two ball bearings that allow the reduction of friction during the rotation of the shaft.The latter gave us a lot of problems because with a very small force acting on the pulley there was considerable friction.This problem has been solved by removing the shield and removing the internal grease and lubricating it with oil.The bearings present were suitable for rotation speeds much higher than ours. Finally, the supporting structure has been mounted on two plywood axes that support the tank where the system will be placed.

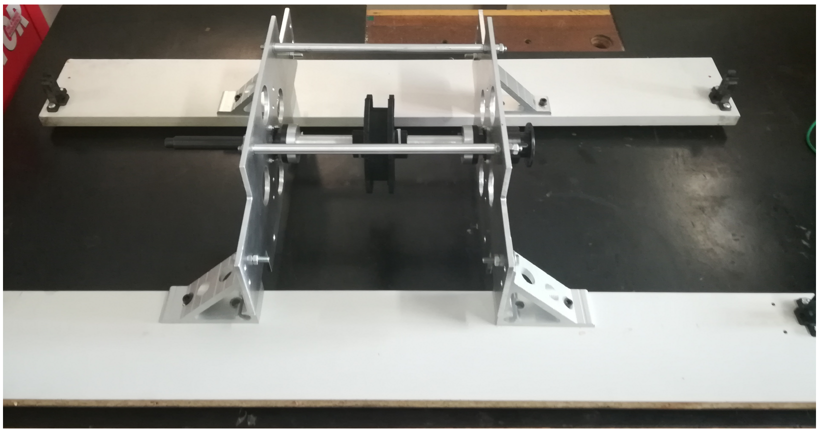

Figure 8.15. The structure fixed on wood component.

8.2.2 Measurement instruments

Load cell

The load cell is fixed by an end to the supporting structure, instead by the other with an arm attached to the brushless motor. The instrument used is a FN3030 series Load Cell Tension and Compression and it gives an electrical tension signal proportional to the effort with this equation:

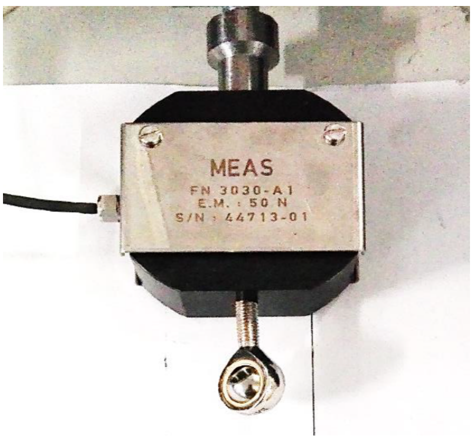

Figure 8.16. Load cell used.

$$1V \ = \ 25N$$

$$GAIN\ LOAD\ CELL = 0.4N/V$$

Encoder

Encoder is a position transducer that converts the angular position of the shaft of our system into a digital electric mustard.
Encoder model code encoder: AMS22S5A1BHBFL336 (RS code: 789-9343)

Features

- Non-contacting magnetic technology
- Highly resistant to vibration/shock
- Highly resistant to fluid/dust ingress
- Programmable at factory for zero position
- Robust design for industrial applications
- Highly repeatable
- RoHS compliant*

AMS22S Non-Contacting Analog Rotary Position Sensor

Electrical Characteristics[1] (@ 25 °C)	
VDD Supply Voltage	5 V ± 10 %
Supply Current [2]	
For Low Speed Processing (Code L)	10 mA max.
For High Speed Processing (Code H)	20 mA max.
Output Signal (Single)	Analog
Independent Linearity	±0.5 % (±0.3 % available on request)
Hysteresis	0.2 % VDD max.
Effective Electrical Angle [3]	340 °
Programmable Electrical Angle	10 ° to 360 ° (10 ° increments)
Voltage Output (Programmable)	1 to 99 % VDD ±1 %
Output Resolution	12 bit @ 360 °
Load Resistance Recommended	10K ohms to ∞
Overvoltage Protection	+20 VDC
Reverse Voltage Protection	-10 VDC

Environmental Characteristics	
Operating Temperature	-40 ° to +125 °C
Rotational Life (Shaft Revolutions)	50 million
Vibration	15 G
Shock	50 G
IP Rating	IP50
ESD Rating	2 kV max.

Mechanical Characteristics (@ 25 °C)	
Mechanical Angle	Continuous
Shaft/RPM	120 RPM max.
Torque (Starting & Running)	1.06 N-cm. (1.5 oz-in.) max.
Shaft Material	Stainless steel
Terminals	Brass / 100 % matte tin over Ni Strike (e3)
Bearing	Bronze sleeve

Product Dimensions

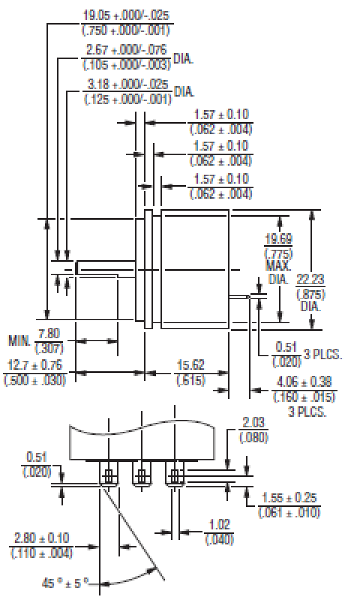

Figure 8.17. Data sheet Encorder.

8.2.3 Data acquisition instruments

MyRio

MyRIO was used for data acquisition and system stifness and damping. MyRIO is a real-time embedded evaluation board made by National Instruments. It is used to develop applications that utilize its onboard FPGA and microprocessor. It requires Labview. It is geared towards students and basic applications.

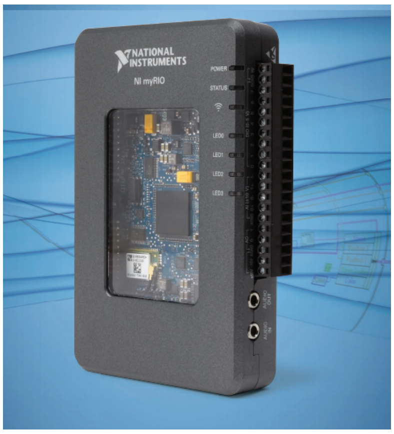

Figure 8.18. MYRIO used

Motor driver

Motor drives are circuits used to run a motor. In other words, they are commonly used for motor interfacing. These drive circuits can be easily interfaced with the motor and their selection depends upon the type of motor being used and their ratings (current, voltage).

Figure 8.19. Driver model used.

Electric motor

The PTO used is a brushless motor-generator that works in direct current. A support about 10 cm long has been applied for the connection with the load cell. In this way you can know the torque discharged from the engine. Moreover it is important to remember that there is also a reducer with a reduction ratio of 16.

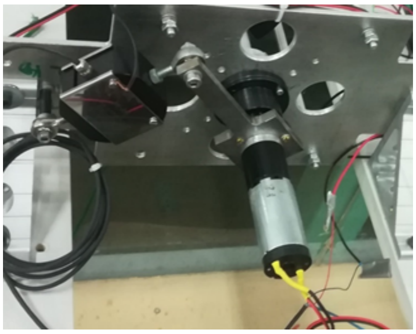

Figure 8.20. Motor brushless and load cell used.

8.2.4 Complete system

In this section is shown the complete system, on the two wooden axes were fixed all the components mentioned before. Now the structure is usual and ready to be fixed on the tank of the laboratory. As you can see in the image on the left you have the MyRIO and the driver instead in the middle you have the structure which is present the pulley and the PTO.

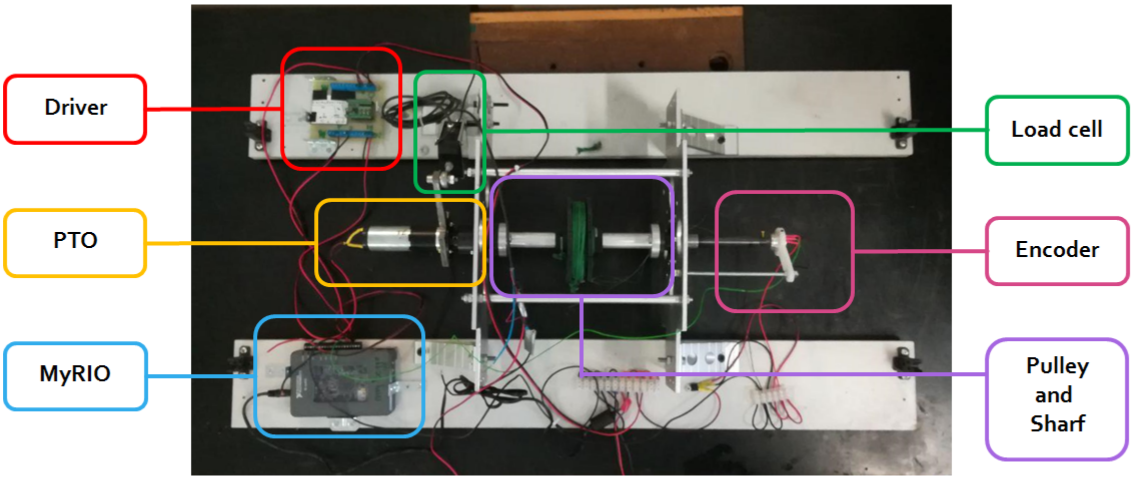

Figure 8.21. System complete.

8.3 Laboratory

8.3.1 Flume

The experimental campaign took place in the flume of the of the laboratory 'G.Bidone' od the department of hydraulics in Politecnico di Torino. The electrically driven wave maker can generate regular waves up to the frequency of 1,7 Hz and heights of about 85 mm when the flume is filled with 700 mm of water. The flume is 50.4 m long, 930 mm deep and 610 mm wide and its sidewalls are made of Plexiglass to observe the experimentation. It can be filled in few minutes thanks to a big duct directly connecting a raised reservoir to the flume. The reservoir is filled from a underground channel flowing under the entire Hydraulics laboratory.

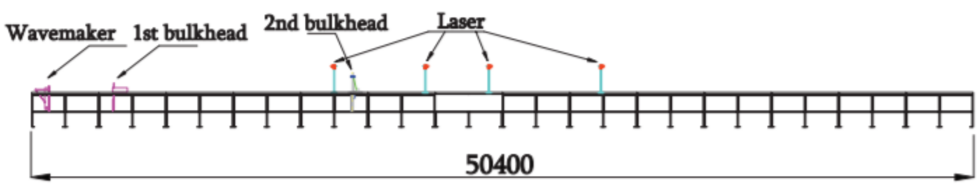

Figure 8.22. Schematic representation of the flume.

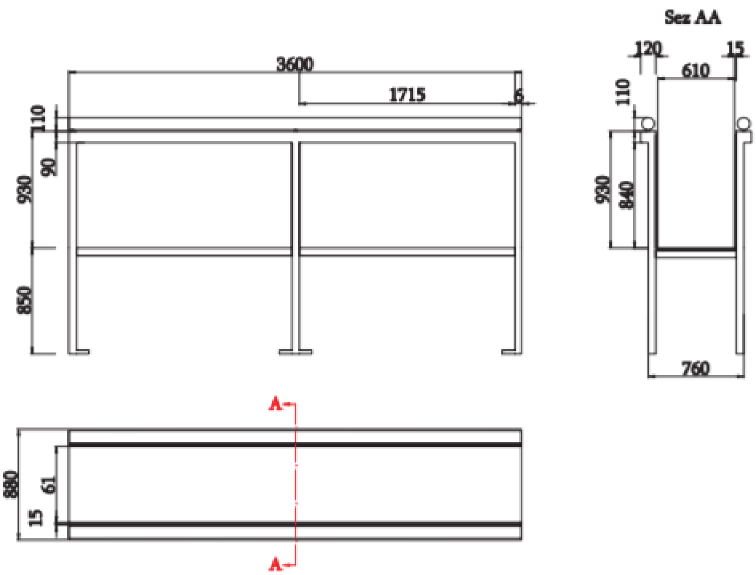

Figure 8.23. Dimensions of the flume.

It is important to remember that in the final part of the tank was placed a beach for the destruction of the waves otherwise they would have been reflected partially reducing the time valid for the acquisition of the data. In the figure below are the large and the Wave maker.

Figure 8.24. Left: Wave maker; Right:Flume

8.3.2 Data acquisition

Flume sensor

In the flume is equipped with a series of 5 ultrasonic sensors, which instantly measure the amplitude and the wave period. A remote computer using LabVIEW controls this measurement system and records data about wave characteristics. In this way, a post control of the produced waves can be done in order to ensure that the entire system functions properly. The sensor used for the campaign is the "fae FA 18-800/I-S" for measurement and distance control and level on liquids and solids.

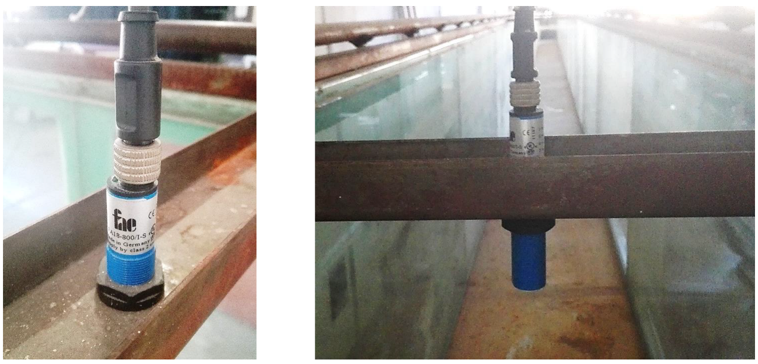

Figure 8.25. FaeFA 18-800/I-S sensor [41].

Video acquisition

For what concerns acquisition of the motion of the submerged hull, the oscillation of the body has been recorded by a motion tracking system in every single experiment. Afterwards, using a post processing motion tracking code in Matlab, the movement of the body was calculated (only heave and surge). It is reminded that the side wall of the flume is made from glass and, as a result, the video recording was feasible.

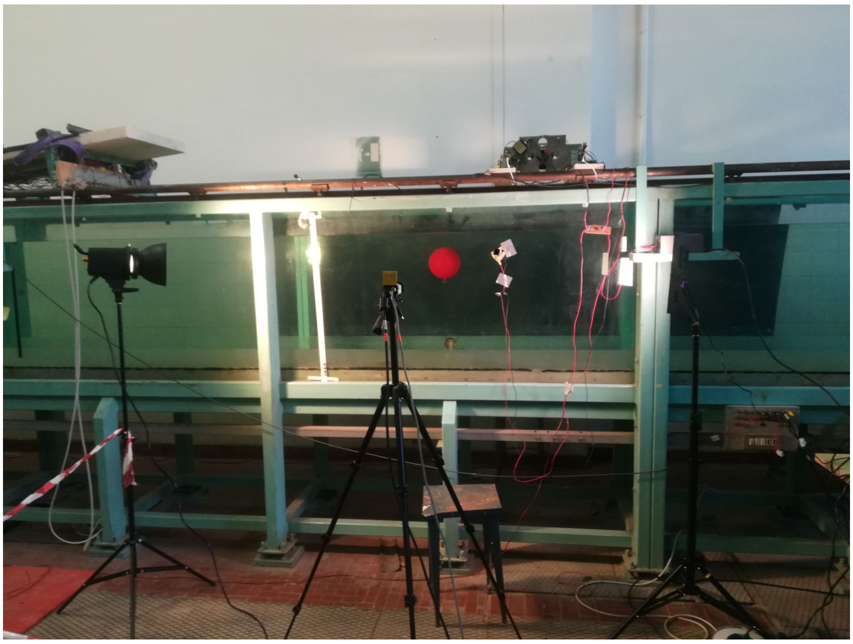

Figure 8.26. Recording the motion of the submerged device.

In order to achieve the best possible contrast between the spherical hull coloured in red and the black background, special professional lamps were used. The light contrast between the hull and the dark background was necessary for the image process for the identification of the hull's motion. The camera is a Basler Scout camera that offers a wide variety of resolutions and speeds. In particular, the model used is FireWire-b interface provided, a technology that lets you get the maximum performance from each sensor. The Basler Scout family features a GenICam compliant API and uses new drivers. FireWire-b cameras are also compatible with Basler's existing BCAM driver and API for FireWire cameras. Along with the drivers, GUI based software is provided that lets users easily set camera parameters, adjust image quality, and control cameras from a remote computer. Moreover, a special optical lens has been mounted that allows to not suffering the refraction phenomenon due to the glass and the water in which the device is immersed. [42]

8.4 Placement in the flume

In order to be able to carry out the tests and to comply with the design scheme for the position of the various components in relation to the point absorber, modifications have been made to the supporting structure. On which were placed MYrio and driver, and finally all connected with cables.

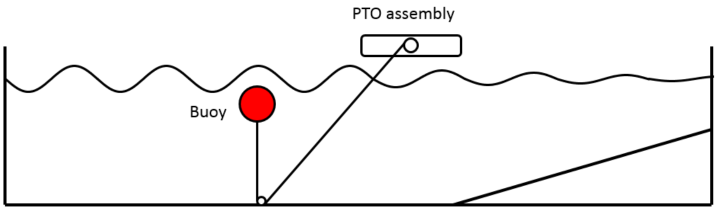

Figure 8.27. Layout system.

The entire PTO system was mounted on two plywood boards with the purpose of being fixed on the tank because it was initially too narrow and had no structure to rest on.

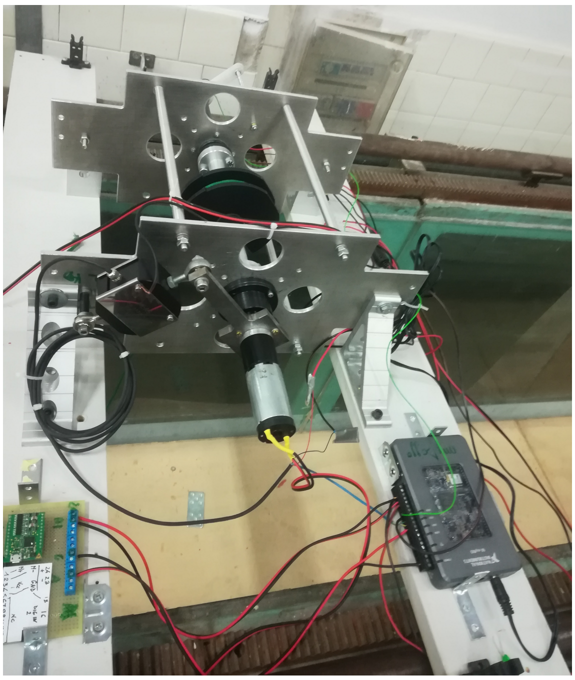

Figure 8.28. System fixed over the flume.

Moreover a trigger has been fixed, that is a led that will be turned on to command from the pc used for the acquisitions so that this led appears in the video in order to be able to synchronize from the acquisitions. The trigger connects all acquisition systems: the PC with the tank's sensor acquisitions, the cameras, the PC with MYRIO's acquisitions.The system is powered with a 0-20V DC power supply.

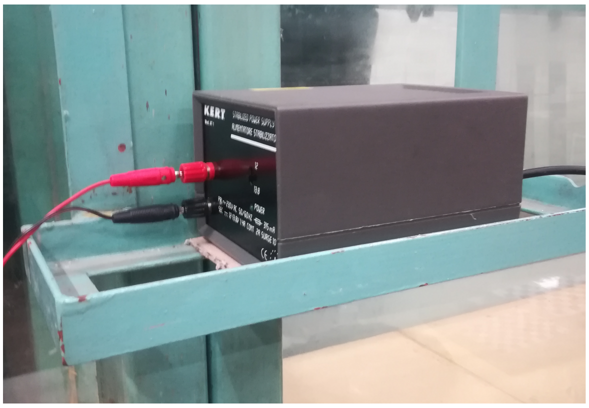

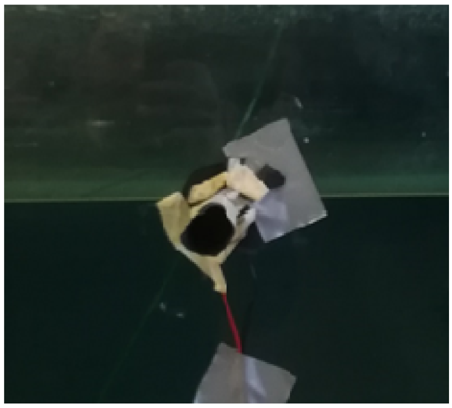

Figure 8.29. Left: trigger; Right: alimentator DC current.

Finally, a pulley anchored to the bottom of the tank with cast iron weights was built.The test piece shall be heavy enough not to move during testing, and the pulley must resist the least possible resistance to rotation because the forces in play are really very small and every detail is important.

Figure 8.30. pulley on the back drop.

As you can see in the next photo all the previously treated items were used to recreate the working layout of the figure at the beginning of the chapter. In the image you can see the whole system ready to perform an experimental test because the point absorber is at the correct distance below the surface, the camera is ready to shoot. you can notice that the rope is tight because you need to give a preload to the engine to ensure that the ball remains under the surface.

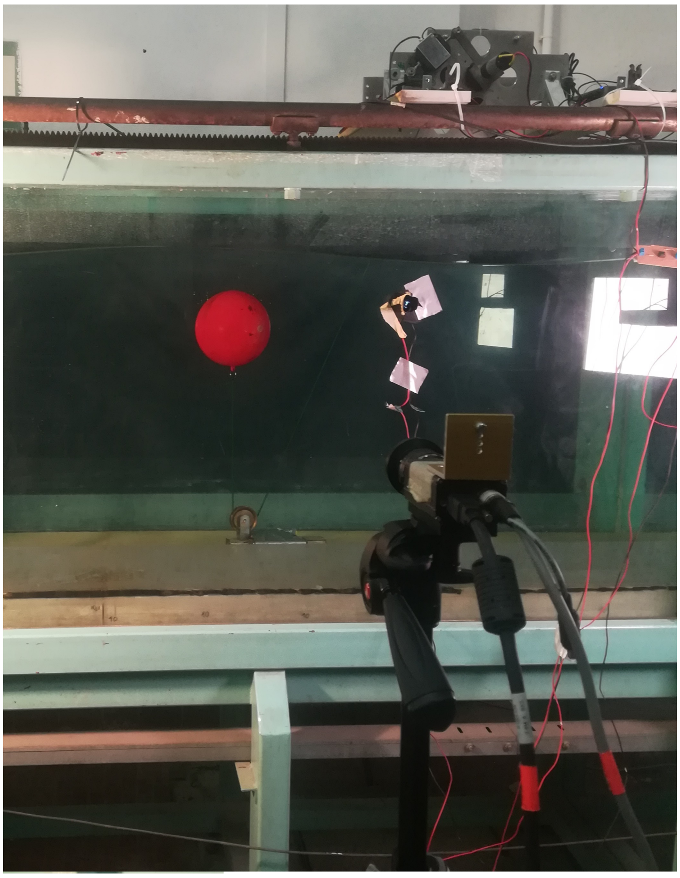

Figure 8.31. Layout system in laboratory.

8.5 Conducting the test

In the previous chapters the components composing our system used to perform the tests have been explained. The aim is to observe the response and behavior of our point absorber subjected to regular waves of constant height but with different frequency, The waves used in the laboratory had a height of 3 cm and a frequency range from 0.62854 Hz to 1.6162 Hz. In the next table the last column are scaled waves and correspond in reality to waves of 1 m of amplitude and with period ranging from 9 to 3.5 respectively.

T[s] Real scale	f [Hz] Small Scale	T[s] Small Scale
3,5	1,6162	0,6187
4	1,4142	0,7071
4,5	1,2571	0,7955
5	1,1314	0,8839
5,5	1,0285	0,9723
6	0,9428	1,0607
6,5	0,8703	1,1490
7	0,8081	1,2374
7,5	0,7542	1,3258
8	0,7071	1,4142
8,5	0,6655	1,5026
9	0,6285	1,5910

Table 8.4. Wave's frequency used.

To realize this experimental campaign the laboratory has used the total layout present in figure where were two control stations with dedicated pc. The first station composed of two pcs that can be observed on the right has been used to create the waves and for the acquisitions of the data coming from the sensors present on the tank. The second station also consisted of two PCs one for recording videos for tracking motion and another for the MYrio data acquisition and for modifying the rigidity and damping of the system.

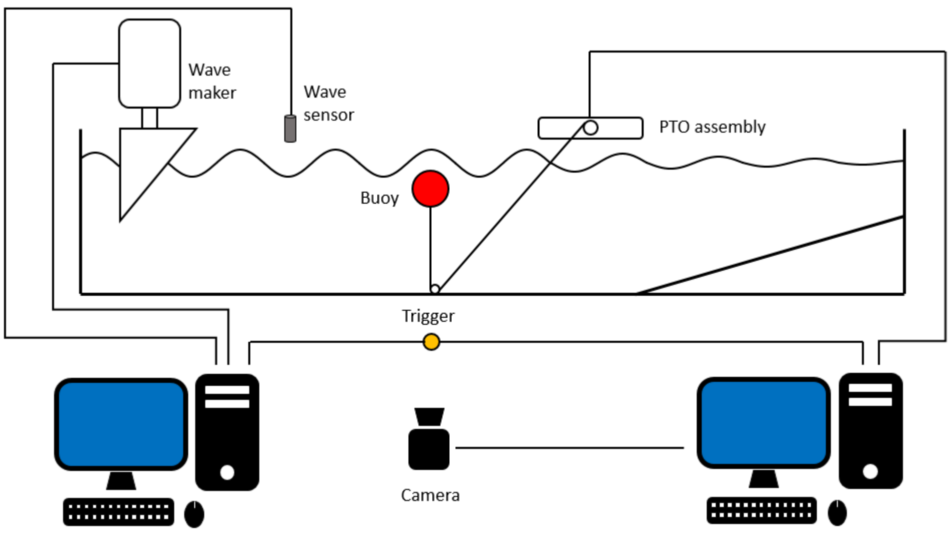

Figure 8.32. General layout.

It is very important to remember that the two stations are connected by the trigger signal that will serve to synchronize the acquisitions.

Figure 8.33. Pc zone for control wave maker.

The procedure by which the tests were carried out:

- Control of the water level of the tank that has to be adjusted for the wave that is about to be created;
- Point absorber position at the correct depth below the surface,Zero of the encoder that was done manually by rotating the pulley very gently because the sensitivity of the instrument was high. Process that had to be performed in pairs, one person moved the pulley the other controlled the position on the display;
- Lubrication of bearings for as little friction as possible;
- Wait for the water to calm down, rest time was about 8 minutes;
- Proceed with the creation of the wave by inserting on the pc that controls the wave maker amplitude and frequency. It is important to remember that the amplitude used was not that of the wave but a magnitude in volts. Indeed, the correct values identified during calibration had to be used;
- Video recording starts when the desired waves arrive at the location where the point absorber has been placed;

- The acquisition of the sensors present in the tank starts only after the start of the video;
- The acquisition of signals from the load cell and encoder starts;
- Trigger is triggered to synchronize the data collected during post-processing but only after performing the previous operations of the given order;
- Trigger deactivated after about 30 seconds;
- All acquisitions terminate;
- Return to starting point with a new wave;

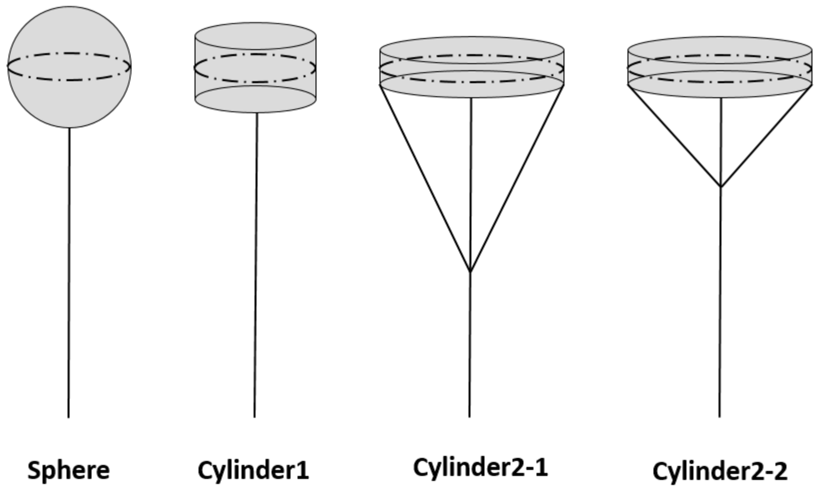

Figure 8.34. Type device used.

The value of $k = 170N/m$ is the optimal value for the sphere with the wave of 1.1313 seconds period (real scale T=5s). This procedure was carried out for the following cases:

- Sphere stiffness constant ($k = 170N/m$);
- Sphere optimal stiffness ($k = resonance$)where problems with acquisitions were found;
- Sphere optimal stiffness ($k = resonance$);
- Cylinder1 stiffness constant ($k = 170N/m$);
- Cylinder2-1 stiffness constant ($k = 170N/m$);
- Cylinder2-2 stiffness constant ($k = 170N/m$);

Chapter 9

Experimental result

The experimental laboratory campaign it was done with the aim of obtaining data that were subsequently analyzed and interpreted. The experimental campaign lasted two weeks during which 92 tests were carried out with our prototypes. Not all the tests were successful but a significant amount of data were obtained and processed.

The data we collected are:

- MyRIO data from the encoder and the load cell from Labview and also the stiffness and damping applied to the engine-generator. These data are in file form .txt;
- Video recorded by the camera;
- Tank sensor data containing the water position for each instant of time in the form of .txt file;

The purpose of the experimental campaign was to validate the model above all with regard to the movement of the point absorber. Another important goal was to test different geometries between them and evaluate the different behaviors. The use of small-scale prototypes did not allow you to evaluate the power with the model in the best way because there was friction in the system.

9.1 Video data

The video recorded with the camera has been processed with Matlab with the aim of extract the buoy motion. In this process it was necessary to locate the object in motion and its color, on the trigger was performed the same procedure. The program produced output .txt file. with the movement data of the center of mass (heave and surge) expressed in pixels.

The following operations were subsequently carried out:

- Saved heave and surge pixels variables of the mass center of the sphere;
- Calculation min, max, mean and rms of heave and surge ;
- Create the following graphs representing the behaviour of the floating body at different frequencies;

In the next figure it is possible to observe the different behaviour at different frequencies of the same device in Heave with two different stiffness values. The first ball was tested with a constant value of $\kappa = 170N/m$, the other was tested with the values corresponding to the resonance stiffness. The value of $\kappa = 170N/m$ is the resonant stiffness of the test at a frequency of 1,1313 Hz . The relative values of the spheres in resonance are greater than the first sphere expected from theory.

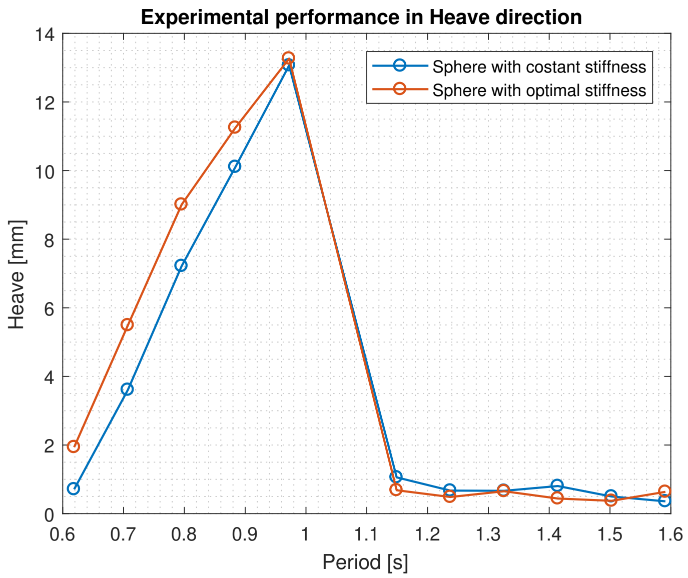

Figure 9.1. Rms Heave different spheres.

The resonance width increase in the optimal case. As it is possible to see in the previous figure after a certain frequency there is a collapse of the amplitude of oscillation, it becomes over-damped for too many frictions present in the system. In the following table there are the resonance stiffness used during the tests.

f $[hz]$	T $[s]$ $small$ $scale$	K $[N/m]$
1,6162	0,6187	260
1,4142	0,7071	240
1,2571	0,7955	200
1,1314	0,8839	170
1,0285	0,9723	140
0,9428	1,0607	120
0,8703	1,1490	100
0,8081	1,2374	87
0,7542	1,3258	75
0,7071	1,4142	66
0,6655	1,5026	58
0,6285	1,5910	52

Table 9.1. Stifness used for the experiment.

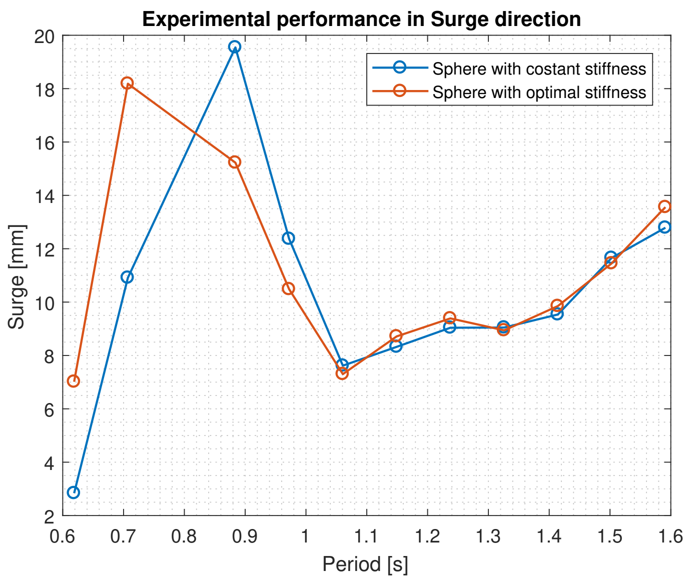

Figure 9.2. Rms surge different spheres.

The behavior of the motion in surge direction is different to the heave direction because the are the drift force that are very difficult to estimate. In this case the resonance width don't increase because the optimal stiffness is related to the heave direction. It is very important remember that in surge motion there is a double frequencies of motion as it's possible see in the following figure.

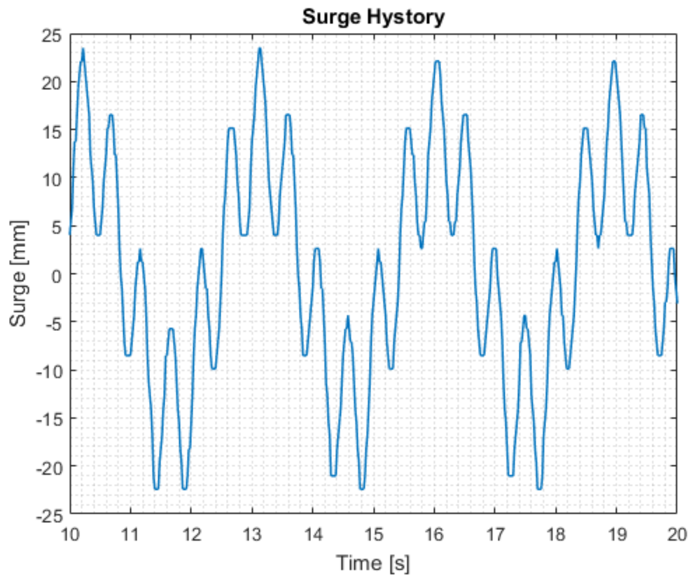

Figure 9.3. Surge motion.

9.2 PTO data

MyRIO acquired in the form of files . txt numerous data from load cell, encoder from PTO. The obtained data are:

- Space expressed in mm signal from encoder;
- Speed expressed in mm/s signal from encoder;
- load expressed in V signal from the load cell;
- K expressed in N/m stifness used during the test;
- C expressed as ks/m damping used during the test;
- F0 expressed in N preload force used to hold the point absorber underwater at the correct depth;
- gain load cell =0.4NV;
- V-offset preload force expressed in volts;
- Load cell arm b=102mm
- R pulley 0.04m;

- Ratio reducer=14;
- MyRIO ticks number of ticks;
- dt ticks expressed in ms;
- Trigger indicates whether it is on or off;

First of all, the .txt file data was processed. data with that aim to derive the quantities of interest analyze the behavior of the device. In following part there are the operation used to obtain the .mat files with the final data.

- Time: calculated knowing the time between every acquisition

$$time = dt\ ticks \cdot number\ of\ tick$$

- Position saved by imposing an upper and lower limit, filtered at 20 Hz , the transient was eliminated by erasing the first seconds of acquisition;
- Speed saved by imposing an upper and lower limit when needed, filtered at 20 Hz the transient was eliminated by erasing the first seconds of acquisition;
- Load: the initial data saved by imposing an upper and lower limit when necessary, filtered at 20 Hz ,the transient was eliminated by erasing the first seconds of acquisition:

$$F_{0PTO} = mean\ F_{0PTO} first\ load\ datas\ acquisition$$

The preloading value is the first load data obtained considered better than mean or rms value

$$Load = Load\ data\ acquisited - F_{0PTO}$$

Finally imposing an upper and lower limit (only for one abnormal)

- Force calculated:

$$Force = \frac{Load}{Gain\ Load\ cell}$$

- Torque calculated:

$$Torque = Force \cdot lever\ arm\ load\ cell$$

- Angular velocity calculated:

$$\omega = \frac{velocity}{radius\ pulley}$$

- Power calculated:

$$Power = |\omega \cdot Torque| = Force \cdot velocity$$

9.2.1 Sphere data from PTO

Data elaboration produced the following plots. Where there are two curves that represent two different devices. It is possible to see the power produced at the various frequencies in next figure.

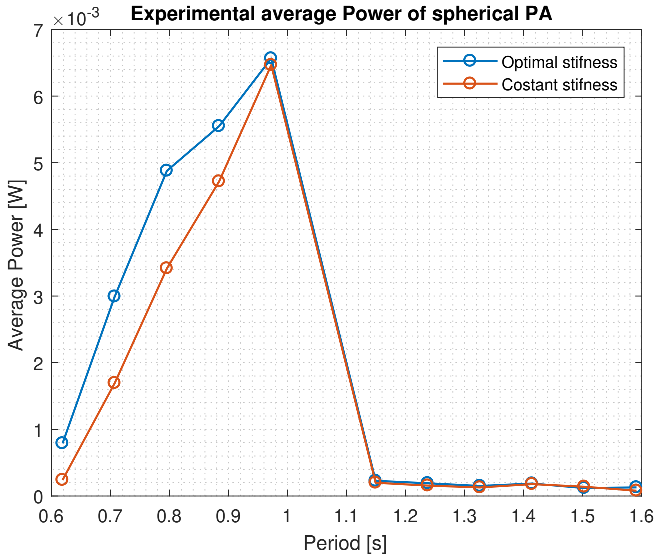

Figure 9.4. Mean power different spheres.

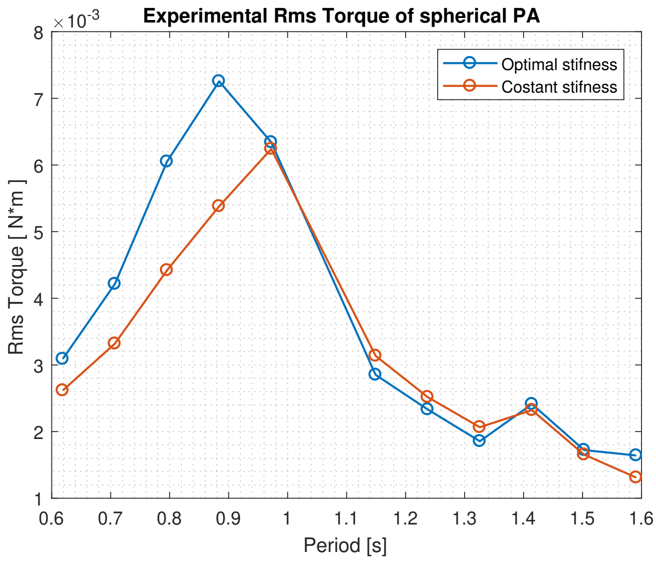

Figure 9.5. Rms torque different spheres.

In the previous graphs it is possible also to observe the trend of torque at different frequencies, which together with the angular speed give the power as previously exposed. In all the graphs presented, it can be seen that the sphere that is always in resonance produces slightly better results in all fields.

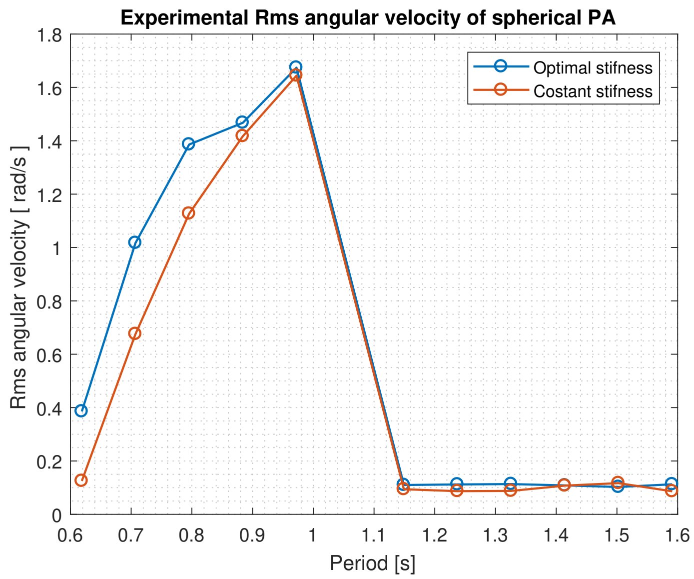

Figure 9.6. RAO rms w different spheres.

The system realized and tested in the laboratory has been built to validate the mathematical model with regard to the movement of the buoy and not of the power because in a model of such small dimensions there are coherent frictions. In fact, as you can see in the graphs, the value of power produced is really low and after a certain frequency there is a collapse of the acquisitions because the system becomes over-damped.

9.2.2 Cylinder data from PTO

Data elaboration produced the following plots. Where three curves represent two different cylinders fixed to the rope in different way as previously exposed. Then it is possible see the power produced at the various frequencies in figure. In the following graphs it is possible also to observe the trend of torque at different frequencies, which together with the angular speed give the power as previously exposed.

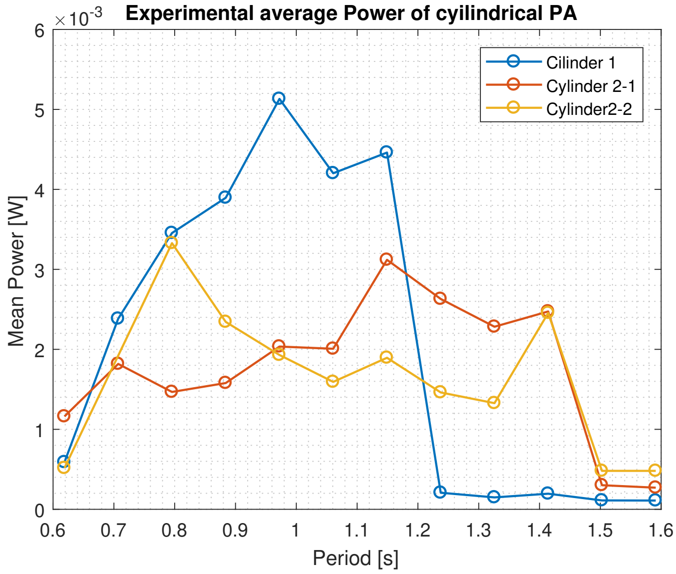

Figure 9.7. Mean power different cylinder.

It can be seen that the cylinder1 has a greater peak power. Instead the other cylinders are able to absorb power on more frequencies having a wider curve. The main difference between the two configurations used for the cylinder2 is that they have the power peak at different frequencies but of similar absolute value.

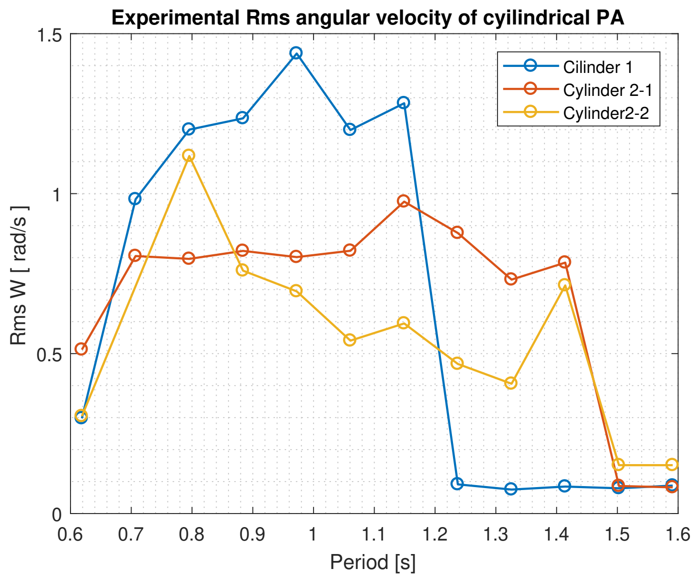

Figure 9.8. Rms ω different cylinders .

9.3 Comparison with different geometries

In this section all the various devices used in all their configurations are compared, In this way a direct comparison between the Sphere, the cylinder1 and the cylinder2-1 is obtained.

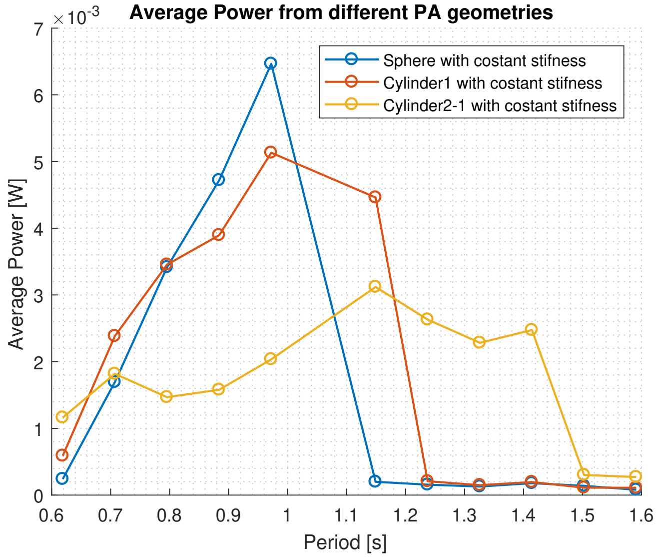

Figure 9.9. Mean power different device.

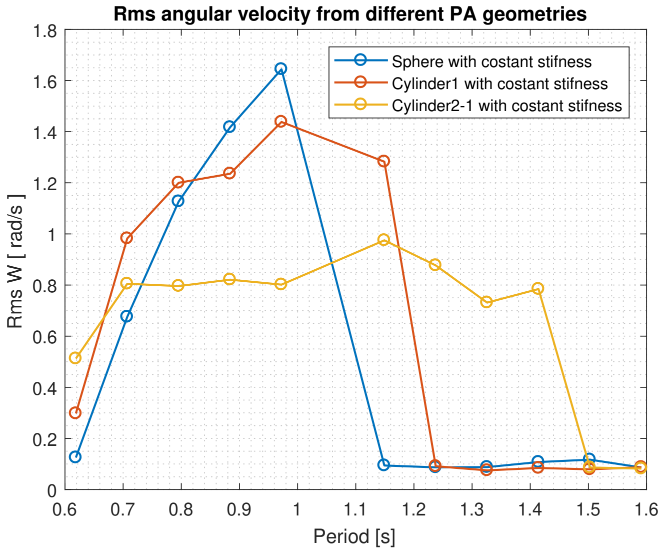

Figure 9.10. Rms angular velocity different device.

All the tests were carried out in the same exact conditions or with constant stiffness. In these graphs it can be seen that the sphere one has a greater peak power and angular velocity but it can be use in a small range of frequencies. Instead the cylinders has a smaller peak of power but they are able to absorb power on more frequencies having a wider curve.

9.4 Model prevision

9.4.1 Model prevision of sphere

In this section the results of the simulations performed with the mathematical model are presented. Average and heave power trends have been derived. It is important to note that the power of the model has been derived with the formulation formula from the potential flow theory:

$$Power = \frac{1}{2} \cdot B_{PTO} \cdot |\dot{x}|^2$$

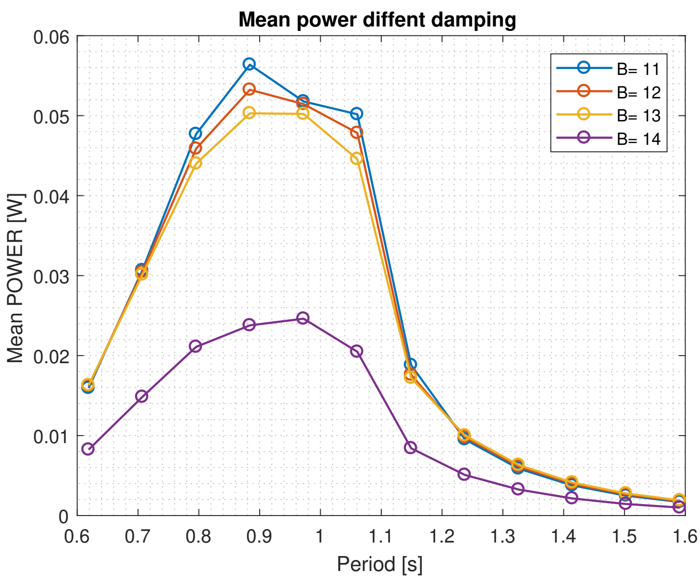

Figure 9.11. Mean Power with different damping from sphere model.

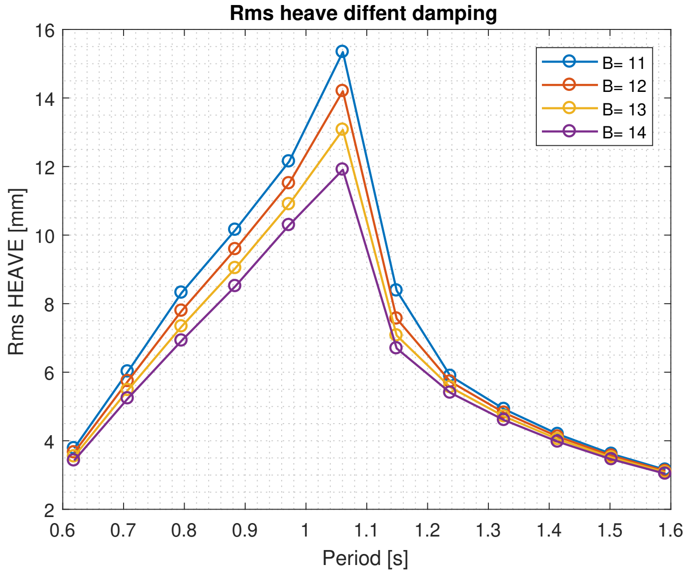

Figure 9.12. Rms heave with different damping from sphere model.

It is important to note that by decreasing the damping value the buoy movement increases and consequently the power produced. Moreover the damping value must be sufficiently large to be able to guarantee a power absorption because having damping equal to zero there is no power.

9.5 Comparison with model

9.5.1 Comparison with Spherical model

In this chapter there is the comparison between the Simulink model and the acquired data. The following two graphs refer to heave and surge. The sphere curve tested with constant stiffness is represented, the experimental data used are obtained from the videos in the first section of the chapter. Model used with $damping = 11[Ns/m]$. Furthermore, the linear regression of the data was produced which produces two lines The more the two lines are similar, the more the model can be considered reliable. For this purpose the linear regression coefficient was calculated. If this number is between 0.7 and 1, it can be considered a reliable model.

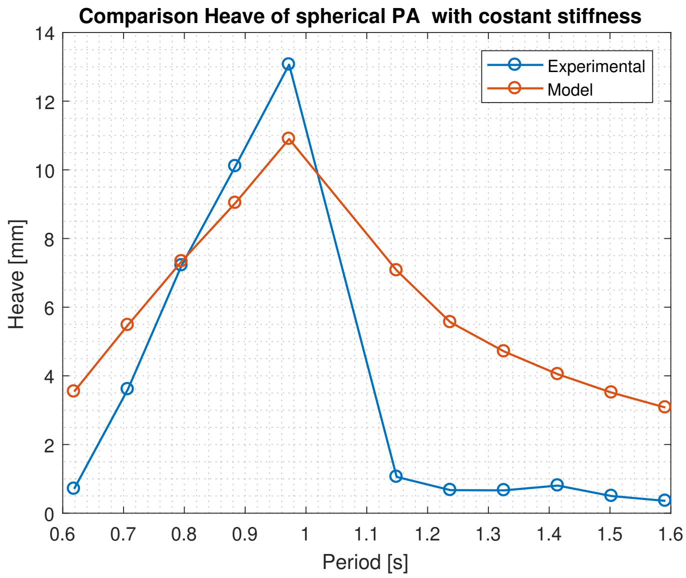

Figure 9.13. Comparison rms Heave between experimental and sphere Model.

As you can see from these graphs our model can be considered reliable because values of the coefficient greater than 0.7 have been obtained. In the graph showing the direction in the direction of heave it can be seen that after a frequent frequency the system becomes over-damped.

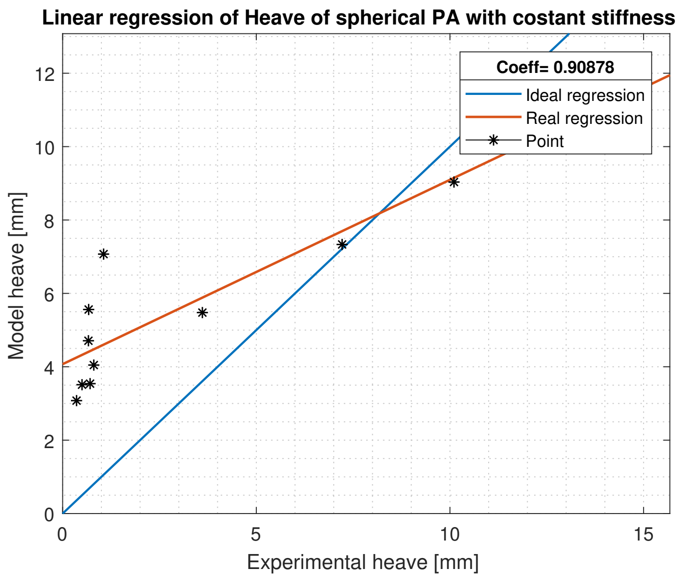

Figure 9.14. Linear regression rms Heave between experimental and sphere Model.

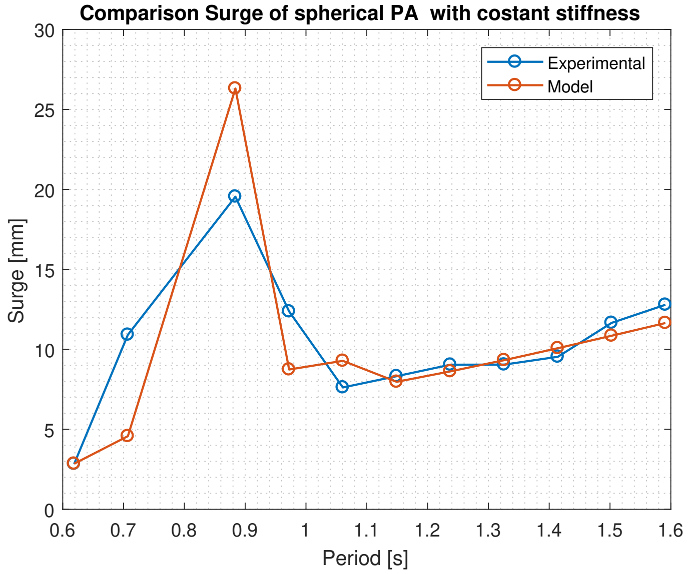

Figure 9.15. Comparison rms surge between Sperimental and sphere Model.

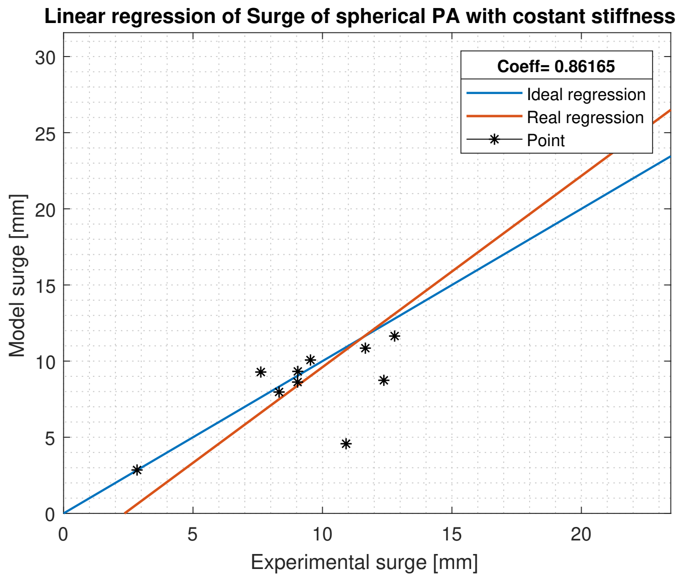

Figure 9.16. Linear regression rms surge between experimental and sphere Model.

In the two previous figures it can be noticed that the model is very approachable with what happens in reality. There are a similar maximum values and in this type of analysis the presence of friction is not particularly noticeable. The following three graphs instead represent angular speed, torque, and power.The experimental data was obtained from data from the PTO.

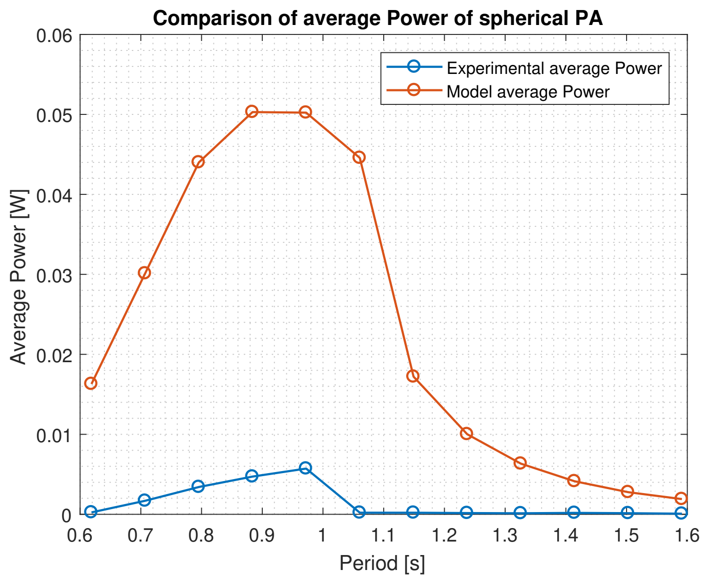

Figure 9.17. Comparison mean power.

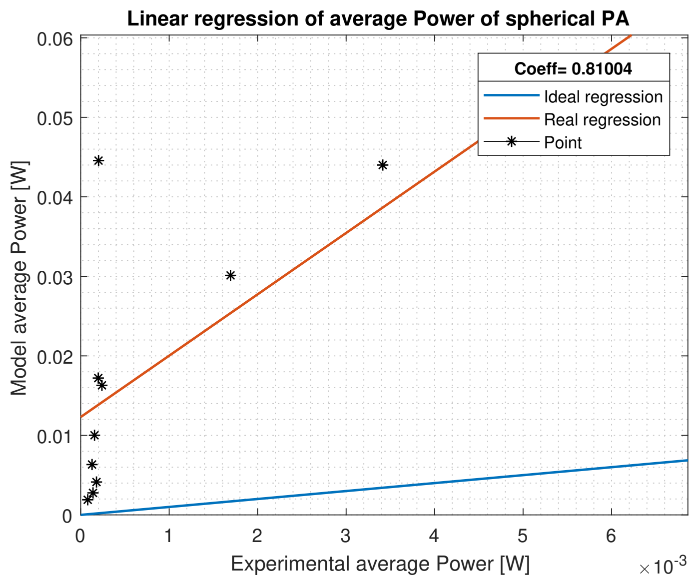

Figure 9.18. Regression mean power between experimental and sphere Model.

As expected, the powers predicted by the model are superior in all the frequencies because there are several frictions' phenomena in the system. This is a big problem that is often reported in small scale prototypes.

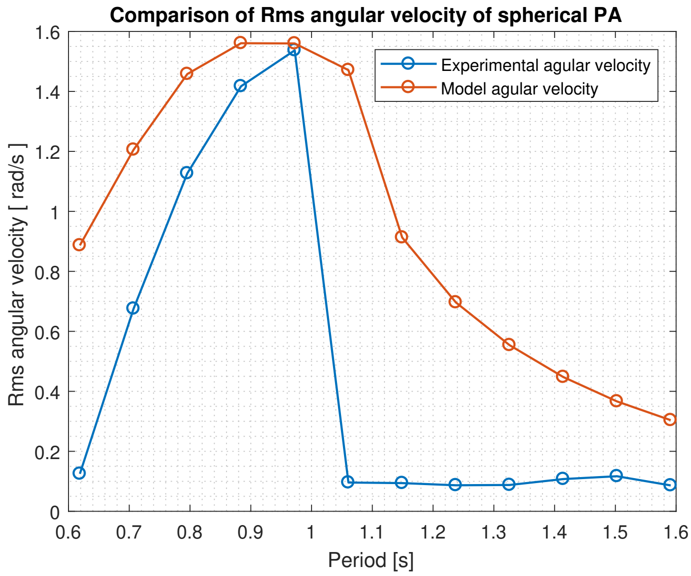

Figure 9.19. Comparison rms ω between experimental and sphere Model.

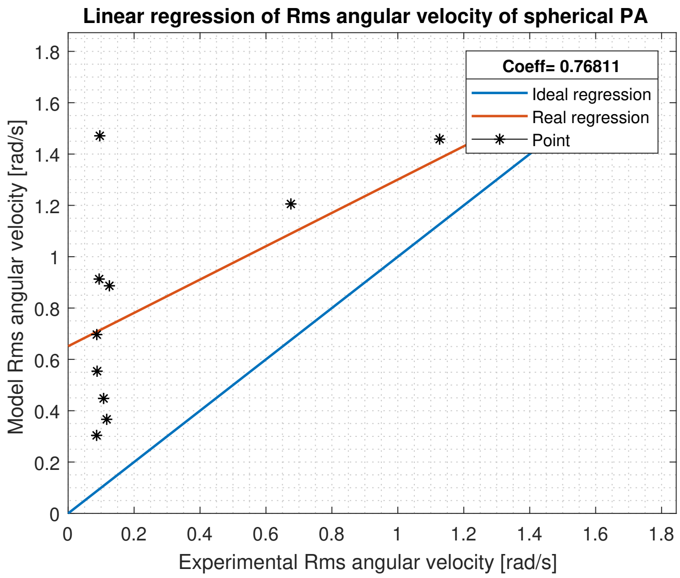

Figure 9.20. Linear regression rms ω between experimental and sphere Model.

The system realized and tested in the laboratory has been built to validate the mathematical model with regard to the movement of the buoy and not of the power because in a model of such small dimensions there are coherent frictions. In fact, as you can see in the graphs, the value of power produced is really low and after a certain frequency there is a collapse of the acquisitions because the system becomes over-damped. Moreover the model does not take into account the frictions and for this one obtains an over estimation of the power.

Chapter 10

Conclusion

The development of a submerged point absorber is on progress in Politecnico di Torino, Italy. The design of the wave energy converter is concentrated in the Mediterranean Sea and specifically in the island of Pantelleria. For the selection of the technical characteristics of the WEC a method proposed by Falnes and Budal is followed. The scatter of Pantellria sea with the device designed is:

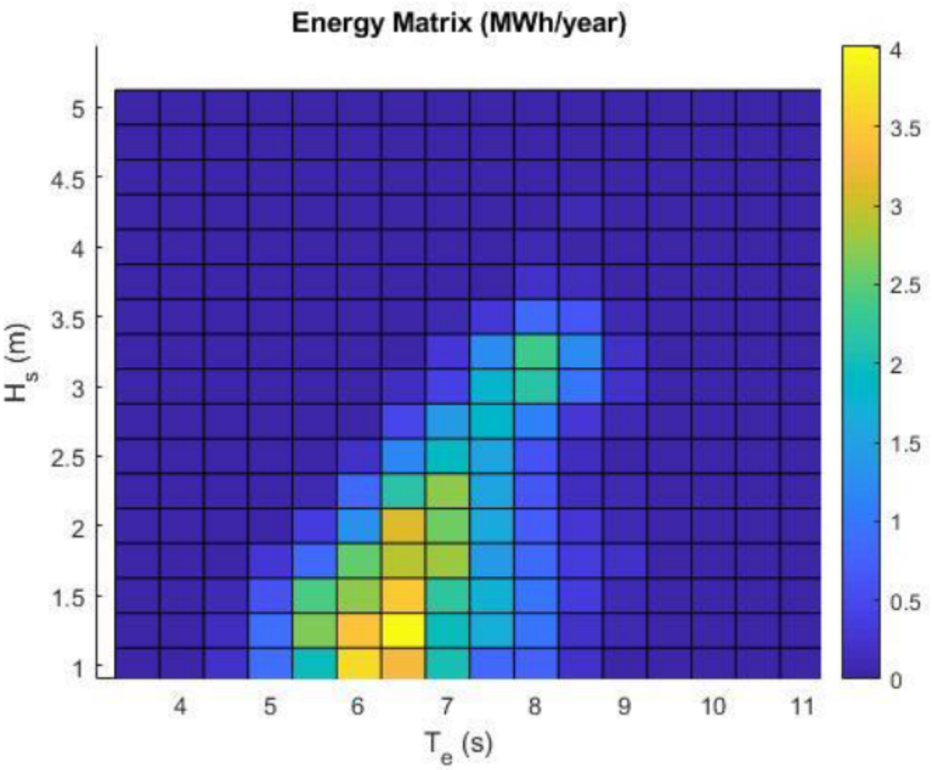

Figure 10.1. Scatter with the device designed [34].

In order to design and test the performance of the device in different situations, a mathematical model has been constructed in Matlab Simulink based on the Cummins Equation. The device designed have the following features:

Feature	value	
$Diameter$	5,14	$[m]$
$Volume$	71,1	$[m^3]$
$Mass$	63960,3	$[Kg]$
S_{3max}	1,55	$[m]$
$SweptVolume$	64,5	$[m^3]$
ds	4,53	$[m]$
$Seadepth$	30	$[m]$
$Mooring\ length$	22,8	$[m]$
$Power/Volume$	240	$[W/m^3]$
$Powerpeak$	20000	$[W]$

Table 10.1. Features of the device rea scale in Pantelleria.

After the experimental campaign that took place in the laboratories of Politecnico di Torino in january 2019 the following conclusions were reached:

- Mathematical model is valid in the wave frequencies that have been tested. It is important to specify that the model is validated with regard to the motion of the buoy and not the power because there were too large frictions with such a reduced scale model. This fact was observed previously in the graphs since after a certain frequency the movement of the sphere collapsed because the frictions of the system were considerable and were over-damped preventing any movement;

- Several geometries have been successfully tested with different anchoring methods, with notable differences. The most productive geometry was the ball in spite of the different cylinders which are slightly smaller. An important observation is that the curve of the sphere is very 'narrow' 'that is it has acceptable power values for few frequencies instead as regards the cylinders they are productive on many more frequencies having a curve more' 'wide' '. The cylinders were able to move significantly even at low frequencies which the sphere does not do. Finally it was a very interesting behavior of the cylinders, which have a great pitch movement especially at low frequencies that with the anchoring system it was not possible to absorb;

- According to Falnes' theory, the geometry found at the end of the 5.14 m diameter design located at pantelleria would be worth and produce with a strong power to volume ratio giving a significant weight to the device;

For what concerns the future work of the development of the point absorber, the following objectives are proposed:

- Complete experimental campaign of the point absorber in the entire frequency domain aiming to valid the numerical model in major scale;
- Design cylindrical point absorber with type of mooring with the aim of absorb the pitch movement;
- CFD analysis in different geometries in order to discover the best performance solution;

Bibliography

[1] https://setis.ec.europa.eu/system/files/Technology Information Sheet Ocean Energy.pdf

[2] BP: Statistical Review of World Energy, Workbook (xlsx), London, 2016

[3] Denise Warkentin-Glenn in “Electric Power Industry in Nontechnical Language”

[4] Phillips, O.M. (1977). The dynamics of the upper ocean(2nd ed.). Cambridge University Press. ISBN 978-0-521-29801-8.

[5] Wiegel, R.L.; Johnson, J.W. (1950), "Elements of wave theory", Proceedings 1st International Conference on Coastal Engineering, Long Beach, California: ASCE, pp. 5–21

[6] https://en.wikipedia.org/ wiki/Wind wave

[7] https://en.wikipedia.org/wiki/Wave power

[8] KNMI/ERA-40 WAVE ATLAS.

[9] B. Czech, P. Bauer, “Wave Energy Converter Concepts, Design Challenges and Classification” IEEE Industrial Electronics Magazine, June 2012.

[10] GUIDE FOR WAVE ANALISYS: Secretariat of the World Meteorological Organization – Geneva – Switzerland 1998

[11] http://folk.ntnu.no/oivarn/hercules_ ntnu/LWTcourse/lwt_ new_ 2000_ Part_ A.pdf

[12] “Ocean Waves and oscillating Systems Johannes Falnes

[13] Thesis: Michele Pasquotto Reduction of power oscillations in Wave Energy Converters using prediction techniques based on Autoregressive Models

[14] A. Babarit,Jørgen Hals Todalshaug . On the maximum and actual capture width ratio of wave energy converters

[15] https://www.peacelink.it/ecologia/a/42640.html

[16] http://theliquidgrid.com/the-tech-pool/wave-energy-converters/

[17] https://www.researchgate.net/figure/Artists-sketch-of-the-Oyster-WEC-concept-online-figure-in-colour fig1 261291083

[18] An axial turbine in an innovative oscillating water column (OWC) device for sea-wave energy conversion Author links open overlay panelI.HashemaH.S.Abdel HameedaM.H.Mohamed

[19] Overtopping Wave Energy Converters: general aspects and stage of development Giovanna Bevilacqua (1), Barbara Zanuttigh (2)

[20] Prospects of Wave power in Bangladesh Md Monjur, Shah Md. Salimullah , M R I Sheikh,S M Showybul Islam Shakib

[21] N.Y. Sergiienko, B.S. Cazzolato, B. Ding, P. Hardy, M. Arjomandi, 'Performance comparison of the floating and fully submerged quasi-point absorber wave energy converters', August 2016, Renewable Energy ELSEVIER

[22] https://tethys.pnnl.gov/technology-type/wave

[23] Johannes Falnes, Jorgen Hals, 'Heaving buoys, point absorbers and arrays', 2012, Philosophical Transactions of the royal society

[24] B. Drew, A. R. Plummer, M. N. Sahinkaya, "A review of wave energy converter technology", Department of Mechanical Engineering, University of Bath (UK), 2009

[25] MARINET, 'CETO Unit Hydrodynamic Testing and Validation', 2014, Infrastructure Access report

[26] Giles Parkinson 'New generation wave energy: Could provide one third of Australia's electricity?', December 2015, Retrieved from https://www.theguardian.com

[27] Erik Lejerskog ,Cecilia Boström ,Ling Hai ,Rafael Waters ,Mats Leijon, 'Experimental results on power absorption from a wave energy converter at the Lysekil wave energy research site', May 2015, ELSEVIER Renewable Energy

[28] Mike Mekhiche, Kathleen A. Edwards, 'OCEAN POWER TECHNOLOGIES POWERBUOY®: SYSTEM-LEVEL DESIGN, DEVELOPMENT AND VALIDATION METHODOLOGY',2014, 2nd Marine Energy Technology Symposium

[29] J. Weber, F. Mouwen , A. Parish and D. Robertson, 'Wavebob – Research and Development Network and Tools in the Context of Systems Engineering'

[30] Horizon 2020, Call: H2020-LCE-2015-2, Topic: LCE-03-2015, Type of action: IA, Proposal number: 691905, Proposal acronym: SeaCURE, European Comission

[31] Gunnar Mork, Steve Barstow, Alina K.Kabuth, M. Teresa Pontes, 'Assessing the Global Wave Energy Potential', June 2010, 29th International Conference on Ocean, Offshore Mechanics and Arctic Engineering

[32] G. Besiom, L. Mentaschi, A. Mazzino, 'Wave energy resource assessment in the Mediterranean Sea on the basis of a 35-year hindcast', January 2016, Energy ELSEVIER

[33] Google Maps, 2018, Retrieved from https://www.google.com/maps

[34] P. Dafnakis, M. Bonfanti, S. A. Sirigu, G. Bracco, G. Mattiazzo, A submerged point absorber wave energy converter for the meditterranean sea, in: Proceedings of the 13rd European Wave and Tidal Energy Conference, 2019

[35] Jorgen Hals Todalshaug, 'Practical limits to the power that can be captured from ocean waves by oscillating bodies, 2013, International journal of marine energy, ELSEVIER

[36] W.E. Cummins, 'The impulse response function and ship motions', October 1962, Symposium on Ship Theory at the Institut flir Schiffbau der Universitit

Hamburg
[37] Nicola Pozzi, ‘Numerical Modeling and Experimental Testing of a Pendulum Wave Energy Converter (PeWEC)’, 2018, Doctoral Thesis, Politecnico Di Torino
[38] Gregory Payne, ‘Guidance for the experimental tank testing of wave energy converters’,2008, SUPERGEAN MARINE
[39] Sea-state based maximum power point tracking damping control of a fully submerged oscillating buoy. Boyin Dinga, , Benjamin S. Cazzolatoa, Maziar Arjomandia, Peter Hardya, Bruce Millsb
[40] Numerical Prediction of Extreme Loads on the CETO Wave Energy Converter Ashkan Rafiee, Jonathan Fiévez
[41] Salvatore Franco, Giuliana Mattiazzo, ‘Hydrodynamic and Performance analysis of a submerged point absorber WEC’, Master Thesis 2017, Politecnico di Torino
[42] Basler Scout Series Retrieved from https://www.baslerweb.com/en/products/cameras/areascan-cameras/scout/
https://www.offshorewind.biz